1 OF 2
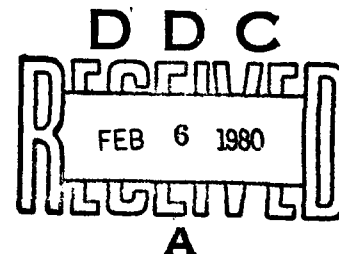
LEVEL

RADC-TR-79-284
Final Technical Report
December 1979

# INVESTIGATION INTO THE FEASIBILITY OF DESIGNING A FAIL SAFE OPTICAL DATA LINK

Sperry Research Center

D. H. McMahon
W. Spillman

D D C

FEB 6 1980

A

**ROME AIR DEVELOPMENT CENTER**
**Air Force Systems Command**
**Griffiss Air Force Base, New York 13441**

80    2    4    032

This report has been reviewed by the RADC Public Affairs Office (PA) and is releasable to the National Technical Information Service (NTIS). At NTIS it will be releasable to the general public, including foreign nations.

RADC-TR-79-284 has been reviewed and is approved for publication.

APPROVED:

RUDOLPH BRADBURY
Contract Monitor

APPROVED:

ROBERT M. BARRETT, Director
Solid State Sciences Division

| Accession For | |
|---|---|
| NTIS GRA&I | ☑ |
| DDC TAB | ☐ |
| Unannounced | ☐ |
| Justification | |
| By | |
| Distribution/ | |
| Availability Codes | |
| Dist | Avail and/or special |

FOR THE COMMANDER:

JOHN P. HUSS
Acting Chief, Plans Office

| REPORT DOCUMENTATION PAGE | | READ INSTRUCTIONS BEFORE COMPLETING FORM |
|---|---|---|
| 1. REPORT NUMBER<br>RADC-TR-79-284 | 2. GOVT ACCESSION NO. | 3. RECIPIENT'S CATALOG NUMBER |
| 4. TITLE (and Subtitle)<br>INVESTIGATION INTO THE FEASIBILITY OF DESIGNING A FAIL SAFE OPTICAL DATA LINK | | 5. TYPE OF REPORT & PERIOD COVERED<br>Final Technical Report<br>1 Jan 77 — 31 Dec 77 |
| | | 6. PERFORMING ORG. REPORT NUMBER<br>SCRC-CR-78-11 |
| 7. AUTHOR(s)<br>D. H. McMahon<br>W. Spillman | | 8. CONTRACT OR GRANT NUMBER(s)<br>F19628-77-C-0055 |
| 9. PERFORMING ORGANIZATION NAME AND ADDRESS<br>Sperry Research Center<br>100 North Road<br>Sudbury MA 01776 | | 10. PROGRAM ELEMENT, PROJECT, TASK AREA & WORK UNIT NUMBERS<br>62702F<br>46001921 |
| 11. CONTROLLING OFFICE NAME AND ADDRESS<br>Deputy for Electronic Technology (RADC/ESO)<br>Hanscom AFB MA 01731 | | 12. REPORT DATE<br>December 1979 |
| | | 13. NUMBER OF PAGES<br>146 |
| 14. MONITORING AGENCY NAME & ADDRESS(if different from Controlling Office)<br>Deputy for Electronic Technology (RADC/ESO)<br>Hanscom AFB MA 01731 | | 15. SECURITY CLASS. (of this report)<br>UNCLASSIFIED |
| | | 15a. DECLASSIFICATION/DOWNGRADING SCHEDULE<br>N/A |

16. DISTRIBUTION STATEMENT (of this Report)

Approved for public release; distribution unlimited.

17. DISTRIBUTION STATEMENT (of the abstract entered in Block 20, if different from Report)

Same

18. SUPPLEMENTARY NOTES
RADC Project Engineer: Rudolph Bradbury (ESO)

19. KEY WORDS (Continue on reverse side if necessary and identify by block number)

| | |
|---|---|
| Fail Safe | Serial Data Bus |
| Optical Data Link | Numerical Aperature |
| Terminal | Lithium Tantalate (LiTaO$_3$) |
| Fiber Optic | Optical Insertion Loss |

20. ABSTRACT (Continue on reverse side if necessary and identify by block number)

This report describes the development of a fail safe optical data link terminal and the construction of a serial fiber optic data bus system which uses several of these terminals. Such a system consists of a master terminal containing a CPU, an LED source, and a photodiode detector; and several remote send/receive terminals, each containing an electro-optic modulator and a photodiode detector. Multimode monofibers are the transmission media, and data can be impressed or tapped off at each remote terminal. The main thrust of this contract was to develop a serial data bus system which continues to

DD $_{1\ JAN\ 73}^{FORM}$ 1473

operate if power fails at one or more remote terminals. After consideration of several types of terminals, an augle collimation terminal and a mirror terminal were constructed. Both were designed to be compatible with Corning low loss multimode glass fibers (NA = .15) and both used ~85 (μm) thick $LiTaO_3$ crystals to control light flow by the electro-optic effect. Because of its superior optical insertion loss (5.7 dB) and modulation depth (51% with 100 V applied), the mirror terminal was selected for system implementation. From three additional mirror terminals constructed, the best two were chosen for the system and permanently butt coupled to fiber terminations. The two terminals and a master terminal were then assembled into a complete system and tested. Overall performance met or approached system objectives and the fail safe nature of the system was clearly shown.

# TABLE OF CONTENTS

iii

TABLE OF CONTENTS (CONT.)

# LIST OF ILLUSTRATIONS

LIST OF ILLUSTRATIONS (CONT.)

## LIST OF ILLUSTRATIONS (CONT.)

# LIST OF TABLES

EVALUATION

Three fail safe optical data link terminals were designed, constructed and supplied to RADC/ETS which demonstrate the feasibility of the fail safe concept.  During the course of this work a minor terminal was invented which improved the fail safe loss from 9.5 to 5.7 db.  This work is ˜f value since it conclusively demonstrated the application of the fail safe ȷ ˙nciple to optical data links.

RUDOLPH BRADBURY
Project Engineer

## 1. INTRODUCTION AND SUMMARY

The principal objective of this contract is the development of a fail safe optical data link terminal and the construction of a serial fiber optic data bus system which utilizes a number of these terminals. An example of such a system is shown in Fig. 1. It consists of a master terminal containing a central processing unit, an LED source and a photodiode detector, and a number of remote send/receive terminals, each containing an electro-optic modulator and a photodiode detector. Multimode monofibers are the transmission media and data can be impressed onto the bus or tapped off it at each remote send/receive terminal. The main thrust of this contract is the development of a serial data bus system which will continue to operate even though power fails at one or more of the remote terminals; i.e., the system is fail safe. It is also necessary that each remote terminal have a low optical insertion loss so that many terminals can be cascaded in the system. Furthermore, it is expected that each remote terminal have a maximum bus throughput in the fail safe or zero applied voltage condition and to operate in its active mode from a low voltage power supply.

This report details work carried out during a one year period beginning in January 1977. In that time period, several different types of fail safe optical data link terminals were considered. Two distinct types were actually constructed: an angle collimation terminal and a mirror terminal. These were designed to be compatible with Corning low loss multimode glass fibers with a numerical aperture of .15, and both utilize thin crystals ($\sim 85$ $\mu$m) of $LiTaO_3$ to control light flow via the electro-optic effect when voltages are applied to appropriate surface electrodes. The mirror terminal was chosen for incorporation into the final system by

-1-
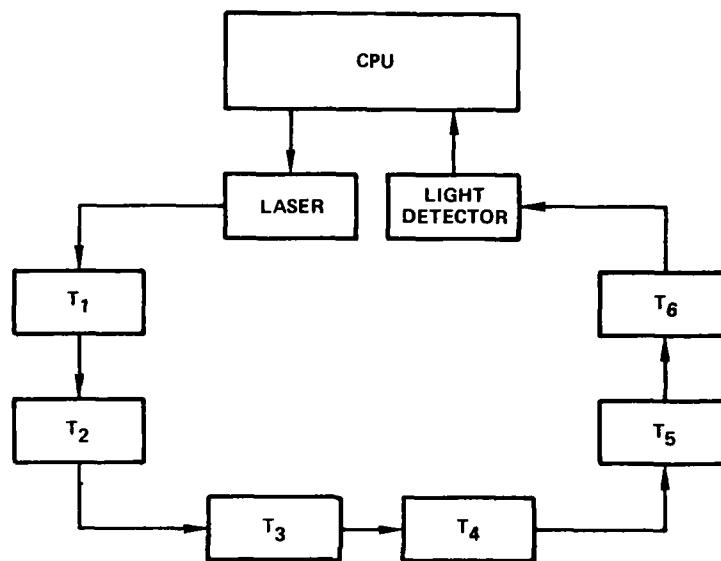
FIG. 1    Fail safe optical link structure.

virtue of the fact that its theoretical and actual performance was superior to the performance of the angle collimation terminal. An optical insertion loss of 5.7 dB was obtained for the best mirror terminal in the fail safe mode as compared with a 7.3 dB loss for the best angle collimation terminal. Although these two losses are comparable, the performance of the angle collimation terminal is at its theoretical maximum while, in theory, a 5-4 dB improvement in insertion loss using the mirror terminal should be possible. Also, the modulation depth achieved by the best angle collimation terminal was 38% for 100 volts applied, whereas the mirror terminal obtained a modulation depth of 51% with the same applied voltage.

Three mirror terminals were constructed and the two with the best performance characteristics were chosen for the final system. These mirror terminals were permanently butt coupled to fiber terminations. They were then tested and found to meet or approach the desired performance characteristics of this contract.

The feasibility of a serial fiber optic data bus system incorporating fail safe optical data link terminals was then demonstrated by the assembly and testing of a complete system which consisted of one master terminal and two remote send/receive fail safe terminals. The fail safe nature of the system was clearly shown by its continued operation in the absence of power at either one or both of the remote terminals.

The remaining sections of this report present in detail the progress which has been made. Section 2 discusses the general principles involved in the use of the multimode optical switching devices developed at the Sperry Research Center (SCRC). The electro-optic effect in thin crystals of $LiTaO_3$ is exploited by evaporating electrodes on opposite faces of the crystal so that, when voltage is applied, the induced change in the index of refraction directly between the electrodes creates a channel waveguide or switching elements and thus allows one to direct the flow of light within it. The input and output ends of the crystals are directly butt coupled to multimode fibers. Furthermore, if the fibers are butt coupled at non-normal incidence, it is possible to collimate the incoming light and

de-collimate the output, thereby allowing the use of optical fibers having relatively large numerical apertures.

The theory and development of the angle collimation terminal are discussed in Sec. 3. This type of device uses a non-normal incidence butt coupling of fibers to crystal to collimate the incoming light. The light is then guided and/or modulated via the electro-optic effect. The best insertion loss achieved with one of these devices in the fail safe mode was 7.3 dB. However, this result was only achieved once and repeatability could not be obtained. A more typical insertion loss would be in the neighborhood of 10 dB. This high insertion loss and difficulties in obtaining the optimum alignment of the fibers to be butt coupled at non-normal incidence contributed to the abandonment of this design for use in the final system.

In Sec. 4, the theory and development of the mirror terminal are discussed. The principle behind the mirror terminal concept is quite straightforward. The light from an input fiber is allowed to spread freely in the plane of the crystal, is reflected by a cylindrical mirror evaporated on the other end of the crystal and focused onto an output fiber. Voltage applied to appropriate electrode patterns evaporated on opposite faces of the crystal spoils the focus of the cylindrical mirror via the electro-optic effect and hence is used to modulate the bus throughput. The best insertion loss in the fail safe mode achieved with this design was 5.7 dB. This fact, together with its theoretical insertion loss of ~2 dB, caused the mirror terminal concept to be chosen for use in the final system. The principal difficulty in device fabrication and the major source of insertion loss seems to lie with the creation of the cylindrical mirror end of the crystal. Significant improvement in this area can be anticipated although the termination of the contract precluded the complete solution of this problem.

In Sec. 5, fiber/device coupling and packaging are discussed. In the coupling together of an electro-optic device and optical fibers, very close tolerances must be observed in order to keep the losses down to an acceptable level. For this reason, the methods used to couple the

-4-

electro-optic devices to optical fibers in a permanent fashion while maintaining close tolerances are discussed, as well as the final packaging techniques.

The components used in the prototype fail safe optical data link system are discussed in Sec. 6. Included are: the fiber-fiber connectors, the LED source, the source-fiber connector, the photodiode detectors, the mirror terminal, and the electronics associated with all of the above.

Section 7 details the complete results of tests run on the mirror terminals and on the complete serial fiber optic data bus system. No significant differences were noted between the performance of the packaged devices and their performance before packaging. The complete system was delivered to ETSD/RADC, while another system was constructed for further experimentation at SCRC.

Finally, a brief summation of the research is given in Sec. 8 along with suggestions for future improvements and research.

## 2. THEORY OF MULTIMODE OPTICAL DEVICES

The theory behind the multimode optical devices developed and used at SCRC has been detailed in the proposal for this contract and in the quarterly status reports QSR-1, -2 and -3. For purposes of completeness, the more important points are summarized here.

### 2.1 Electro-Optic Planar Waveguides

The basic electro-optic planar waveguide is a very simple structure, as shown in Fig. 2. In essence, it is a thin slab of a material whose index of refraction $n$ may be changed an amount $\Delta n$ by the application of an appropriate electric field (Pockel's effect). In the absence of any applied field, light entering one end of the guide parallel to the $\hat{y}$ direction is confined within it in the $\hat{z}$ direction due to the dielectric discontinuities in that direction, but free to spread in the $\hat{x}$ direction. At SCRC, the materials most commonly used are $LiTaO_3$ and $LiNbO_3$ due to their easy availability in pure form, their large electro-optic coefficient,

and excellent mechanical properties.

## 2.2  The Electro-Optic Effect

The electro-optic or Pockel effect states that a change in the index of refraction of a material may be caused by the application to it of a suitable electric field.  For c-cut crystals having the $LiTaO_3$ structure, and with an applied field $E_z$ along the c-axis, the required relationships are:

$$\Delta n_z = \tfrac{1}{2}n_z^3 \, r_{33} \, E_z \quad \text{(TM modes)} \tag{1}$$

and

$$\Delta n_x = \tfrac{1}{2}n_x^3 \, r_{13} \, E_z \quad \text{(TE modes)} \tag{2}$$

where the electro-optic coefficients $r_{33} = 30 \times 10^{-12}$ m/V and $r_{13} = 7 \times 10^{-12}$ m/V are relevant for TM and TE modes, respectively, in $LiTaO_3$.

## 2.3  Light Guiding via the Electro-Optic Effect

For a typical multimode fiber, the fiber cone of light will spread geometrically by $\pm\theta_m$ in a crystal of $LiTaO_3$ if the fiber end is butt coupled to a polished $\hat{x}$ or $\hat{y}$ face of the crystal, where $\theta_m$ depends upon the numerical aperture of the fiber.  By carrying out an analysis using Snell's law at grazing angles of incidence, it can be shown that the index change $\Delta n$ required to contain light of a maximum angle $\theta_m$ is given by

$$\Delta n = \frac{\theta_m^2 n}{2} \quad . \tag{3}$$

Two distinct methods of light guiding are possible using the electro-optic effect.  The first involves the use of a guiding electrode as shown in Fig. 3.  When a voltage of the proper polarity and magnitude is

-6-
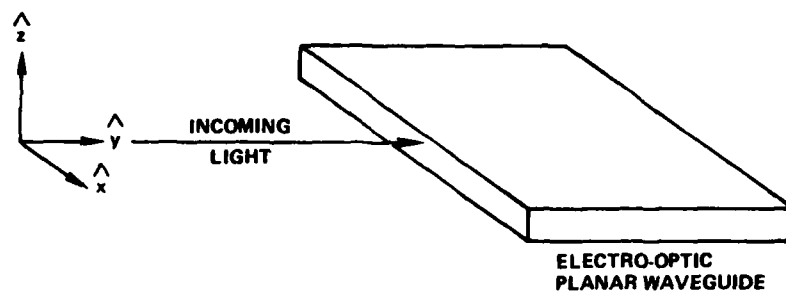
FIG. 2    Typical electro-optic waveguide slab.
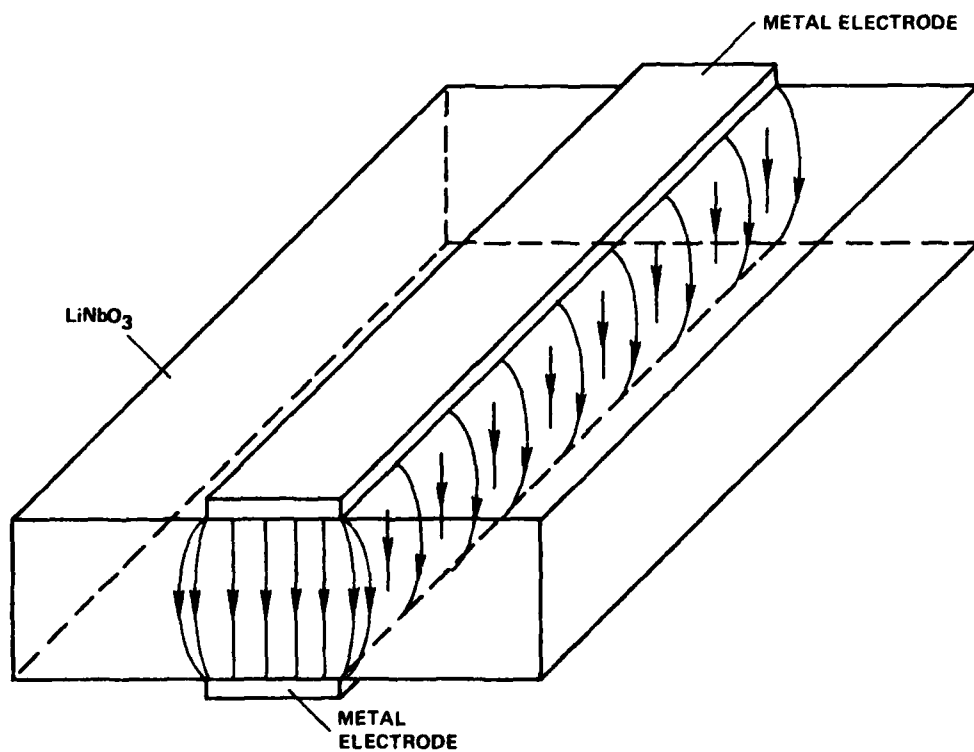


FIG. 3    Basic electro-optic guide structure.

applied to the strip electrodes, the index of refraction is increased in the crystal region between the electrodes by an amount $\Delta n$, so that, as indicated by Eq. (3), light making an angle of $\theta_m$ or less with the channel walls will be guided. The second method involves the use of two anti-guiding strip electrodes as shown in Fig. 4. In this case, the index of refraction is decreased an amount $\Delta n$ in the regions between the electrodes, so that light will be confined to the non-electrode channel of relatively higher index. The advantage of this second method is that the guided light will neither experience reflection losses from being incident upon the electrodes nor will it travel through the high field regions, thereby removing the possibility of optical damage due to photoelectric effects.

## 2.4  Polarization Effects

As shown in Eqs. (1) and (2) of Sec. 2.2, the electro-optic effect implies that TM-polarized light sees a different change of index than does TE-polarized light for a given applied field due to the 4-fold difference in the electro-optic coefficients $r_{33}$ and $r_{13}$. However, since the critical angle for total reflection $\theta_m$ depends on the square root of the induced index change, the difference in the magnitude of the electro-optic coefficients implies that a given applied field along the c-axis guides TM modes about twice as efficiently as TE modes.

## 2.5  Sources of Loss

There exist three readily apparent sources of loss in the use of electro-optic planar waveguides. The first is due to mismatches between the input and/or output cross-sectional areas and the crystal input and/or output areas. The second is due to reflection and scattering at the fiber/crystal interfaces. Finally, the third is due to the fact that the angular spread of light within the crystal might be greater than can be guided via the electro-optic effect.

The problem of minimizing the three sources of loss discussed above was carefully addressed during consideration of the angle collimation terminal, which is analyzed in detail in the next section.
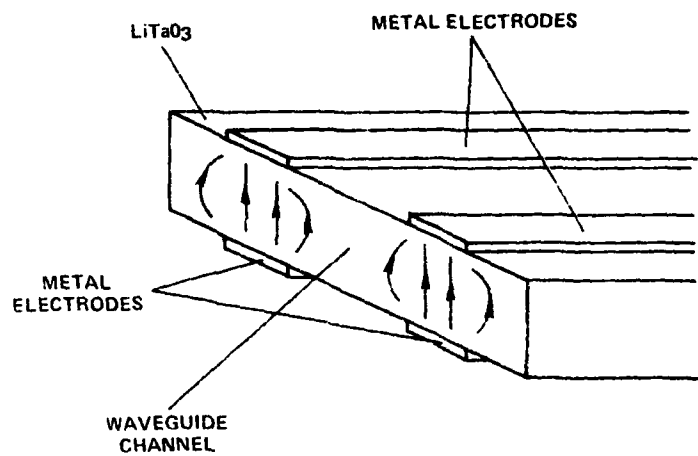
FIG. 4    Electro-optic guide with antiguiding electrodes.

## 3. THE ANGLE COLLIMATION TERMINAL

In the development of a send/receive terminal to be compatible with the fail safe concept, the logical first step is to attempt to use an electro-optic planar waveguide with a single strip electrode to guide and/or modulate the light. An example of such a device is shown in Fig. 5. It consists of a thin crystal of $LiTaO_3$ or $LiNbO_3$ which has an appropriate Cr/Au strip electrode evaporated on each side. Multimode fibers are butt coupled to the input and output ends of the device. Voltage of the correct polarity applied to the electrodes guides the input light to the but output fiber, while voltage of the opposite polarity (i.e., anti-guiding) deflects the input light away from the bus output fiber and thereby allows the device to modulate the bus throughput. In order for this device to function as a fail safe terminal, enough light must reach the output fiber in the absence of voltage applied to the electrode waveguides to insure a large bus throughput. To maximize this throughput, the light in the crystal should have the smallest possible angular spread, so that the loss due to the spreading of the unguided light beyond the cross-sectional area inter-cepted by the butt coupled output fiber is minimized. A minimum angular spread also allows for more efficient guiding and/or modulating of the bus throughput in that the percentage of light exceeding the critical angle for electro-optic guiding can be greatly reduced. This leads to a consideration of the idea of angular collimation.

### 3.1 The Angle Collimation Concept

A typical multimode fiber having a numerical aperture of .15 has an angular spread in air of $\sim \pm 8^{\circ}$. If this fiber is butt coupled at normal incidence to a platelet of $LiTaO_3$, the angular spread in the crystal is reduced to $\sim \pm 3.7^{\circ}$ due to the high index of refraction (n=2.2) of this material. However, in order to guide TM modes using a single strip elec-trode on a 3 mil crystal of $LiTaO_3$, a voltage of 2400 V across the 3 mils is required. This voltage is higher than the breakdown voltage of the crystal. The required voltage can be reduced by a factor of two by using a triple stripe structure in which a voltage is applied to two electrode

strips parallel and adjacent to the main waveguide channel. *This voltage
is opposite in polarity to that applied to the central electrode,* so that
the net index difference between the main waveguide channel and the
adjacent channels is $2\Delta n$. However, the voltages required are still too
high to be practical.

In order to further reduce the necessary operating voltage, it is
necessary to further collimate the light within the crystal. This can be
accomplished by butt coupling the fiber to the crystal at a non-normal
incidence angle. The collimation effect follows directly from Snell's law
which states that light rays incident at a larger angle are bent more
towards the normal than those rays incident at a smaller angle. It can
therefore be shown that a cone of light incident at $66^{o}$ is collimated by
a factor of two, three-fold collimation requires an incident angle of $75^{o}$,
etc. The angle collimation factor vs incident light angle is shown in
Fig. 6. The ability to collimate the light within the crystal is extremely
important due to the quadratic dependence of the total internal reflection
angle $\theta_m$ on the induced change in the index of refraction, given by Eq. (3),
i.e.,

$$\theta_m = \sqrt{\frac{2\Delta m}{n}} \quad .$$

Therefore, if the spreading angle is reduced by a factor of two, the index
change required to contain the light is reduced by a factor of four. It is
evident, then, that angle collimation allows the voltage requirements for
light guiding and modulation to be reduced substantially.

3.2 Device Design and Construction

All of the electro-optic devices discussed in this report follow
the same basic fabrication procedure in which they have electrode patterns
evaporated onto both sides and are permanently bonded in a glass sandwich.
A brief summary of this procedure is described below.

The crystals of $LiTaO_3$ to be used for electro-optic devices were

-11-

3 MIL CRYSTAL OF LiNbO$_3$
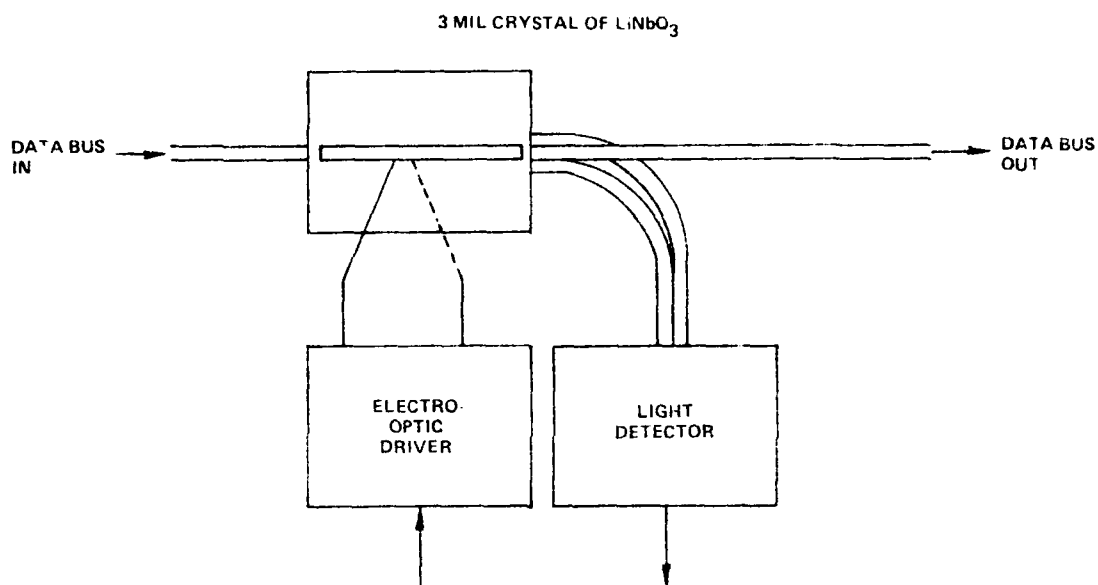


FIG. 5    Fail safe data terminal structure.
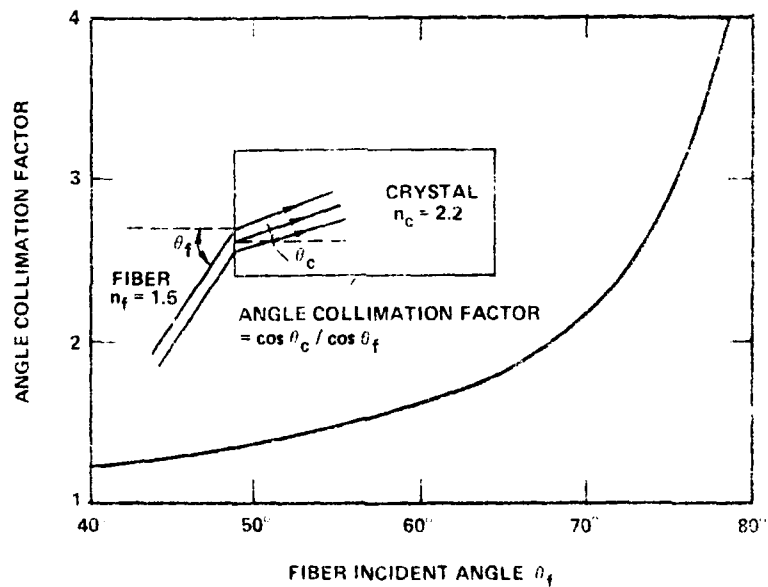


FIG. 6    Angle collimation factor vs incident light angle for LiTaO$_3$.

obtained from Crystal Technology, Inc. A typical size for the crystal wafer is 1" × ½" × .003". It was specified as selected acoustic grade crystal with an inspection polish on both faces, and was delivered bonded to a piece of glass with glycolphthalate for support. This backing material was used throughout the fabrication process to minimize the change of damaging the very thin crystal wafer.

To prepare the crystal for fabrication, the exposed side of the crystal wafer is first cleaned. Then, the desired metal electrode pattern is created on the crystal face using a photoresist lift-off technique. The crystal/glass structure is then heated to ~$100^{o}$C to melt the glycolpthalate, the crystal is turned over, and the device is allowed to cool so that the crystal is again bonded to the glass. The newly exposed surface is then cleaned, and the appropriate electrode pattern is laid down directly opposite the first. The electrode patterns are formed by first using a 10 Å flash of Cr for adhesion and following that with a 1000-3000 Å layer of Au.

Once the electrode patterns have been formed on the crystal wafer, the crystal/glass structure is again heated to ~$100^{o}$C and the crystal is transferred to a piece of glass cut to allow access to the pad electrodes. A second similarly cut glass plate is then bonded on top of the crystal and the whole glass/crystal/glass sandwich is allowed to cool. The glass/ crystal/glass sandwich is then placed in a diamond saw, and the edges are cut at the proper angle relative to the electrode pattern. The edges are then polished down beginning with a 600 grit paper and continuing down to a syton polishing medium. This process yields an excellent surface polish. For the last step in the process, electrodes are attached with conductive epoxy to the crystal electrode pads, and the device is ready for testing.

In designing the devices to be actually constructed, it was decided for the reasons discussed in the previous section to use the triple stripe geometry for the electrode and to use either 3-fold or 4-fold collimation when butt coupling the fibers to the crystal. The angle col- limation technique allowed the spreading loss in the fail safe mode to be

reduced to an acceptable level. However, other sources of loss had to be considered.

One important source of loss is the mismatch between the input/output areas of the crystal and the cross-sectional fiber areas butted against them. In Table 1, the relative input and output efficiencies for normal incidence fibers of 85 μm diameter butted against varying thicknesses of crystal are listed. As can be seen, there is very little difference in total coupling efficiency for thicknesses ranging from 75% to 100% of the fiber core diameter. However, an unavoidable insertion loss of ~1 dB occurs from the mismatch, even under optimum conditions.

The other principal source of loss comes from reflection and scattering at the fiber/crystal interface. For a device requiring a four-fold collimation, the angle between the fiber and the crystal input/output surfaces is $79.2^0$. For this geometry and a c-cut crystal, it is possible to calculate the reflection losses at each interface for TM and TE modes by applying the Fresnel formulae:

$$T_{TE} = 4\frac{n_c}{n_f}\frac{\cos\theta'}{\cos\theta}\left[\frac{n_c}{n_f} + \frac{\cos\theta'}{\cos\theta}\right]^{-2} \tag{4}$$

and

$$T_{TM} = 4\frac{n_c}{n_f}\frac{\cos\theta'}{\cos\theta}\left[1 + \frac{n_c}{n_f}\frac{\cos\theta'}{\cos\theta}\right]^{-2} \tag{5}$$

where $n_c$ is the index of refraction of the crystal, $n_f$ the index of refraction of the fiber core, $\theta$ the angle between the fiber and the surface normal ($79.2^0$) and $\theta'$ obtained from Snell's law ($n_c \sin\theta' = n_f \sin\theta$). $T_{TE}$ and $T_{TM}$ then represent the fractional transmitted power of TE and TM polarized light. If $n_f = 1.47$, $n_c = 2.17$ for LiTaO$_3$ and $\theta = 79.2^0$, it is found that $T_{TE} = .79$ and $T_{TM} = .49$. This imples that the total loss from reflections at both interfaces totals 3.6 dB, which represents an

-14-

# TABLE 1

## Fiber/Device/Fiber Coupling Efficiency as a Function of Device Thickness

| Crystal Thickness ($\mu$m) | Relative Input Coupling Efficiency | Relative Output Coupling Efficiency | Total Coupling Efficiency |
|---|---|---|---|
| 85 | 1 | .79 | .79 |
| 80 | .98 | .82 | .80 |
| 75 | .95 | .85 | .81 |
| 70 | .91 | .87 | .79 |
| 65 | .97 | .89 | .77 |
| 60 | .82 | .91 | .75 |
| 55 | .76 | .93 | .71 |
| 50 | .70 | .94 | .66 |

Input Efficiency $= 1 - \dfrac{2}{\pi}\left(\arccos(t/d) - \dfrac{t}{d}\sin(\arccos(t/d))\right)$

Output Efficiency $= 1/2 \sin(\arccos(t/d)) + \dfrac{\pi d}{4t} - \dfrac{d}{2t}\arccos(t/d)$

$t =$ crystal thickness        $d =$ fiber core diam $= 85\ \mu$m

unacceptable figure. The problem is compounded by the fact that the TM modes, which are the most easily guided by the electro-optic effect, are the ones which suffer the greater reflection loss. However, it has been found[1] that, by the use of anti-reflection coatings, the total loss can be reduced to .5 dB, which represents a much more reasonable figure.

Several angle collimation terminals have been constructed and tested.[2] These all used a Cr/Au triple stripe electrode pattern evaporated on both sides of the crystal. The fibers used were Corning low loss fibers with a numerical aperture of .15 and a core diameter of 85 $\mu$m. The optical insertion loss in the fail safe mode was found as a function of length and collimation from a computer program previously developed. In this program, a number of input parameters are used to determine the output light intensity as a function of position at the output edge of the crystal. These parameters are: fiber core index, fiber numerical aperture, fiber core size, crystal index, crystal thickness, crystal length, degree of collimation, refractive index of matching fluid between fiber and crystal, and light polarization. Furthermore, the fiber geometry is taken into account as well as the variability of reflection losses, the degree of collimation over the full cone angle of the input fiber, and the finite width of the fiber. A sample output is shown in Fig. 7, for fiber NA= .16, 4-fold collimation, core diameter = 13.6 mils, total length = .5". The relative throughput may be found by computing the total power under the curve in a 13.6 mil length and dividing this figure by the total input power. The computer program therefore provides a theoretical best case insertion loss for the fail safe mode.

The most successful angle collimation device tested, designated LT-10, was 2.8 cm long, used three-fold collimation, had a thickness of 90 $\mu$m, and was designed to be used with fibers of a .15 numerical aperture. The theoretical loss due to light spreading the crystal in the fail safe mode was determined using the computer program described above. This loss was found to be ~5.0 dB for TE light and ~5.4 for TM light. The total reflection loss was calculated to be 2.1 dB for TE modes and 6.2 dB for

-16-

TM modes. However, with an anti-reflection fluid with index of $n = 1.62$ inserted between the fiber and the crystal, it was calculated that the reflection loss would be minimized. In fact, the loss becomes .64 dB for TE modes and 2.4 dB for TM modes. The third major loss is due to the mismatch between the input/output areas of the crystal and, since the fiber core diameter was 85 μm, was calculated to be 1.2 dB. All of these effects combine to produce a theoretical minimum loss of ~7.8 dB. In addition, there might be other minor sources of loss due to imperfections in device construction, but these are estimated to contribute .5 dB or less to the total insertion loss.

The determination of theoretical losses for the device discussed above in the active mode, i.e., with a non-zero voltage applied to the electrodes, presents a much more difficult problem than the calculations for the fail safe case. The major difficulty is contained in the necessity to know the strength and spatial distribution of the fringing electric fields in the bulk material away from the electrode edges, and then to perform a complicated ray tracing for a two-dimensional system without circular symmetry. However, a simplified calculation considering only ray motion in the plane of the crystal has been carried out for crystals using normal incidence butt coupling. This calculation indicates that the intensity distribution shown in Fig. 8 provides a good approximation to the actual situation. Triple stripe electrodes as shown in Fig. 9 were used on the device where the width W of the central stripe is the fiber core diameter times the collimation factor, or 225 μm. The guard channel electrodes are separated from the central electrode by one crystal thickness t to prevent electrical breakdown. It is theoretically possible to completely channel TM modes with this device with an applied voltage of 100 volts, but 50% of the TE modes will be lost due to the difference between the electro-optic coefficients $r_{33}$ and $r_{13}$.

From the analysis above, it is possible to obtain an expression representing the ratio of the light guided beneath the central electrode to the total amount of light guided by the central electrode plus the fringing
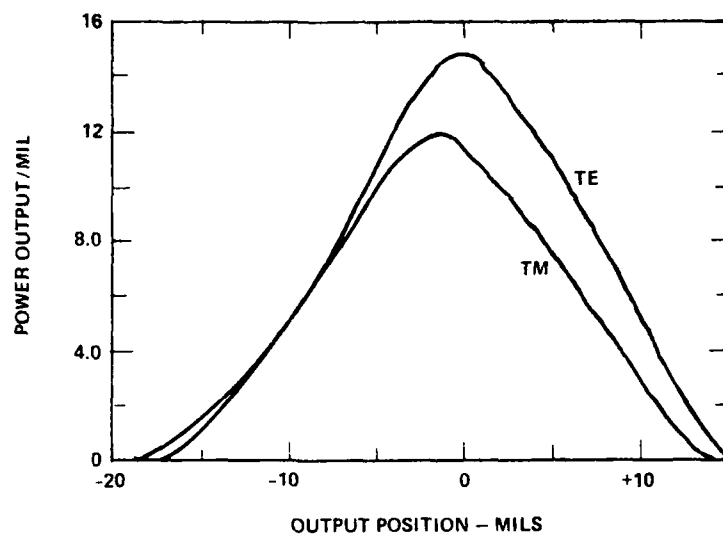
-17-

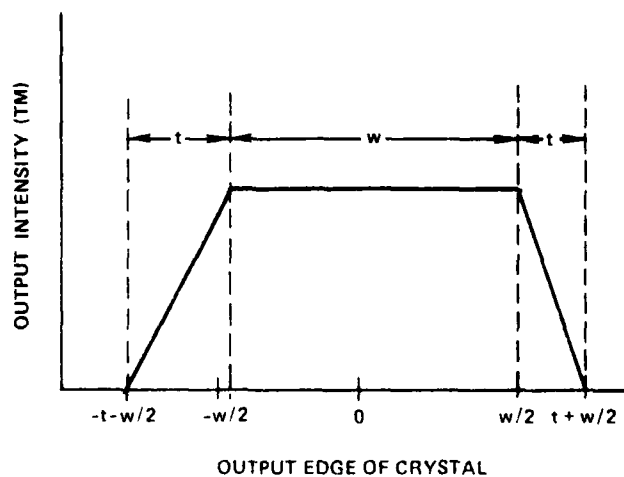FIG. 7    Power output at end of .5 inch crystal for NA = .16 input.



FIG. 8    Approximate output intensity distribution with applied
voltage.  w = width of center electrode and t = thickness
of crystal.

-18-

fields. This yields the loss at the output fiber due to the fringing fields, and is equal to 1.3 dB for TM modes and 1.3 dB + 3 dB = 4.3 dB for TE modes at V ≃ 100 volts. In addition, there are the same reflection and size mismatch losses as in the fail safe case, so that the total theoretical losses are ~5.5 dB for a bias voltage of 100 volts. It is also possible to carry out the same analysis to obtain the total insertion loss as a function of voltage, merely by assuming the same profile for the output intensity as shown in Fig. 8. In fact, this was done for the device under discussion and the results will be presented in the next section.

## 3.3 Experimental Results

The preceding section provided an analysis of theoretical total insertion loss for angle collimation device LT-10. In Fig. 10, the total insertion loss, both experimental and theoretical, is presented as a function of voltage. As can be seen, the experimental and theoretical curves differ by less than ~.5 dB over the voltage range -100 volts to +200 volts. This agreement indicates both that the approximations involved in the calculation of the fringing field loss were justified, and that the performance of LT-10 is at its theoretical limit; i.e., a total insertion loss of no better than 7.3 dB can be obtained for the fail safe mode. In addition, the modulation depth obtained was only 32% for a bias of 100 volts.

## 3.4 The Status of Angle Collimation Terminals

The device discussed in the preceding section, LT-10, displayed the best performance characteristics of any of the angle collimation terminals which were constructed. As has previously been reported (see QSR-1, QSR-2, and QSR-3, which are attached to the present report as appendices), others have been constructed: one with two-fold collimation, one with three-fold collimation, and one with four-fold collimation. The four-fold collimation and the other three-fold collimation device both exhibited losses 3 dB greater than the theoretical prediction. It has been found that there is considerable alignment difficulty involved in the construction of the angle collimation devices. The proper positioning of each fiber relative to the device requires a simultaneous optimization of three
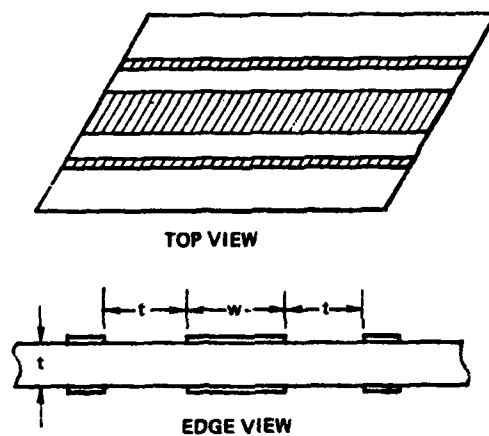
-19-

**FIG. 9** Triple stripe electrode geometry used for LT-10.
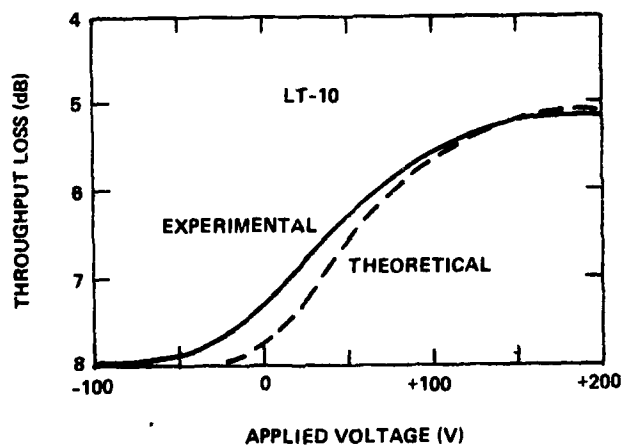


**FIG. 10** Theoretical and experimental throughput loss vs voltage for LT-10.

coordinate positions and three angular degrees of freedom. This is very
difficult to achieve and the required tolerances to be maintained are even
closer and more critical than for normal incidence butt coupling. It is
probable, therefore, that most of the loss greater than the theoretical
estimates is due to misalignment of crystal and fiber. However, alignment
difficulties encountered do not make the angle collimation terminal an
attractive prospect for the production of any significant number of devices.
Since minimum insertion loss of the fail safe mode is not predicted to be
less than the 7.3 dB loss attained by LT-10, other lower loss concepts had
to be devised. The most promising of these, and the one in fact chosen for
incorporation into the final system, was the mirror terminal concept. This
is discussed in detail in the next section.

## 4. THE MIRROR TERMINAL

The problems encountered in the attempt to make the angle col-
limation terminal compatible with the fail safe concept were believed
to be due largely to the extreme sensitivity of the angle collimation
terminal to misalignments in the non-normal-incidence fiber/crystal coupling.
For that reason, a way was again sought to incorporate normal incidence
coupling into a fail safe data terminal. The resulting device, the mirror
terminal, is described below.

### 4.1 The Mirror Terminal Concept

The mirror terminal concept is based upon the fact that, for a
cylindrical mirror, the plane perpendicular to the optic axis of the mirror
and passing through its center of curvature represents the focal plane for
1-to-1 imaging. The mirror terminal illustrated in Fig. 11 makes use of
this passive focusing property. Figure 11 shows schematically a top view
of the mirror terminal structure (x-y plane) with an imput and an output
fiber. The thickness of the crystal plate (along the $\hat{z}$ axis) is chosen to
be compatible with the fiber core diameter. The light inserted into the
terminal has a non-zero $\hat{z}$ component and makes multiple bounces in the
vertical plane (not shown). The cylindrical mirror, however, affects the

-21-

propagation direction only in the x-y plane as shown. The useful property of the mirror in this case is that any extended object in the 1-to-1 plane a distance d from the center of curvature will form an image of the same size a distance d on the other side of c. Therefore, the bus fibers are positioned symmetrically about the center of curvature. This allows almost all of the divergent light from one fiber to be collected by the other. The focusing action works equally well for TM and TE modes, and does not depend on the fiber numerical aperture.

Modulation by the mirror terminal is accomplished by spoiling the focus of the cylindrical mirror via the electro-optic effect as is discussed in the next section. Also, the terminal is an active multimode directional coupler, i.e., a tap-off device, with several options available as to where the tapoff occurs. The device is capable of very fast switching and its operation is independent of wavelength in the visible and near infrared regions of the spectrum. The most important features of the terminal, as discussed below, are its fail safe transmission and its low optical insertion loss.

The specifics of mirror terminal design and construction are discussed in the next section.

## 4.2  Device Design and Construction

A perspective drawing of the active portion of a typical device is shown in Fig. 12. The basic fabrication process is identical in most respects to that of the angle collimation terminal; i.e., the electro-optic material is $\hat{z}$-cut single crystal $LiTaO_3$ sandwiched between protective glass plates and bonded with an insulating cement, which serves to trap light strongly in the $\hat{z}$-direction. The electrode patterns were formed on the crystal surfaces using the same photolithographic technique as for the angle collimation terminals and consisted of a flash of chromium followed by a 3000 Å deposition of gold.

The input end of the crystal, i.e., the planar surface where the fibers are to be butt coupled at normal incidence, is ground and

-22-

FOCAL
PLANE
FOR 1:1
IMAGING

CIRCULAR
MIRROR

INPUT FIBER

OPTIC AXIS

C

V

OUTPUT FIBER

IN/OUT
PLANE

Z ○——→ X

Y

FIG. 11   Optical ray paths within terminal.



MODULATION
VOLTAGE
(DATA IN)

CONTROL
ELECTRODE

METALIZATION
FOR CYLINDER
MIRROR

$LiTaO_3$
CRYSTAL

FIBER
INPUT
(DATA BUS)

FIBER
OUTPUT
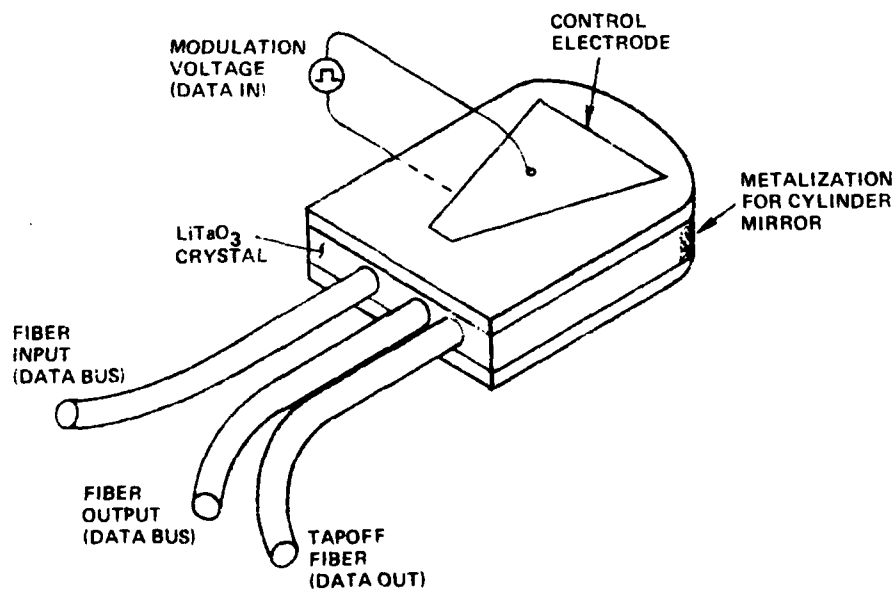(DATA BUS)

TAPOFF
FIBER
(DATA OUT)
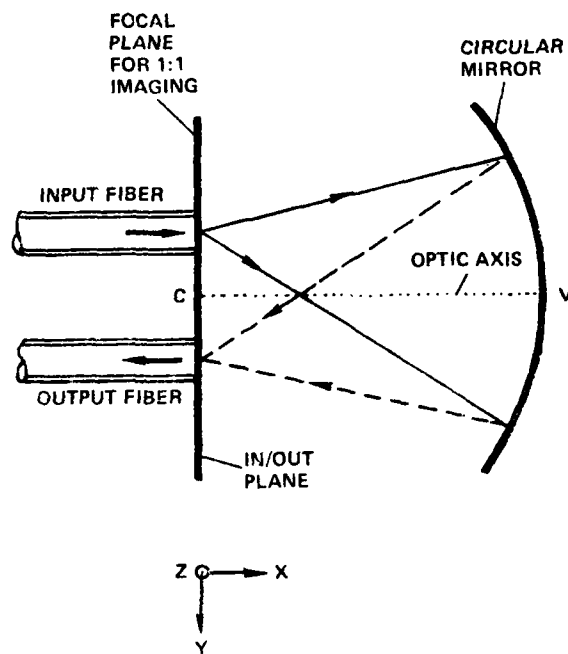
FIG. 12   Perspective view of fail safe mirror terminal.

-23-

polished flat. The other end of the crystal is then formed into the shape of a cylindrical mirror whose radius of curvature lies along the axis of the previously formed electrodes and extends to the center of the input end of the crystal. This is done using special polishing equipment developed at Sperry. A metallic coating consisting again of a flash of chromium and a 3000 Å deposition of gold is then evaporated onto the cylindrically shaped end of the crystal to make it totally reflecting.

The fibers which are to be butt coupled to the mirror terminal consist of a bus input, a bus output, and a local tapoff. The tap-off fiber can be located at any one of three positions: adjacent to the output fiber off-axis as in Fig. 12, between the bus fibers, on the optic axis, or on the optic axis at a small opening in the mirror film. In the last case, a circular area of the mirror surface may either have a fiber or a photo-diode detector butt coupled against the mirror terminal at that point and, since the amount of light which is tapped off is not greatly affected by the modulation voltage, this tap is virtually voltage independent. The other two possible positions for the tap-off fiber are definitely voltage depend-ent. It is expected that the optical intensity in the tap fiber will have its lowest value in the fail safe mode and its largest value in the active mode. The voltage dependent tap can then be used for multimode optical switching or multiplexing, if necessary.

The modulation function of the mirror terminal is accomplished through the use of spoiler electrodes. These function by diverting or deflecting the light rays from the paths which they follow in the fail safe mode. This defocusing increases the insertion loss and thereby allows modulation. The defocusing occurs for either the guiding or anti-guiding polarity of voltage applied to the electrodes. As was stated in the section on the angle collimation terminal, the TM modes are perturbed four times as much as the TE modes due to the anisotropy of the electro-optic effect in $LiTaO_3$. The estimated response of a mirror terminal to applied voltage is shown in Fig. 13, which displays the fraction of input optical power reach-ing the bus output and the tap-off fibers as a function of voltage. This

-24-

result is obtained for the tap-off fiber adjacent to the bus output fiber and displays the fail safe nature of the terminal; i.e., maximum bus throughput occurs when there is zero applied voltage.

## 4.3 Theoretical Insertion Losses

The major theoretical optical losses in the mirror terminal concept come from several distinct sources: mirror loss, fiber/crystal input/output area mismatches, and reflection losses between fiber and crystal. These losses combine, as will be seen below, to yield a total theoretical insertion loss figure significantly better than that obtained for the angle collimation terminal.

The first loss to be considered is that due to the mirror coating. If one assumes incident light with a wavelength of 6300 Å, the reflection losses for various commonly used mirror coatings are as follows: chromium, 7.5 dB loss; aluminum, .97 dB loss; copper, .34 dB loss; gold, .36 dB loss. Because of its resistance to oxidation, it was decided to use gold as the mirror coating for the mirror terminals.

The second source of optical loss is distortion of the shape of the focal spot. This is due to the fact that the cylindrical mirror focuses light in only the x-y plane and not in the $\hat{z}$ direction. If a laser is focused into a point on the input surface, the output image is a sharp line. Similarly, the circular input from an optical fiber images as a rectangle. These two situations are shown in Fig. 14. Since the output fiber has the same diameter as the input fiber, some fraction of the output light will not be intercepted by the output fiber. Similar losses can occur due to a mismatch between the input fiber and the input surface. As has been shown in Table 1, the total loss due to area mismatches between the fiber and crystal input/output surfaces remains close to 1 dB for crystal thicknesses ranging from 75% to 100% of the fiber core diameter.

Reflection losses at the fiber/crystal interface comprise the third contribution to the total theoretical insertion loss. These have been previously discussed in Sec. 3.2. Here, because normal incidence
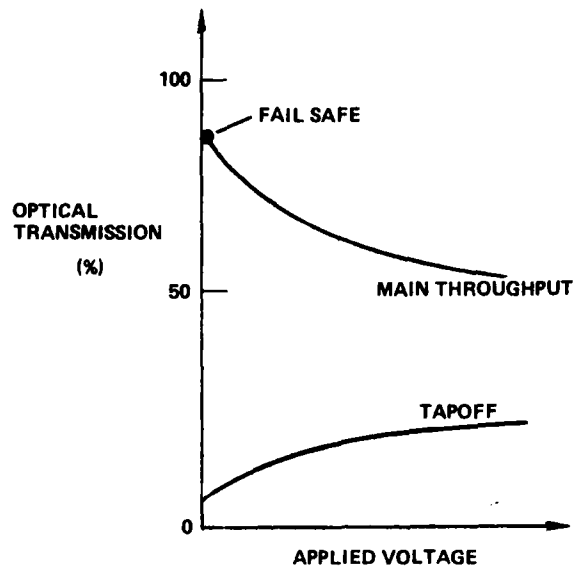
-25-

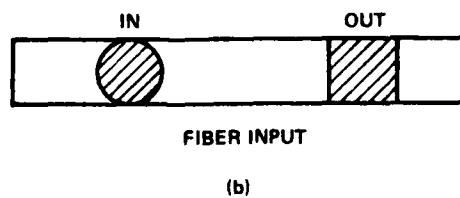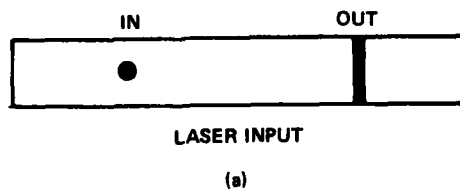FIG. 13   Anticipated effect of modulation voltage.



FIG. 14   End view of mirror terminal showing incident and
emergent optical beam shapes.

coupling is used, these losses can be kept below .3 dB by the insertion of an anti-reflection fluid between the fiber and the crystal.

The three loss components discussed above are held to be irreducible; i.e., they follow directly from the design of the mirror terminal and hence are unavoidable. These are seen to total 1.7 dB

A reducible loss component occurs due to the finite numerical aperture of the fibers used. The problem is displayed in Fig. 15. As can be seen, the light from the input fiber is reflected into the output fiber at too large an angle for all of the light to be captured and some of it will therefore be lost. This loss has been estimated for a fiber with an 88 $\mu$m core and numerical aperture .15 being used in conjunction with a device of thickness 85 $\mu$m and radius R = 1". The results, displayed in Table 2, indicate that, for a small separation between the fibers (d < 15 mils), the loss amounts to less than .5 dB. The loss could be reduced or eliminated by butt coupling the output fiber at an angle, although this was not done for the present system. Also, there are other reducible losses, due to improper device fabrication, i.e., poor quality of the mirror surface, chipping, poor quality of the input/output surface, improper focus, improper alignment of the input/output surface relative to the electrode pattern and/or the cylindrical mirror end. A more detailed discussion of these losses and ways to minimize them may be found in QSR-3 (Appendix C). As stated in QSR-3, these losses can probably be reduced below 1 dB. In addition, there are small propagation losses from the scattering of the beam off the electrode pattern, but these are held to be insignificant.

In summary, a mirror terminal having an optical insertion loss in the fail safe mode in the range 2 to 3 dB appears feasible.

4.4 Experimental Results

Several devices have been fabricated using LiTaO$_3$ $\hat{z}$-cut crystals of either 3.5 mil or 9 mil thickness. Typical examples of these two devices are shown in Figs. 16 and 17. They differ only in thickness and shape of electrode pattern. These spoiler electrode patterns were created with

**TABLE 2**

Throughput Loss Due to Center-to-Center Separation D
Between Input and Output Fibers

| D(mils) | Loss(%) |
|---------|---------|
| 5 | 3.3 |
| 10 | 6.7 |
| 15 | 10.0 |
| 20 | 13.0 |
| 30 | 20.0 |

$$\text{Loss} = D/W$$

$$W = \left(\frac{2 \times N.A.}{n_{LT}}\right) \times R \sim N.A. \times R$$
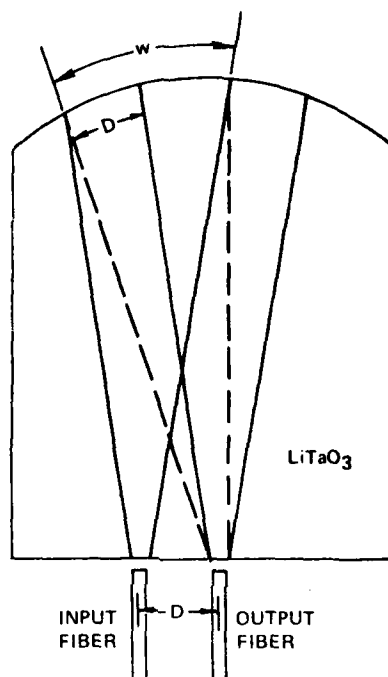
$$N.A. = .15 \qquad R = 1"$$

FIG. 15    Throughput loss due to finite numerical aperture of
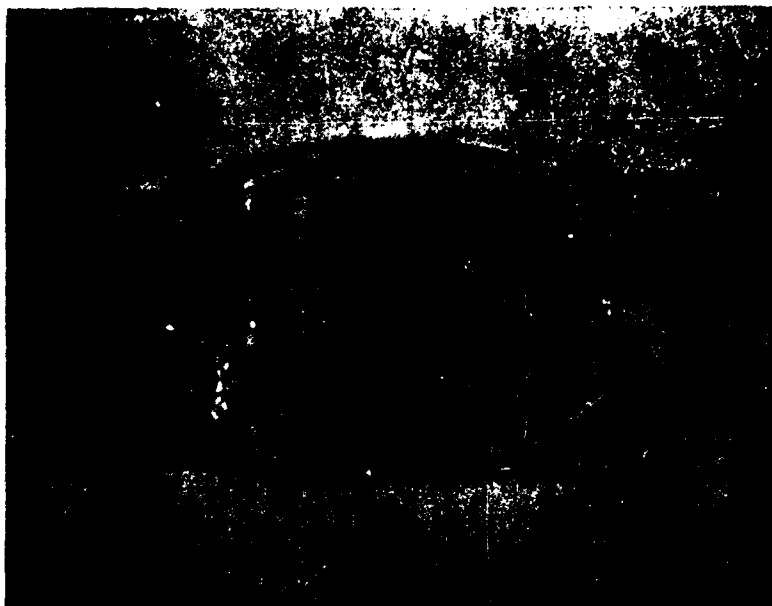output fiber.

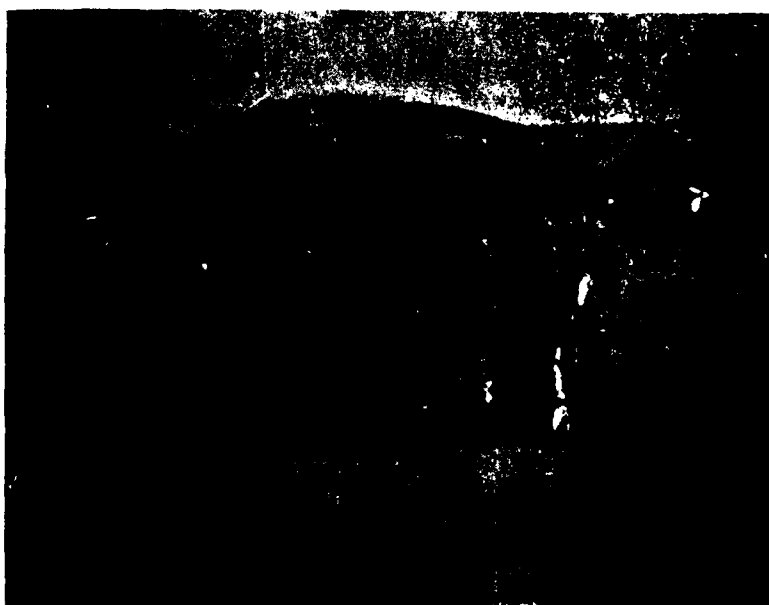FIG. 16   Mirror terminal using 3.5 mil crystal.



FIG. 17   Mirror terminal using 9 mil crystal.

the aid of a computer. Figures 18 and 19 show the patterns used for the 3.5 mil and 9 mil crystals, respectively, with all dimensions in mm. These are radial vanes directed toward the center of curvature. In the thicker crystal, there is wider lateral fringing of the electric field between the electrodes, and therefore a greater spacing between them is required than is necessary for the 3.5 mil crystal.

For the two thicknesses of device constructed, the 3.5 mil crystal was designed to be compatible with Corning low loss fiber with a core diameter of 3.3 mils, while the 9 mil crystal was designed for use with 10 mil core Valtek fiber. For that reason, two multifiber terminations were constructed for insertion loss testing using the two different types of fiber. Figure 20 shows the experimental layout used for testing the mirror terminals. A He-Ne laser in conjunction with focusing optics was used to provide an excitation cone of light to completely fill the numerical aperture of the fiber chosen as input. The amount of light in the input fiber was then carefully measured before the fiber termination was butted up against the mirror terminal input surface. The position of the fiber array was then adjusted to provide the optimum bus throughput in the absence of voltage. Finally, an indexing fluid was inserted between the fiber termination and the input edge of the crystal, and the voltage dependence of the bus throughput and the tapoff were measured. This allowed the insertion loss and the modulation depth to be determined as a function of voltage.

For the fail safe or no voltage condition, the minimum optical insertion loss obtained for a 9 mil device (MT-10) was 5.2 dB, while the best 3.5 mil device (MT-11) yielded a 5.7 dB loss. It is interesting to note that these are the lowest insertion losses measured for any multimode switching device constructed in our laboratory. It was hoped that the 9 mil device would yield a better loss figure than was actually obtained. The problems involved in the creation of the mirror end were anticipated to have much less of an effect upon the 9 mil device as opposed to the 3.5 mil device, though this is clearly not indicated by the results above, where the two insertion losses are nearly the same. The problem of whether excess
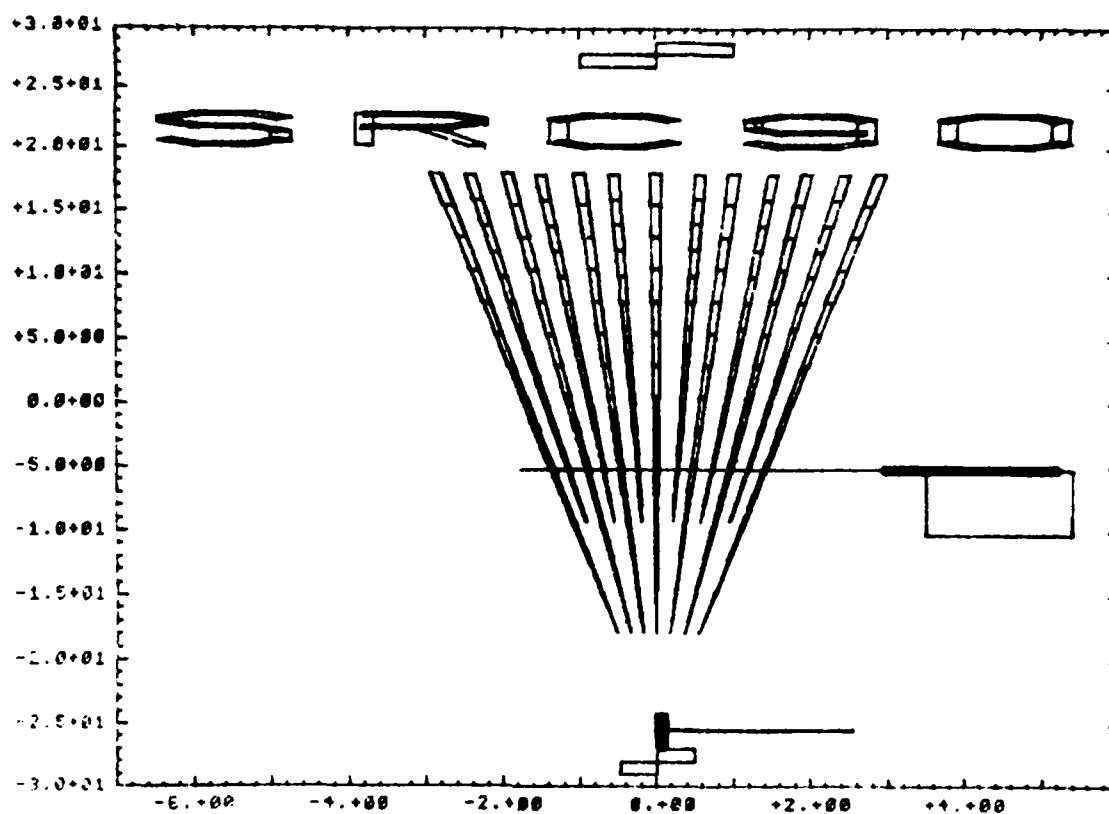
-31-

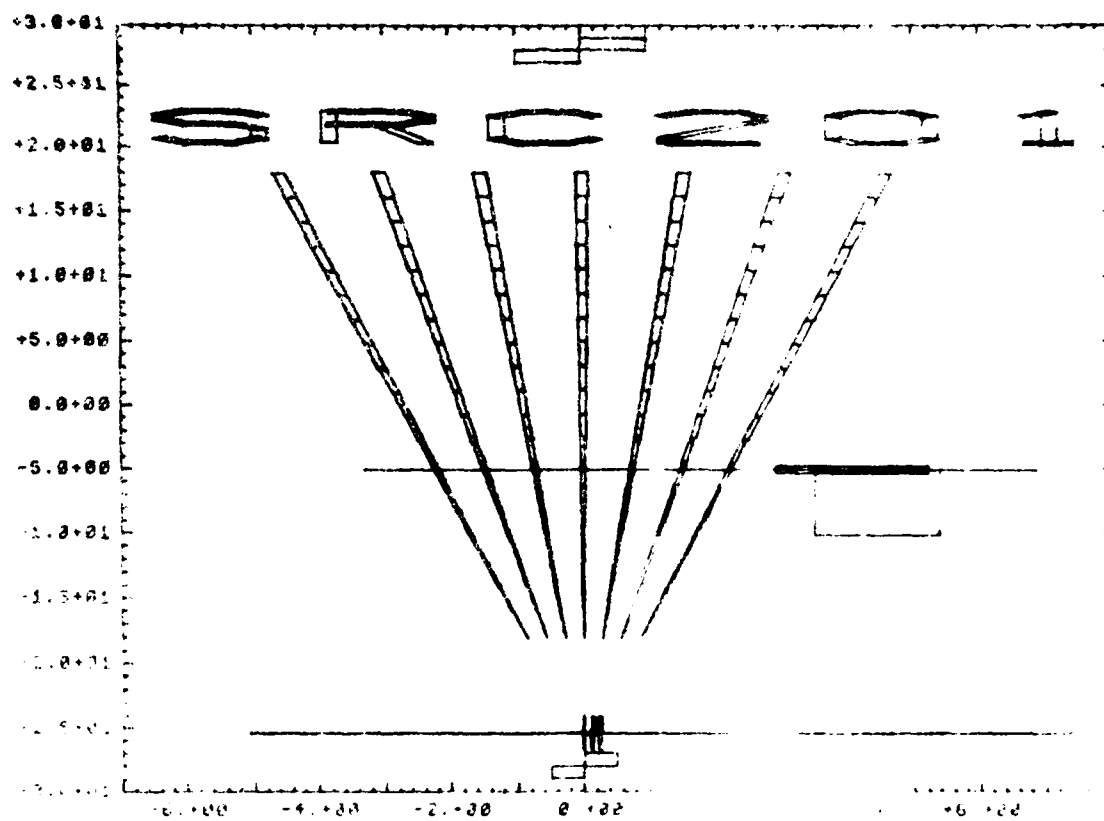FIG. 18    Electrode pattern for 3.5 mil crystal.

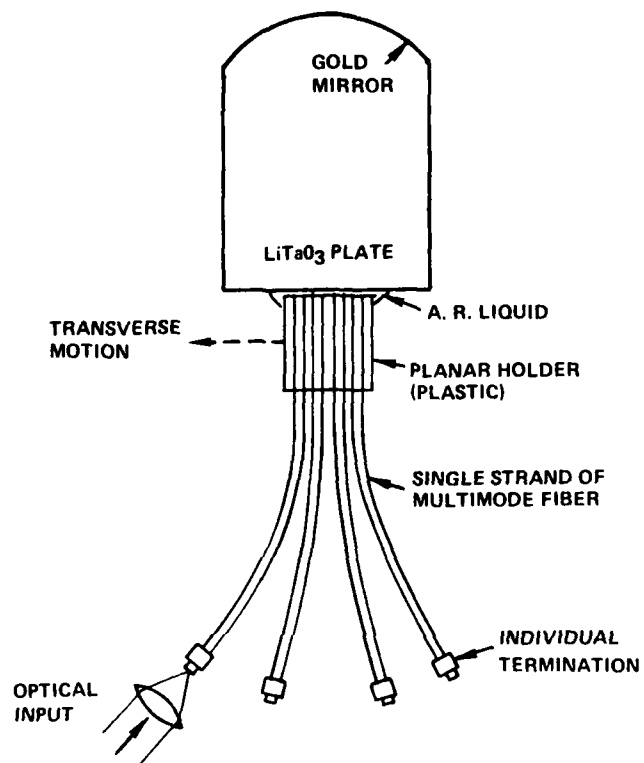FIG. 19   Electrode pattern for 9 mil crystal.

FIG. 20   Layout of the mirror terminal and multiple fiber coupling.

optical insertion loss is due to improper fabrication of the mirror end is unfortunately not resolved by this test. However, since the two insertion losses were comparable in magnitude, a final selection for which thickness of device to be used in the final system could not be based on the insertion loss figures alone. A clear choice is indicated, however, if the variation of modulation depth with voltage is considered for each device. As can be seen in Fig. 21, the modulation depth for a 3.5 mil device is roughly 10 times the modulation depth for a 9 mil device $\left(\frac{m_1}{m_2} \sim \left(\frac{t_2}{t_1}\right)^2\right)$. This means that a switching voltage of 50 volts applied to the 3.5 mil device produces approximately the same effect as a switching voltage of 500 volts applied to the 9 mil crystal. The difficulties inherent in the switching of large voltages led to the decision to use the 3.5 mil devices in the final system. Of the three devices constructed and tested during the contract, the two with the best performance characteristics, MT-11 and MT-15, were chosen for incorporation into the final system. The bus throughput loss and the tapoff loss with respect to input light level, and the modulation depth, are shown as a function of electrode voltage for these devices in Figs. 22 and 23. The better of the two devices exhibits an insertion loss of 5.7 dB and a tap-off ratio of 13.6 dB in the fail safe mode, together with a modulation depth of ~27% for a 50 volts peak-to-peak ac signal.

## 4.5  The Status of the Mirror Terminals

Of the two devices chosen for incorporation into the final system, MT-11 exhibited the better performance characteristics. Even so, the experimental insertion loss of 5.7 dB for this device exceeded the theoretical loss by 3 to 3.5 dB. The reasons for this excess loss, while not yet completely understood, are believed to lie principally with the difficulty involved in the formation of a perfect cylindrical mirror end on the crystal. Rounding effects, misalignment of focus, chipping of the mirror surface, and non-cylindrical shaped surface all probably contribute to the excess loss, and it is expected that improved fabrication techniques will reduce the total insertion loss to a more acceptable level of 3 dB.
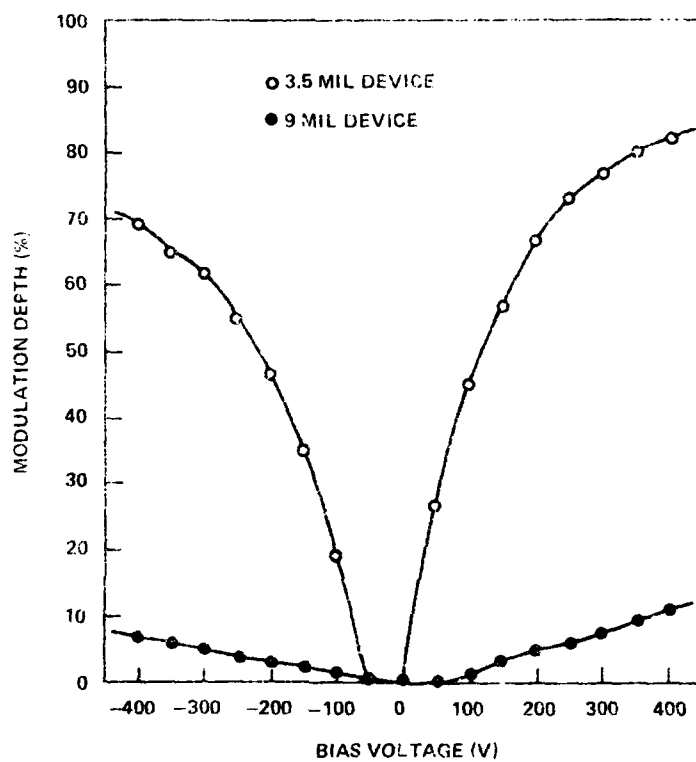
FIG. 21  Modulation depth vs bias voltage for the 9 mil and
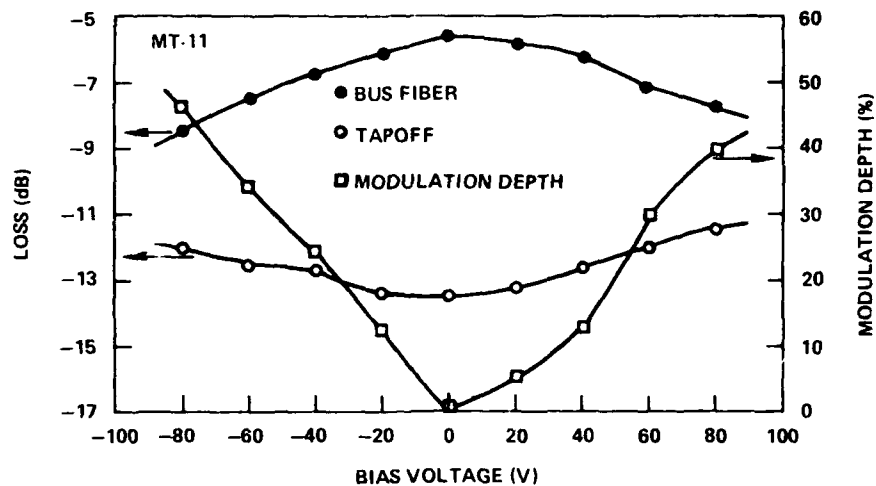3.5 mil devices.

FIG. 22 Insertion loss, tapoff ratio and modulation depth vs bias voltage for MT-11.
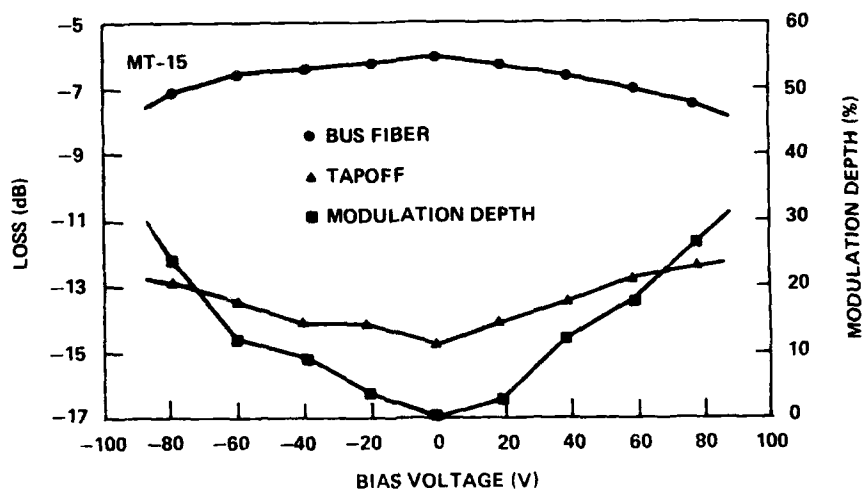


FIG. 23 Insertion loss, tapoff ratio and modulation depth vs bias voltage for MT-15.

-37-

## 5. FIBER/DEVICE COUPLING AND PACKAGING

### 5.1 Fiber/Device Connections

The permanent coupling together of a fiber optic device and a fiber termination in a secure fashion remains one of the most important steps in the fabrication of a complete functioning unit. The actual fiber connections required for a mirror terminal are shown in Fig. 24. Four fibers were used in a plane-parallel array. The bus input fiber (31) and bus output fiber (#3) are positioned symmetrically on each side of the optic axis of the mirror. The local tapoff of light was accomplished using two fibers (#2 and #4) which are positioned on either side of the bus output fiber. To minimize the insertion loss due to the finite numerical aperture of the fibers used, it was necessary to have the separation between the bus input and bus outuput to be as small as possible. This was accomplished in the construction of the fiber terminations, as is discussed below.

### 5.2 Fiber Terminations

The fibers used in the construction of the fiber terminations were Corning low loss fibers with a fused silica core having a numerical aperture of .15. Five fibers were used in each termination to allow for optimization of the bus throughput by having four distinct choices for the complete set of one input fiber, one output fiber and two tap fibers.

The five fibers to be used were first stripped of their buffer coating by immersing them in acetone. They were then positioned on a glass microscope slide so that, at the edge of the slide, they were parallel with their outer cladding in contact. A small drop of glycol phthalate is then used tò fix the fibers in place and a second microscope slide bonded to the fibers from above is used to complete the termination "sandwich". Figure 25 shows a five-fiber array near the edge of glass slide. As can be seen, the fibers are already nearly touching and parallel. The fiber ends which emerge from the glass sandwich are strengthened with Torr Seal epoxy. The fiber ends are then polished down on a succession of abrasive surfaces down to a 1 μm size alumina grit. A typical example of polished fiber ends
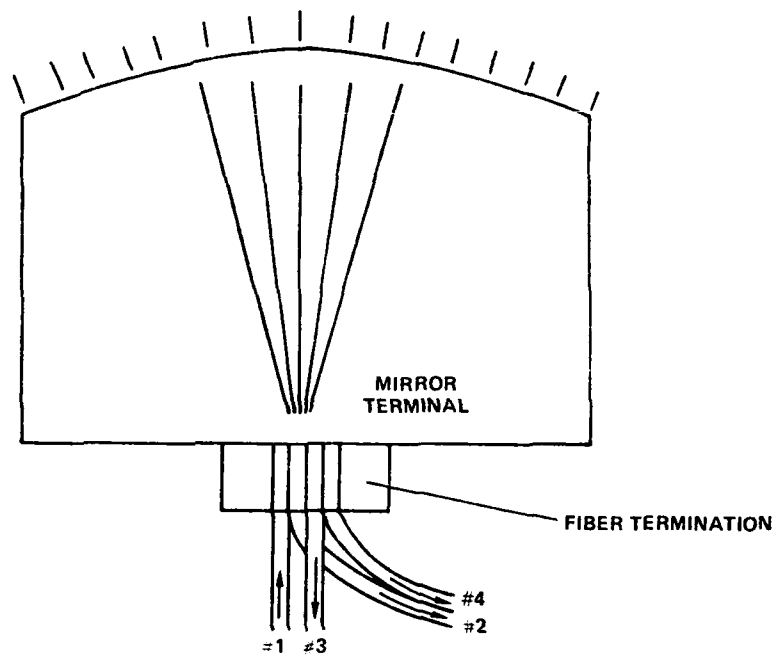
-38-

FIG. 24    Actual coupling of fiber termination to device.



FIG. 25    Interior of fiber termination.

is shown in Fig. 26. As can be seen, any deviation from linearity in the array is very small, the fibers are touching or nearly touching and the surface polish is of good quality. The final step in the fabrication of a termination is the epoxying in place of a glass support sleeve to the glass sandwich at the point where the fibers emerge from thenon-mating side. A completed termination is shown in Fig. 27.

## 5.3 Packaging

When the fiber termination has been completed, it is epoxied to the mirror terminal. This is accomplished by mounting the mirror terminal on an optical post, mounting the fiber termination on a precision translation/rotation positioning device. The bus throughput is optimized by manipulation of the fiber termination relative to the mirror terminal. The two components are then epoxied into position while the bus throughput is continously monitored. Index fluid is then inserted between the fiber termination and the mirror terminal ($\sim$5 $\mu$m gap) to reduce reflection losses.

It was anticipated that the performance of the devices would deteriorate during the epoxying process with respect to the optimized laboratory measurements, but this was not found to be significant. A loss of a few tenths of a dB was measured for the worst case.

Each epoxied device was then packaged as shown in Fig. 28. Contained within the unit is the mirror terminal/fiber array together with a photodiode. The electrical connector pins mate directly with the modulator driver and the detector electronics. The fibers are contained in the PVC jackets and are ready for connection into the data bus circuit.


## 6. FAIL SAFE OPTICAL DATA LINK COMPONENTS

### 6.1 Fiber

The choice of which optical fiber to be used in the fail safe optical data link depended upon which commercially available fiber most closely matched the mirror terminal requirements for core diameter. It was also deemed desirable for the chosen fiber to exhibit low loss at the
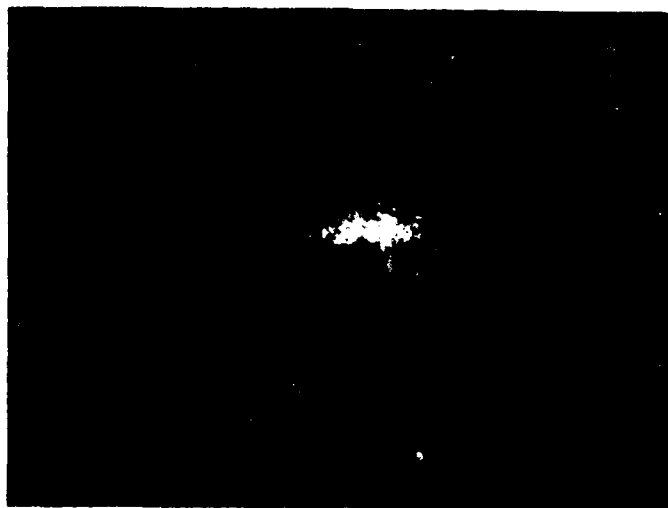
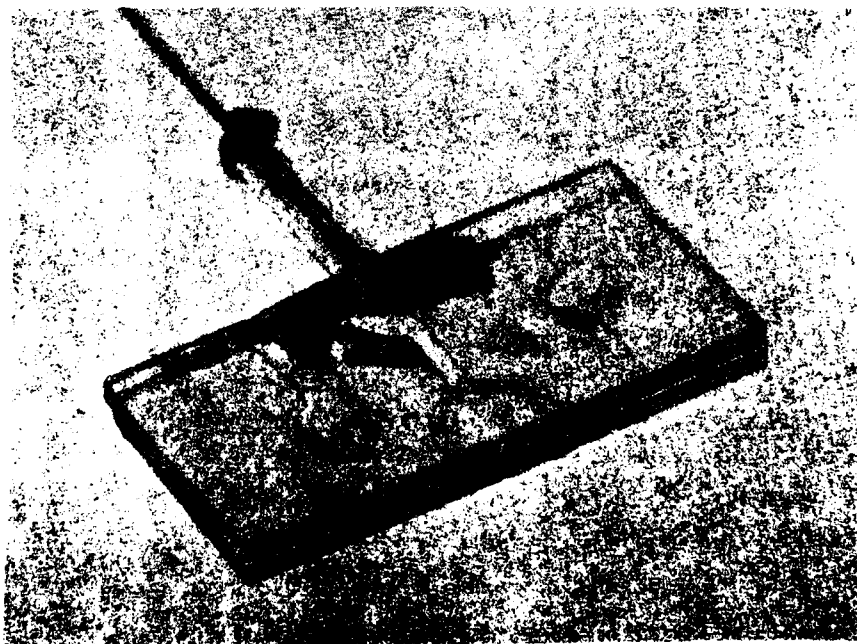FIG. 26   Polished fiber ends in fiber termination.



FIG. 27   Completed fiber termination.

FIG. 28   Packaged mirror terminal device.

frequency of the source. An optimum thickness for the mirror terminals had been found to be ~90 $\mu$m. This thickness represented an acceptable compromise between lowering the modulator drive voltage requirements and having a crystal that was easily manipulatable. For that reason, Corning low loss multimode fiber with a core diameter of 85 $\mu$m was found to be quite satisfactory. Furthermore, it exhibited its lowest optical loss of 30 dB/km at a wavelength of .82 $\mu$m. This matches quite well the wavelength of peak power of the LED source of .90 $\mu$m.

## 6.2 Source Considerations

The only real choice of a source for use with a fail safe optical data link lies between either a laser or an LED. Recently, semiconductor laser sources have been produced which will operate cw or 50% duty cycle at room temperature. However, these devices are at present both costly and somewhat unreliable. For those reasons, it was decided to use an LED in the fail safe system. Commercially produced LED's can now be obtained which have a higher reliability, longer lifetime and much more easily satisfied drive requirements.

For the best match between the minimum loss wavelength of the Corning low loss fiber and the source, a Burrus-type, GaAlAs LED would be preferred. This is because the Burrus geometry, in which the fiber to be used is integrally butt-coupled to the active emitting area, allows a significant amount of optical power to be inserted into a multimode glass fiber with a small core diameter. Furthermore, the GaAlAs composition can be made to emit in the .82 to .85 $\mu$m region, which corresponds exactly to the minimum·loss region (first valley) of most multimode fibers. GaAs, on the other hand, emits maximum optical power at .9 $\mu$m where the loss is somewhat higher. It was not possible to obtain a Burrus-style LED with a GaAlAs composition at reasonable cost. However, it was possible to obtain a Burrus-style (etched well) LED with a GaAs composition, a Plessey HR 954. This type of LED has the Burrus geometry, but is not coupled to any fiber. It is capable of inserting ~50 $\mu$W of optical power into a fiber with a numerical aperture of .15, and this was found to be the case when this

-43-

source had the Corning low loss fiber butt coupled to it at SCRC. This amount of optical power provides a data bus signal of sufficient strength to operate the fail safe optical data link with the number of terminals required for the present contract.

The LED which is supplied with the data link is driven by a circuit which provides the required 200 mA drive current and produces an internally generated 20 kHz square wave operating at a 50% duty cylce. This is done both to provide a bus signal for detection at the two remote receivers and the master receiver, and to operate the LED source more conservatively. The driver circuit is designed to operate from a 5 volt supply which is also provided. A block diagram of this circuit is shown in Fig. 29 while the detailed circuit is shown in Fig. 30.

## 6.3 Detector and Preamp

For the purposes of testing and demonstrating the fail safe optical data link, it is necessary both to detect the data bus signals from the master terminal at each of the remote terminals and to detect the signals impressed by each remote terminal upon the data bus at the master terminal. The data bus signals are optical pulses of 20 kHz repetition rate, and are therefore easily distinguished from the remote terminal modulation pulses operating at a 750 kHz repetition rate.

The same detector was used in the master and remote terminals. This was an EEG, type SHS-100, silicon PIN photodiode, with a 5 $mm^2$ active area and a capacitance of 4 pF. Low cost and relative simplicity caused this diode to be chosen over the more expensive avalanche photodiodes.

Since the amount of optical power injected into the data link was of the order of 50 μW, it was necessary to amplify the signals tapped off at each terminal. A block diagram of this optical receiver is shown in Fig. 31. The detailed circuit diagram is shown in Fig. 32. It is noted that a comparator is used in this circuit so that data output signals have a uniform amplitude independent of their point of reception on the data bus.

-44-

| 5 VOLT SUPPLY | PULSE GENERATOR | HEX INVERTER | BUFFER | LED |
|---|---|---|---|---|

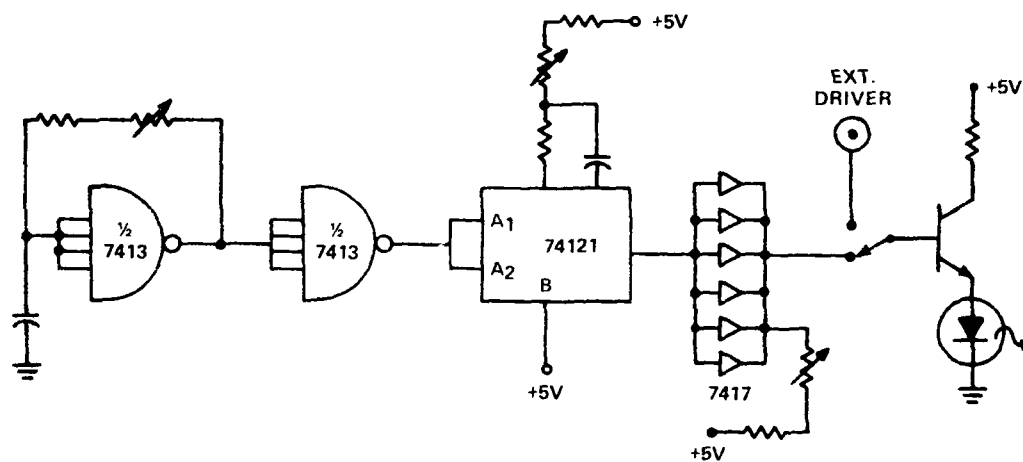FIG. 29   Block diagram of the LED driver.

FIG. 30   The LED driver circuit.
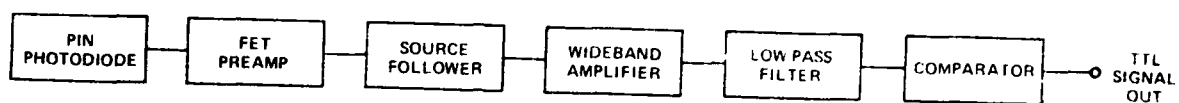
-45-

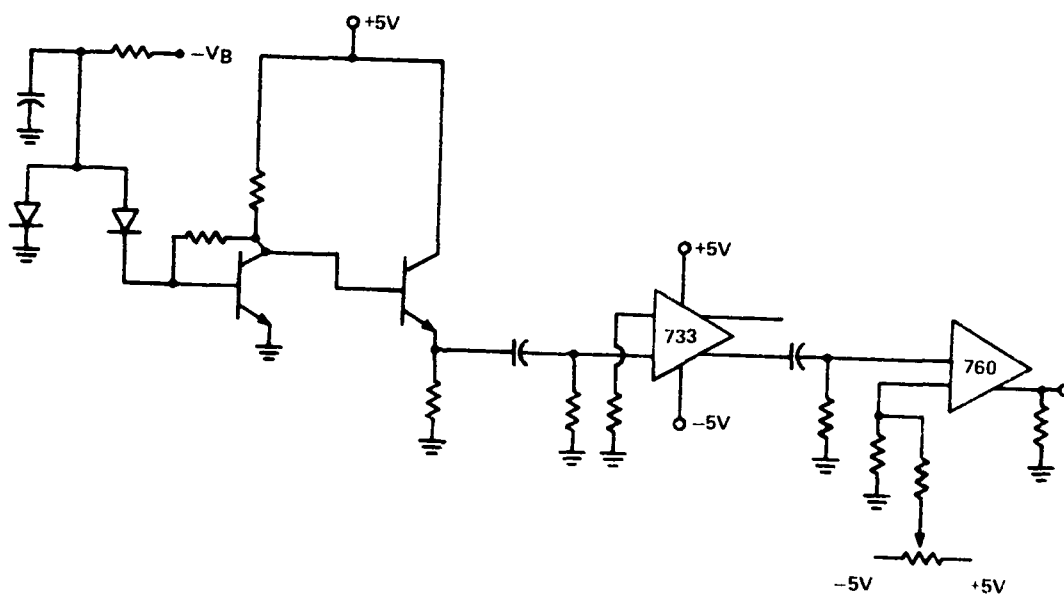FIG. 31   Block diagram of the optical receiver.



FIG. 32   Circuit diagram of the optical receiver.

-46-

## 6.4  Mirror Terminal Modulator

The mirror terminal modulator has been discussed in detail in Sec. 4. The 30 mil devices have a measured capacitance of ~50 pF , and display a modulation depth with voltage as shown in Figs. 22 and 23. They are driven by a circuit virtually identical with the LED driver with two modifications. First, the frequency of the driver pulses is much higher, 750 kHz vs 20 kHz and, secondly, a pulse transformer circuit with a 20:1 turns ratio to provide 100 volts pulses to the mirror terminal modulator from the 5 volt supply. A block diagram of the modulator driver is shown in Fig. 33. It should be emphasized that the capacitance of the mirror terminal modulators implies a maximum modulation rate of ~400 megabits/sec if they are used in conjunction with a 50 $\Omega$ load.

## 6.5  Fiber Connectors

Three types of fiber connectors are used in the fail safe optical data link: source-fiber connector, detector-fiber connector, and fiber-fiber connector. The source-fiber connector accomplishes the butt coupling of the fiber and the Burrus-type or etched well LED. The fiber is positioned in the etched well so as to provide maximum optical power coupled into the fiber. A large plastic sleeve is then pushed down the fiber and permanently epoxied to the LED. The fiber is also epoxied at the point where it emerges from the plastic sleeve. In this way, a rigid and stable coupling between fiber and source is made.

The detector-fiber coupling does not involve the critical positioning required for the source-fiber coupling due to the relatively large active area of the photodiode detectors. The fiber ends are placed as near as possible to the active area of the detector by use of a plexiglass guide. The fibers are then epoxied into place in the guide, and the permanent detector-fiber coupling has been made.

For ease of construction and to demonstrate the modular nature of the data bus, fiber-fiber connectors are used between the modules comprising the complete fail safe optical data link. An example of a

-47-

fiber-fiber coupler is shown in Fig. 34. Basically, it consists of a groove in a plexiglass substrate in which the input and output fibers are butted against one another with an index matching fluid between them. A second piece of plexiglass is then clamped against the first to hold the fibers in position. Although coupling fibers with these connectors requires care, throughput losses averaging .5 dB result when 85 μm core Corning fibers are used. The ease of connector fabrications and the low coupling losses make this coupling scheme attractive for the present application.

## 7. FAIL SAFE OPTICAL DATA LINK

A complete functioning fail safe optical data link was constructed using the components described in Sec. 6. Testing of the link was carried out and the results are presented in this section.

### 7.1 System Configuration

The fail safe optical data link as constructed consisted of three modular units: a master terminal and two remote terminals. These were assembled into a working system using the fiber-fiber connectors described in Sec. 6.5. Figure 35 presents a block diagram of the entire link. As can be seen, the master terminal consists of an LED source and driver together with a photodiode detector and receiver. Provision is made to externally drive the source LED if required. A photograph of the completed master terminal is shown in Fig. 36. The remote terminals are similar to the master terminal with the mirror terminal modulator replacing the LED source. Again, although a .75 megabit/sec internal square-wave generator is provided, provision is made for external driving of the modulator. Figure 37 presents a photograph of one of the completed remote terminals while Fig. 38 is a photograph of the complete system. The operational characteristics of the data link are described in the next section.

### 7.2 Operational Characteristics

The first test to be made on the system was to demonstrate that a data bus signal inserted into the system could be detected by each

| 5 VOLT SUPPLY | PULSE GENERATOR | HEX INVERTER | BUFFER | PULSE TRANSFORMER | MIRROR TERMINAL MODULATOR |
|---|---|---|---|---|---|

FIG. 33    Block diagram of the modulator driver.
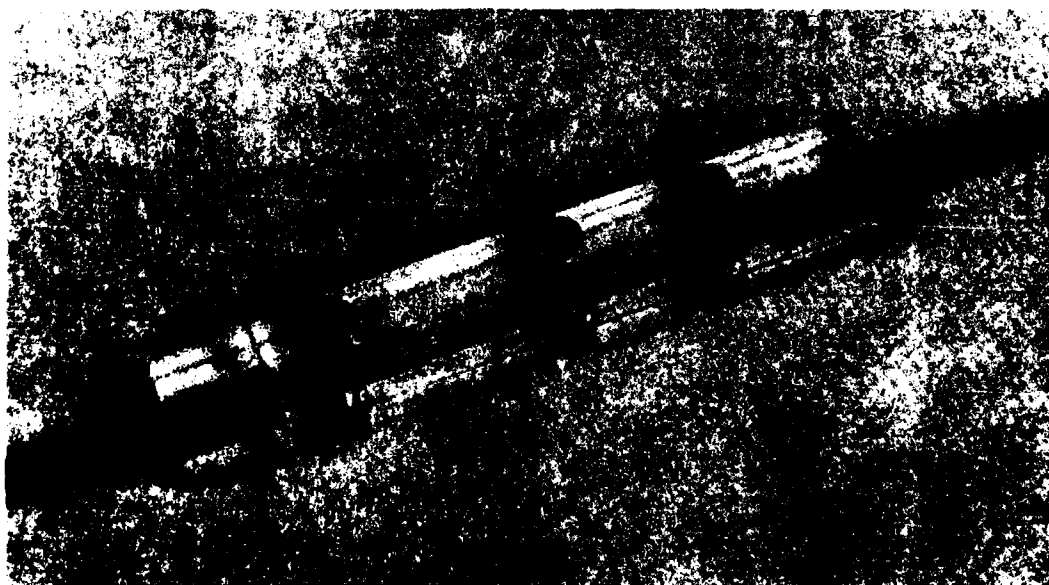


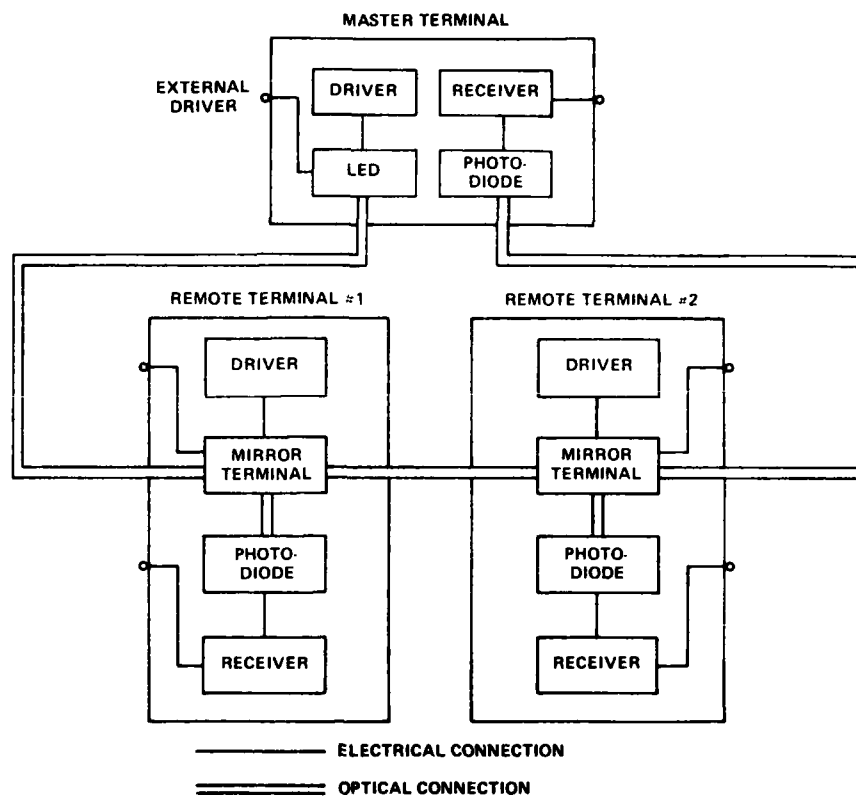FIG. 34    Fiber-fiber connector.

FIG. 35    Block diagram of the fail safe optical data link.


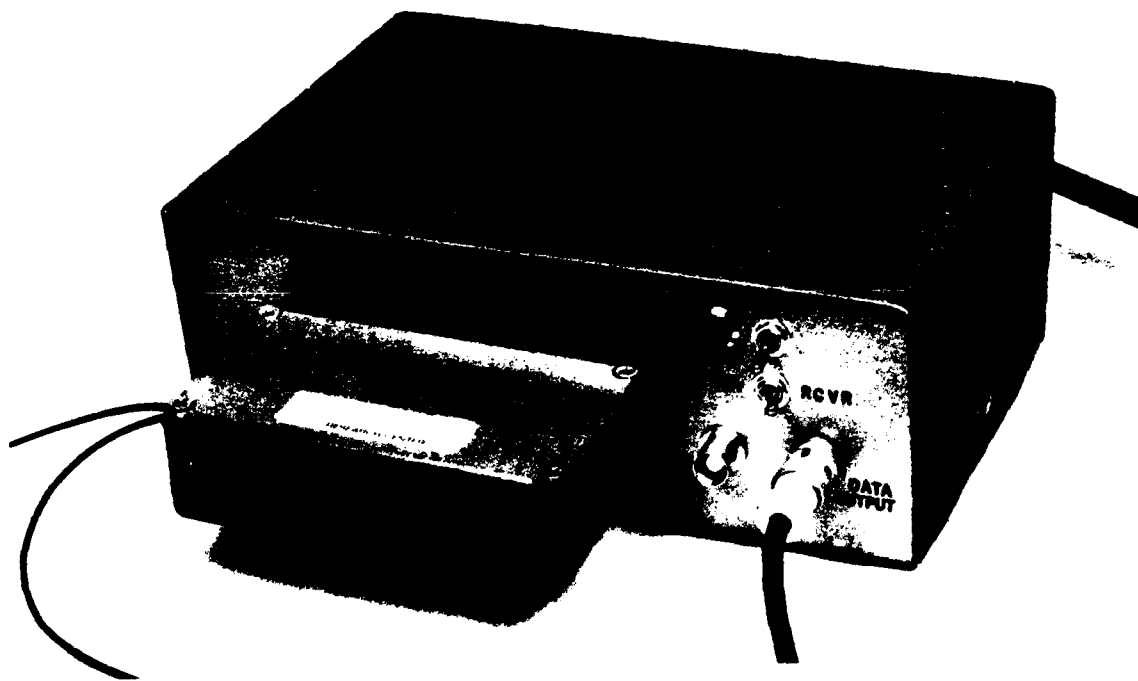
FIG. 36    Fail safe master terminal.
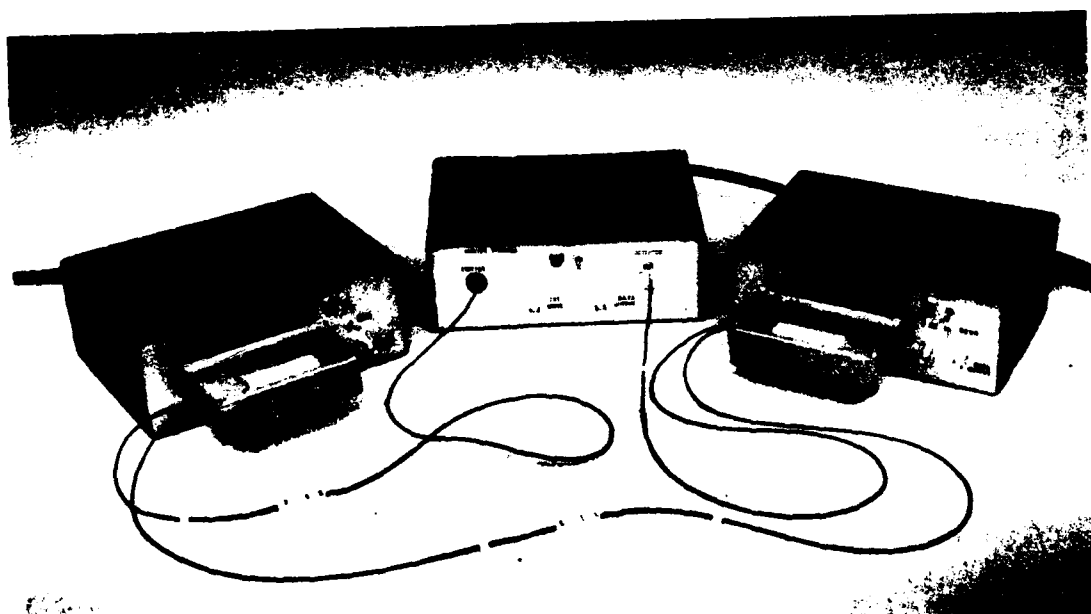
FIG. 37   Fail safe remote terminal.



FIG. 38   Complete fail safe optical data link.

terminal on the link. The source was pulsed at a 20 kHz repetition rate using an external driver. This repetition rate was chosen to be low to distinguish it from the remote terminal modulation. The results are shown in Fig. 39. As can be seen, there is no difficulty in detecting the bus signal, even after it has passed completely around the link. The optical power detected at remote terminal #1 was 14 dB below the optical power inserted into the link, the optical power detected at remote terminal #2 was 22 dB below the inserted optical signal, while the closed loop signal detected at the master terminal was 14 dB below the insertion level of 80 μW. Since the limit of detectability is of the order of 20 nW with available room temperature detectors and receivers, at least two more remote terminals could be added to the link as it currently exists. The detectability limit represents a compromise with bandwidth, and data rates of a few megabits/sec could be achieved at this limit. Figure 40 summarizes the actual measured losses in the system: fiber-fiber connector losses, mirror terminal insertion losses and tapoff losses. These are all relative to the 80 μW of optical power inserted into the link. The figures in parentheses represent the ratio between optical power coupled in at the source and the optical power seen at each detector.

The detectability of the signals impressed upon the data bus by each remote terminal was the next system characteristic to be investigated. With the source at the master terminal driven internally and remote terminal #1 in the transmit mode, Fig. 41 shows the signal detected at the master terminal. Trace (a) shows the signal received with remote terminal #2 in the active receiving mode, and trace (b) shows the signal received with remote terminal #2 without ac electrical power supplied to the modulator. Since these two signals are identical, Fig. 41 shows both the modulation characteristics of remote terminal #1 and the fail-safe nature of remote terminal #2. Similarly, Fig. 42 shows the modulated signal produced by remote terminal #2 and detected at the master terminal with remote terminal #1 (a) in the receive mode and (b) without electrical drive power. Hence, both remote terminals are both experimentally fail safe in nature and

-52-

20mV          100µS

(a)

(b)

(c)

(d)

2V
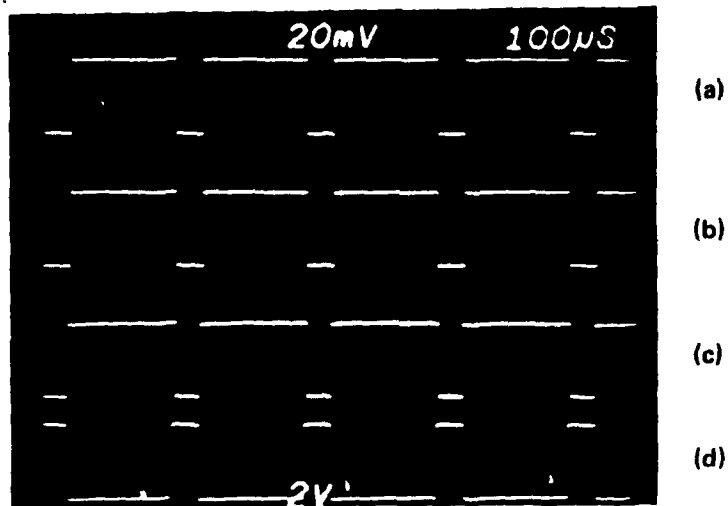
FIG. 39  Data bus signal detected at (a) remote terminal #1, (b) remote
         terminal #2, and (c) the master terminal, with LED driver current
         pulse (d).
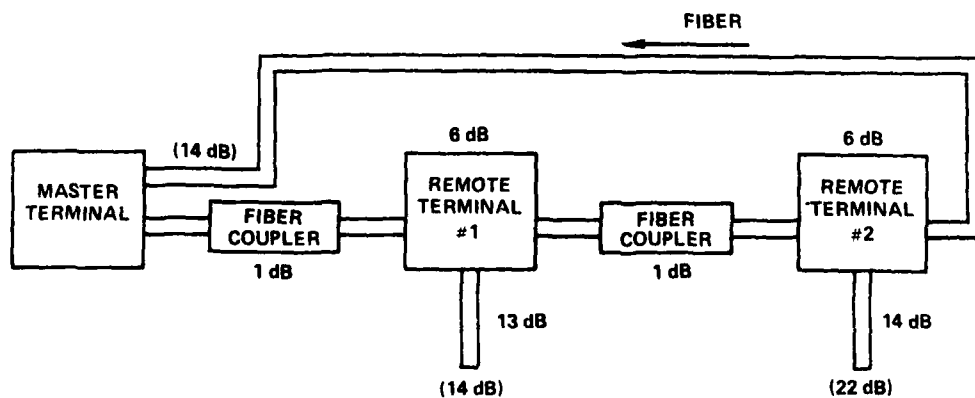


FIG. 40  Block diagram of data link with losses.
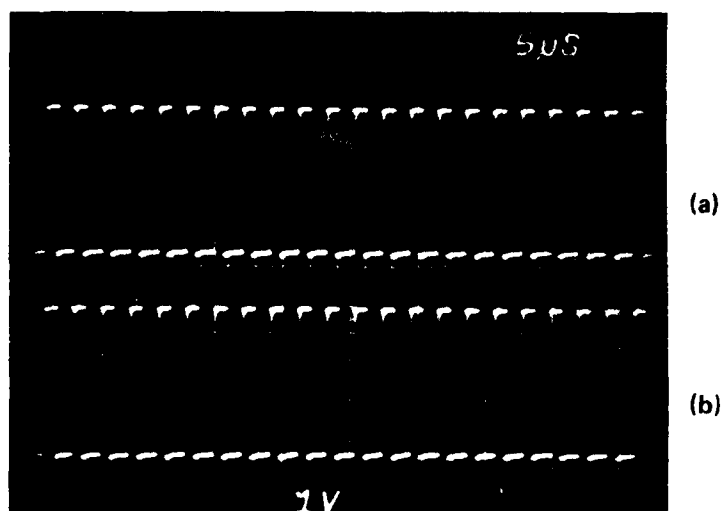
FIG. 41  Signals detected at the master terminal from remote
terminal #1 (a) with remote terminal #2 in the receive
mode and (b) with remote terminal #2 without power.
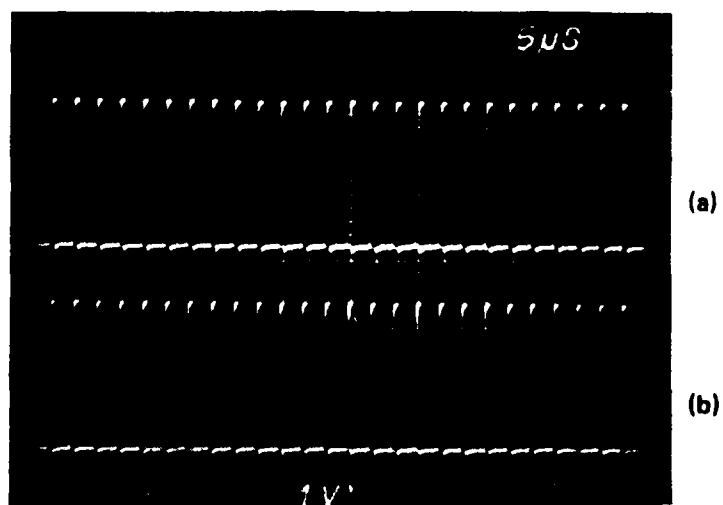


FIG. 42  Signals detected at the master terminal from remote
terminal #2 (a) with remote terminal #1 in the receive
mode and (b) with remote terminal #1 without power.

-54-

can produce a modulated signal capable of being detected at the master terminal.

Finally, the action of the comparator circuit was demonstrated. Figure 43 shows the modulated optical signal from remote terminal #1 being detected at the master terminal. To demonstrate the operation of the comparator, trace (a) shows the signal before it enters the comparator while trace (b) shows the output of the receiver after the comparator. Here, the tapped-off data pulses have been restored to TTL logic levels. Since the receivers at each terminal on the link are detecting signals whose optical power ratios may differ by as much as 8 dB, the comparator circuit is extremely useful in providing a uniformly strong output from the receiver regardless of where a signal is detected on the link.

## 8. SUMMARY AND RECOMMENDED RESEARCH

A fail safe optical data link in the form of a serial data bus has been constructed and tested. The functioning of this link is dependent upon the performance of two identical mirror terminal/modulators. These devices are capable of an optical insertion loss of less than 6 dB in the fail safe mode and a tapoff ratio of 12 to 13 dB. They are designed to be compatible with step index multimode monofibers with a core diameter of 85 $\mu$m and can accept large numerical apertures. Both devices have been permanently butt coupled to fiber arrays at normal incidence. The final packaged devices exhibited a modulation depth approaching 50% for 100 volts applied.

The mirror terminal/modulators were assembled into two remote fail safe terminals which together with a master terminal comprised a demonstration data link. The master terminal consisted of an LED source and driver together with a photodiode detector and receiver. The remote terminals each consisted of a mirror terminal/modulator and driver together with a photodiode detector and receiver. The test system was modular in nature; i.e., non-permanent fiber splices were made between units. The system was demonstrated to be fail safe in that a power failure at either of the remote terminals did not interfere with the functioning of the link
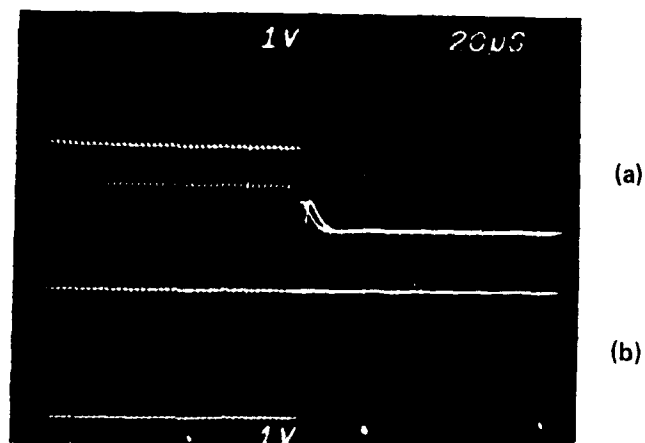
-55-

FIG. 43 Signals from remote terminal #1 detected by the master
terminal (a) before the comparator circuit and (b) after
the comparator circuit.

and, indeed, the smallest optical insertion loss for the mirror terminal/ modulators occurred in the fail safe mode. It was further shown that signals sent by the master terminal could be detected at each terminal on the data link and that each remote terminal could impress a signal upon the bus which could be detected at the master terminal.

The devices described here are capable of being the components of a practical fail safe optical data link as they exist at present if a suitable optical source is used. If one incorporates the components used in the test fail safe optical data link with low loss fiber (attenuation less than 10 dB/km) and a source capable of inserting $\sim$.5 mW of optical power into the link at the wavelength of minimum attenuation for the fiber used, a working system could be constructed. This could consist of a master terminal and as many as five remote terminals using the present mirror terminal/modulators.

The results of this contract have shown that active optical devices can be constructed to have a fail safe character and also to be able to function as send/receive terminals in a fail safe optical data link. These devices have been shown to be compatible with standard step index multi- mode monofibers.

For further research, there are several areas in which activity would be fruitful. The first of these would be the improvement of the per- formance of the mirror terminals so as to make it more nearly approach the theoretical limit. A careful determination of exactly where excess loss occurs should be carried out to identify which steps in the present fabrica- tion process should be modified. At the same time, device fabrication techniques should be developed which will allow device operation over the entire Mil Spec temperature range. Considerable improvement in the mirror terminal performance can be expected.

A second area of investigation is a refinement of the pulse trans- former techniques used in the present contract to increase the bandwidth of signal injection to 10 MHz from the present value of .75 MHz. The alternate method for obtaining high voltage pulses by using a resonant tuned circuit

-57-

should also be analyzed. These two approaches are shown in Figs. 44 and 45.

The third area in which further research would produce useful information is the investigation of other device concepts which are compatible with the fail safe idea. The doped channel waveguide concept is one which deserves attention. This concept was considered briefly during the course of this contract but abandoned due to the ease of fabricating electro-optic channels. The basic idea involved is that a waveguide channel in an electro-optic material can be produced by doping the material with appropriate metallic ions. This permanent waveguide channel would then be incorporated into a design using the triple stripe geometry of the angle collimation terminal with the doped channel replacing the central strip. Normal incidence butt coupling of fibers to device would also be used. Modulation would be produced using the electro-optic effect via the guard electrodes. The necessary modulation voltages could be obtained by the resonant driving or pulse transformation techniques discussed above.

Finally, an analysis should be carried out to determine the tradeoffs involved in choosing either passive or active multimode switching devices for typical fiber bus applications such as tee couplers, star couplers, matrix switches, etc. Such an analysis would provide a basis for determining the optimum approach for a given system application.'

The extension of the current research into the areas described above seems a logical next step in the development and refinement of fail safe optical data links. The attractive attributes of the mirror terminal concept in conjunction with a fail safe optical data link (one source per bus, low optical insertion loss, maximum throughput in the fail safe mode, normal incidence butt coupling of fibers to device, and good modulation depth for reasonable applied voltage) which have been demonstrated in this contract make a strong case for continued development.
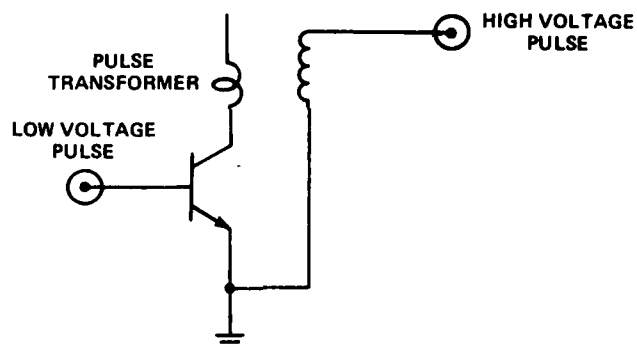
FIG. 44    Pulse transformer approach for generating high voltage
         pulses.
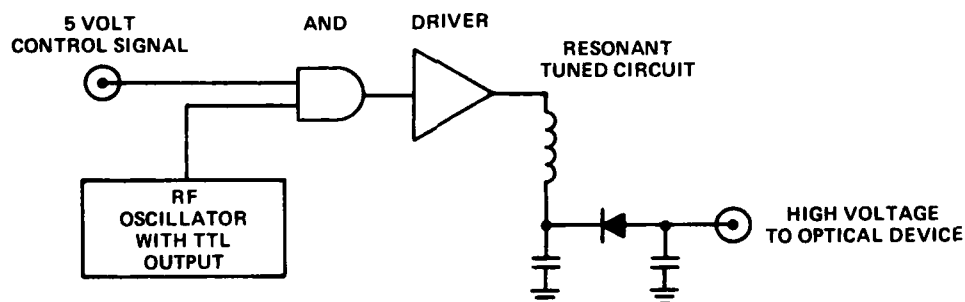


FIG. 45    Resonant circuit approach for generating 500 volts dc
         from 5 volt dc power supply.

APPENDIX A

INVESTIGATION INTO THE FEASIBILITY
OF DESIGNING A FAIL SAFE
OPTICAL DATA LINK

Quarterly Status Report No. 1
Contract No. F19628-77-C-0055

Sperry Research Center
100 North Road
Sudbury, Massachusetts 01776

SCRC-CR-77-26
15 April 1977

Prepared for
ROME AIR DEVELOPMENT CENTER
DEPUTY FOR ELECTRONIC TECHNOLOGY
HANSCOM AIR FORCE BASE
BEDFORD, MASSACHUSETTS 01731

Investigation into the Feasibility of Designing a Fail Safe Optical Data Link

## I. INTRODUCTION

The objective of this program is to investigate and develop a data terminal suitable for use in constructing a highly reliable multi-terminal optical data link system. This reliability is achieved through the development of a terminal structure which allows the link to continue in operation if the power fails at an individual terminal. The specific data bus system is a daisy chain which uses single multimode fibers for the terminal interconnects as shown in Fig. 1. Each individual terminal includes an electro-optic device which can impress information onto the data stream or monitor the data already on the channel and, if power failure does occur, allows adequate optical power to pass through the terminal with zero applied voltage.

The individual terminal is shown schematically in Fig. 2. Basically, the electro-optic device consists of a thin crystal of $LiTaO_3$ or possibly $LiNbO_3$, which has an appropriate electrode pattern evaporated on both faces. The particular device shown in Fig. 2 is a "single stripe" modulator which uses one 3 mil wide Cr/Au stripe electrode on each side of a 3 mil x 3/4" crystal. Multimode fibers with a core diameter of about 3 mils and NA=.15 are butt coupled to the input and the output of the device. Application of a voltage which increases the refractive index creates a light path that guides the light from the input to the output port. The reverse voltage tends to deflect light away from the output port. Thus, in this mode of operation the device is a modulator which impresses information from the data terminal onto the data stream. The tap off of light from the main data stream is accomplished by placing additional fibers at the output to collect a portion of the light which is not confined by the channel. The operation is fail safe in that the terminal must be designed so that, even without a guiding voltage on the device, there must
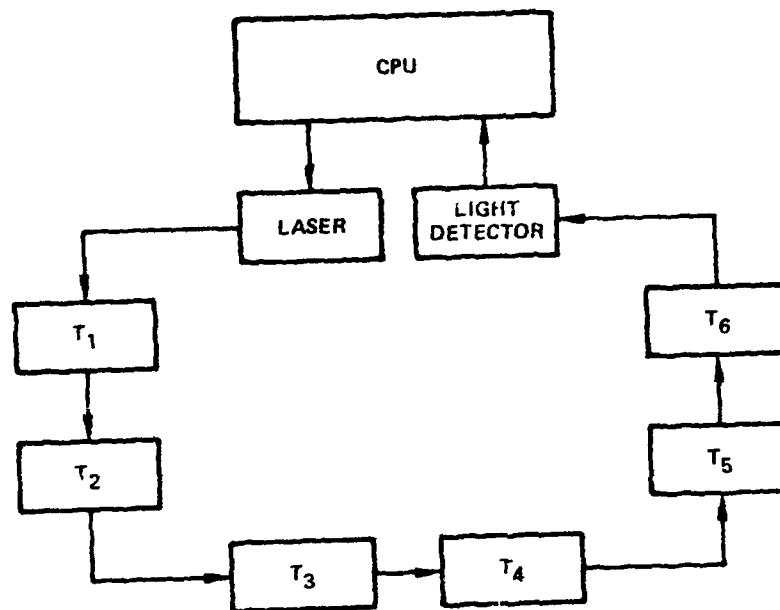
-62-

FIG. 1   Fail safe optical link structure.
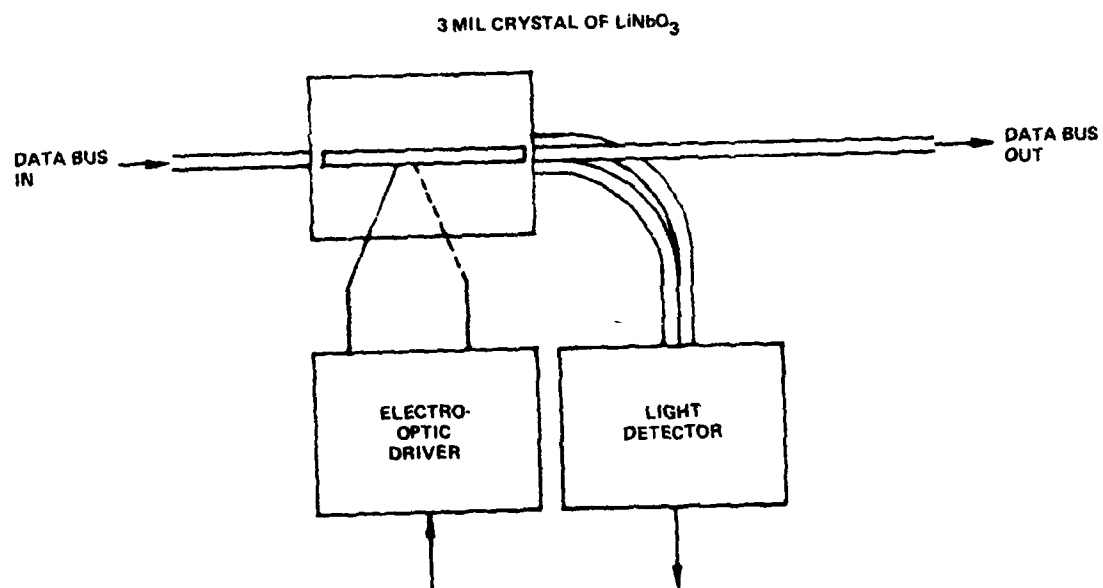
**3 MIL CRYSTAL OF LiNbO$_3$**



FIG. 2   Fail safe data terminal structure.

be enough unguided light falling on the output port to yield a strong
signal through the terminal.

This report covers the first three months (January 1 to April 1,
1977) of effort on this contract. The first quarter has been primarily
a design phase and in the next section we describe the theoretical considera-
tions that have been included in the planning. In addition, some preliminary
device construction has taken place and the finished devices are described.
The final section details some new concepts which have been developed to
potentially improve the device through lower throughput losses or greatly
simplified construction. The plans for the next quarter are then described.

## II. DEVICE DESIGN AND CONSTRUCTION

The simple single stripe modulator described above is inade-
quate as it stands for a useful data terminal, because the voltage required
to confine the light from a typical multimode fiber is well above breakdown
for the crystal. We can compute this voltage as follows. For a typical
multimode fiber (NA=.15), the fiber cone of light is $\pm 3.9^{\circ}$ in the crystal.
Using Snell's law at grazing angles of incidence, we find that the index
change $\Delta n$ required to contain a light ray of maximum angle, $\theta_m$, is given by

$$\Delta n = \frac{\theta_m^2 n}{2}$$

where $n$ is the index of refraction of the crystal. For $\theta_m = 3.9^{\circ}$ and
$n = 2.18$ we have $\Delta n = 5 \times 10^{-3}$. This index change is in turn related to the
required electric field $E_z$ by

$$\Delta n_z = 1/2 \ n_z^2 \ r_{33} E_z \qquad \text{(TM modes)}$$

$$\Delta n_x = 1/2 \ n_x^2 \ r_{13} E_z \qquad \text{(TE modes)}$$

for a $LiTaO_3$ or $LiNbO_3$ crystal structure. For these crystals,

-64-

$r_{33} = 30 \times 10^{-12}$ m/V and $r_{13} = 7 \times 10^{-12}$ m/V. For the TM modes, we can then calculate that $\Delta n = 5 \times 10^{-3}$ implies a voltage of 1900 V across 3 mils well above the breakdown point of approximately 500 V. Due to the smaller $r_{13}$ coefficient, this 1900 V will produce only 1/4 the index change for TE modes, but the quadratic relationship of $\Delta n$ and $\theta_m$ means that 1/2 of the $3.9^\circ$ light cone or about $\pm 2^\circ$ of TE light will be guided.

One relatively simple change in the single stripe electrode structure can drop the required voltage in half. This is accomplished through the use of guard electrodes on either side of the main light path which are connected to the opposite polarity voltage as shown in Fig. 3. With this "triple stripe" arrangement a given V produces a certain $\Delta n$ in the guide region and $-\Delta n$ in the surrounding region for a net index change of $2\Delta n$. Thus the required voltage is reduced by a factor of two.

However, in order to dramatically reduce the voltage down to more reasonable values, it is necessary to collimate the light. Due to the quadratic relationship between $\theta_m$ on $\Delta n$, a decrease of $\theta_m$ by a factor of four reduces the voltage by 16, so that the required applied voltage is approximately 50 V. This collimation procedure is best accomplished by a procedure termed non-normal incidence butt coupling collimation, developed previously at SCRC. As Fig. 4 indicates, if the fiber is cut and polished at an angle, the light entering the crystal is expanded and collimated in one dimension. Four-fold collimation requires an incident angle of $79^\circ$, for example. Such angular coupling procedures have previously been carried out for two- and three-fold collimation.

Another important design parameter is the thickness of the crystal. It might be expected that the optimum device thickness is equal to the fiber core diameter, but this is not so. The input coupling loss increases as the crystal thickness decreases, but the output coupling loss, due to the circular nature of the fiber, decreases as the crystal is made thinner. In Table 1 we list the input and output coupling loss as a function of crystal thickness for 85 μm core fibers. The coupling loss factors listed in the table are relative coupling losses computed from
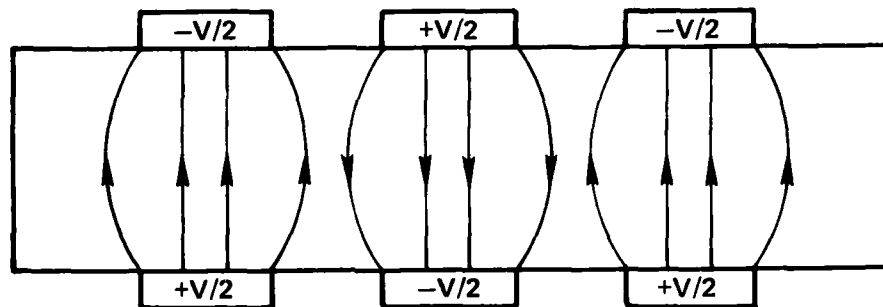
-65-

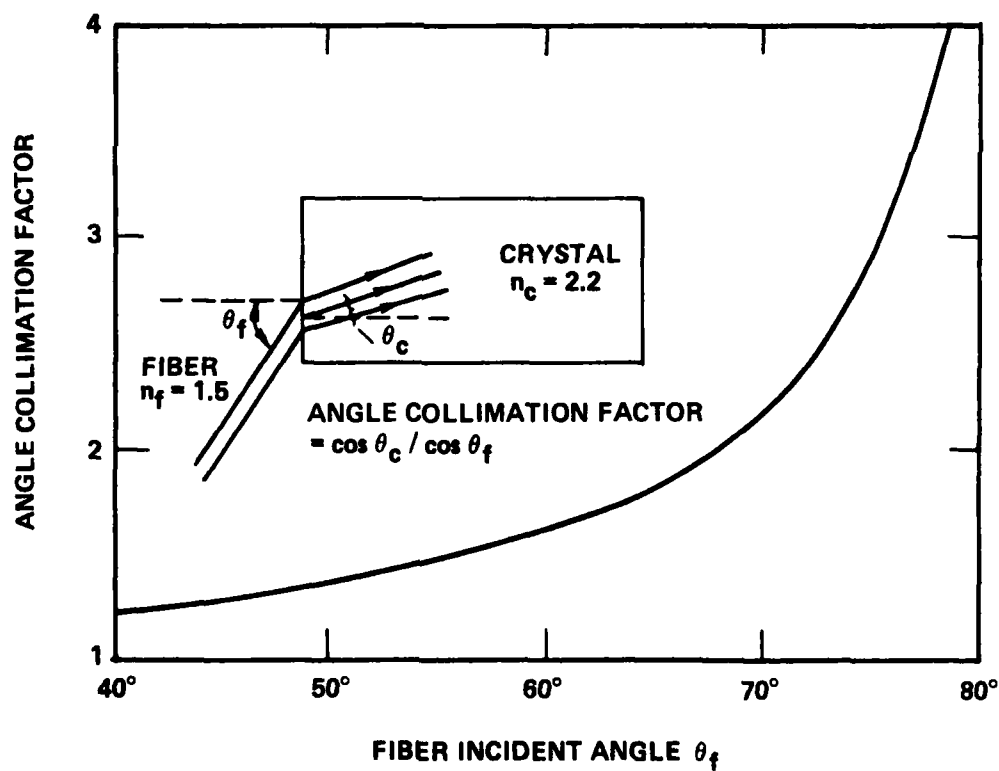FIG. 3    Modified guide structure with guard electrodes.



FIG. 4    Angle collimation factor vs incident light angle for $LiTaO_3$.

simple geometric formulas which compute the area of the circle that
coincides with the crystal geometry, and applies for the V=0 condition only.
Multiplying the input and output coupling factors shows that the optimum
thickness for V=0 is 75 $\mu$m, although there is very little difference from 65
to 85 $\mu$m.

The device design can be summarized thus far as follows: the
Cr/Au electrode pattern uses the triple stripe geometry on both sides of
the crystal. The collimation required is three- or four-fold, and the
required voltage therefore is 40 to 100 V. The thickness of the crystal
is about 75 $\mu$m, slightly less than the core diameter of the 85 $\mu$m multimode
fiber. The length of the crystal depends on the allowed losses and must be
fixed in conjunction with the collimation factor. The central channel width
in the crystal is 3.4 mils times the collimation factor.

The remaining design parameters to be fixed are the length and
degree of collimation, both of which must be adjusted simultaneously for
a compromise between modulation depth and throughput loss, with and without
an applied voltage. The throughput loss with V=0 can be found as a function
of length and collimation from a computer program previously developed.
This program computes the output light intensity as a function of position
at the output edge of the crystal using a number of input parameters as
variables: fiber core index, fiber NA, fiber core size, crystal index,
crystal length, degree of collimation, refractive index of a matching fluid,
and light polarization. The program takes into account the fiber geometry,
the variability of the reflection losses and degree of collimation over the
full cone angle of the input fiber, and the finite width of the fiber. wo
sample outputs are shown in Figs. 5 and 6 for NA=.16, four-fold collimation,
core diameter = 13.6 mils (4 x 3.4 mils), and .5" and 1" length, respec-
tively. The relative throughput is found by computing the total power under
the curve in a 13.6 mil length and dividing by the total input power. In
Table 2 we list typical losses computed with V=0 taking into account all of
the factors mentioned above including the size mismatch of Table 1. If
we arbitrarily adopt about 6 dB as the maximum acceptable throughput loss in
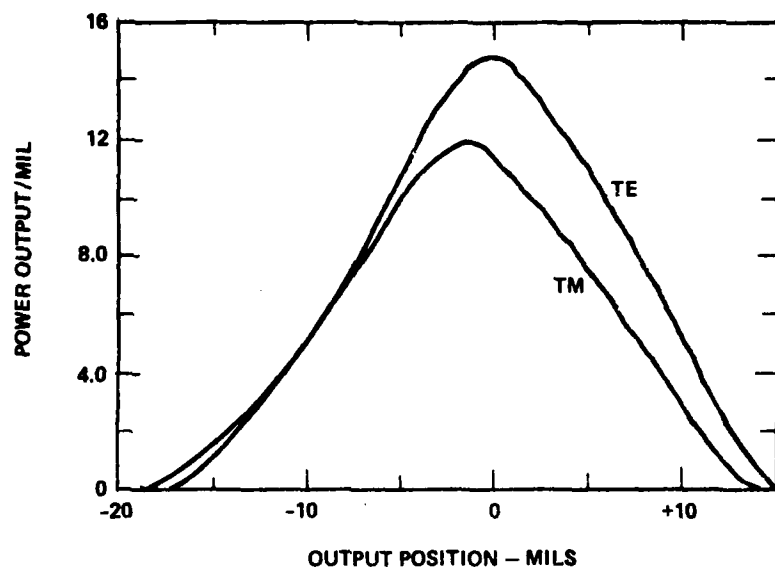
-67-

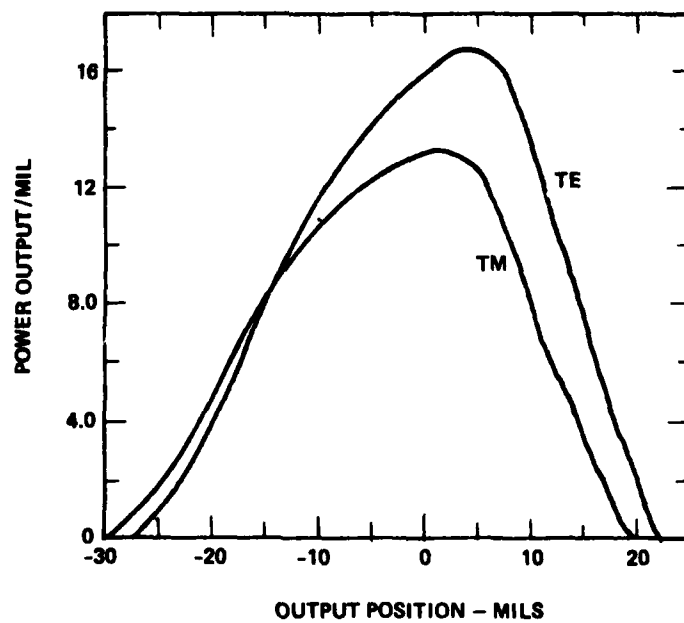FIG. 5    Power output at end of 0.5 inch crystal for NA = .16 input.



FIG. 6    Power output at end of 1 inch crystal for NA = .16 input.

-68-

## TABLE 1

### Fiber/Device/Fiber Coupling Efficiency as a Function of Device Thickness

| Crystal Thickness ($\mu$m) | Relative Input Coupling Efficiency | Relative Output Coupling Efficiency | Total Coupling Efficiency |
|---|---|---|---|
| 85 | 1 | .79 | .79 |
| 80 | .98 | .82 | .80 |
| 75 | .95 | .85 | .81 |
| 70 | .91 | .87 | .79 |
| 65 | .97 | .89 | .77 |
| 60 | .82 | .91 | .75 |
| 55 | .76 | .93 | .71 |
| 50 | .70 | .94 | .66 |

$$\text{Input Efficiency} = 1 - \frac{2}{\pi}\left(arcos\,(t/d) - \frac{t}{d}\sin\,(arcos\,(t/d))\right)$$

$$\text{Output Efficiency} = 1/2\,\sin\,(arcos\,(t/d)) + \frac{\pi d}{4t} - \frac{d}{2t}\,arcos\,(t/d)$$

$t$ = crystal thickness     $d$ = fiber core diam = 85 $\mu$m

## TABLE 2

### Total Throughput Loss in dB for V = 0

| Device Length (in.) | Total Device Loss (V = 0) | | | | | |
|---|---|---|---|---|---|---|
| | 3-Fold Collimation | | | 4-Fold Collimation | | |
| | TM | TE | AVG | TM | TE | AVG |
| .5 | 7 | 6 | 6.5 | 4.7 | 3.7 | 4.2 |
| .75 | 8 | 7 | 7.5 | 5.7 | 4.6 | 5.2 |
| 1.0 | 9 | 8 | 8.5 | 6.5 | 5.6 | 6.0 |

the fail safe condition, then any length under 1" may be acceptable with 4-fold collimation, as well as .5" with 3-fold collimation. With 4-fold collimation we will have lower operating voltages, but the modulation depth may be greater for 3-fold collimation.

It is very difficult to predict accurately the light captured as a function of V, due to the fringing nature of the electric field, and even the V=0 calculations which we have shown above should only be used as a guide to the device design. With that in mind we have chosen two device designs to construct and test initially: .5" long $LiTaO_3$ with 3-fold collimation and .75" long $LiTaO_3$ with 4-fold collimation. The experimental results obtained from these devices will determine the direction to proceed in order to maximize the terminal design. In actual fact there may be more than one optimum device depending on other parameters such as the total number of terminals in the system. This result occurs because the through-put loss and modulation depth are directly related, and the optimum tradeoff between these two factors may be a function of the total number of terminals or other parameters related to the daisy chain link itself.

The mask designed for the 4:1 collimation device is shown in Fig. 7. It uses a 13 mil wide central channel and 2.5 mil guard electrodes with a 3 mil separation on either side. The electrical connections are brought out to large pads on either side of the crystal. The pattern is the same for both faces of the crystal except that the second side is reversed top to bottom with respect to the first side, so that the electrical connection pads do not appear facing each other across the crystal. Figure 8 shows the device after the electrodes have been evaporated on both faces, but before the sawing and polishing operation. All eight connection pads (four on top and four on the bottom) are visible.

The remaining steps in construction include sandwiching the crystal between two pieces of glass with cut-outs for the electrical connections, sawing at the proper angle for collimation, polishing the edges, and epoxying the electrical connections. A completed fail safe device is shown in Fig. 9, mounted on another glass slide for convenience. The

-70-
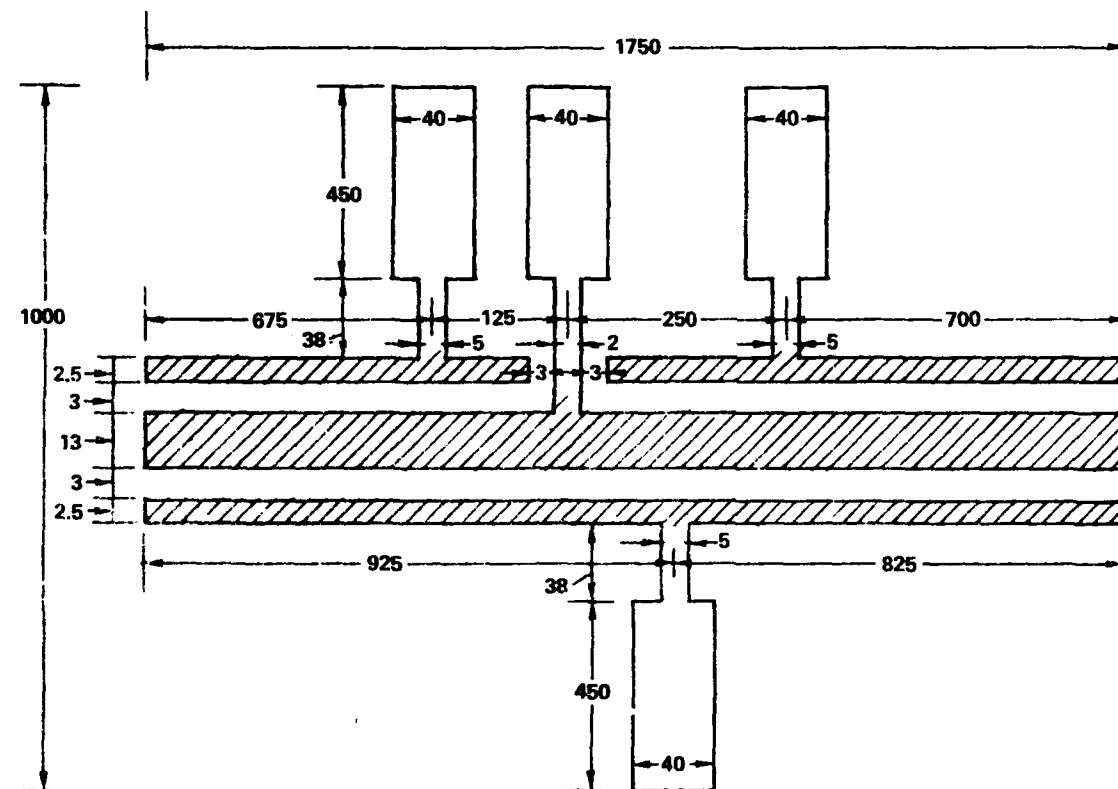
ALL DIMENSIONS IN MILS (.001")

FIG. 7    Mask for four-fold collimation, triple stripe device.
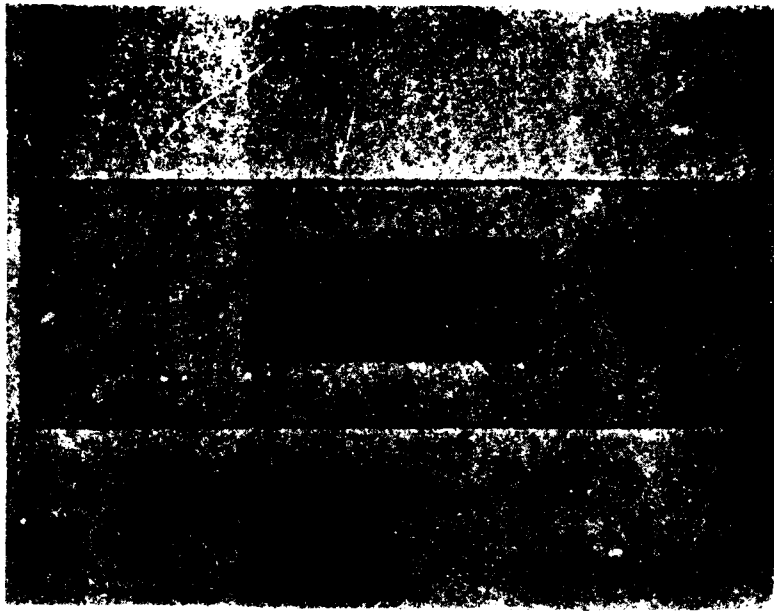
FIG. 8    Photo of four-fold collimation device after electrode evaporation.



FIG. 9    Photo of completed four-fold collimation device.

electrode pattern has been wired so that four electrical connections can be made to the crystal: top and bottom electrodes of the central stripe and top and bottom electrodes for the guard electrodes. The normal connection is to wire the central and guard electrodes on the same side to opposite polarities, although there is the possibility of using a permanent voltage on the barriers and modulating only the central electrode. While one device is complete and another is very near to completion, at this time we have not had the opportunity to evaluate the performance. In addition, for the 4:1 device we are presently in the process of constructing the 4:1 collimation fiber terminations which require the fiber to be sawed and polished at an angle of $79^{o}$. Both the 4:1 fibers and the measurements of the two initial 3:1 and 4:1 collimation devices will be completed soon.

### III. NEW CONCEPTS AND FUTURE PLANS

The original proposed fail safe devices are being constructed and will be optimized, but new designs have been developed which may offer some improvements. For example, it would be advantageous if a procedure could be found to eliminate the non-normal incidence butt coupling, since it leads to excess reflection losses and presents some extra fabrication steps. In order to d this, the light must be collimated by some other means or the waveguide index must be increased so as to confine the uncollimated fiber light.

An alternate means for collimating the fiber light is by use of a taper horn structure which expands and then contracts to gather the light, as shown in Fig. 10(a). The index change is produced by the usual electro-optic effect. This structure could also be considered to be a lens that acts to focus the light from the input to the output fiber and the exact shape of this lens would be determined by a ray tracing procedure to optimize the throughput. Another benefit of this structure is that the modulation depth would be very large, since removing the voltage would greatly reduce the throughput intensity. However, this is also one of the largest drawbacks, in that the fail safe feature is no longer present.
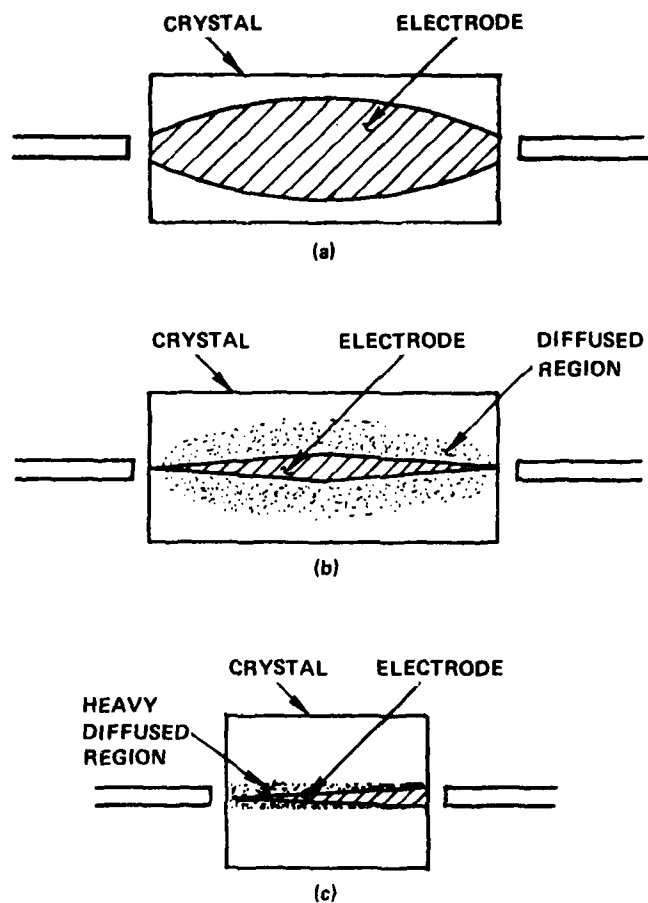
-73-

FIG. 10 (a) -- (c) Proposed methods for eliminating non-normal incidence collimation.

Also, the crystal would be very long, and this adds to the construction cost and difficulty.

Another possibility is shown in Fig. 10(b), where the electro-optic effect is replaced by a diffused lens structure, and modulation is produced by diverting light with the usual electro-optic effect. This would enable us to retain the fail-safe feature of the terminal. The required diffusion would be relatively light, i.e., about $5 \times 10^{-4}$ index change but, from our previous experiments with deep Cu diffusion, we have found an attenuation of 1 dB/cm for such a waveguide. Since the length required for such a device is 5 to 10 cm, the loss, at present, is unacceptable. Also, the length of the device is still a disadvantage.

In Fig. 10(c) another possible diffused channel terminal is shown. In this case, a heavy diffusion ($\Delta n = 5 \times 10^{-3}$) has been used to confine the light. This terminal has ideal characteristics in that it is short, easy to construct and has high throughput for V=0. Modulation is obtained by deflecting light away from the output port with the electrode shown. From our present knowledge of Cu diffusion, the losses would again be unacceptable. However, the potential advantage of this structure justifies further experimentation with deep diffusion of ions in $LiNbO_3$ or investigation into other methods of producing permanent refractive index changes. Other workers have produced excellent single mode guides using Ti diffusion, and the possibility exists of adapting this technique for multi-mode devices. Since the diffusion temperature is above the poling temperature of $LiTaO_3$, $LiNbO_3$ would be used for the terminal. From our experience with this material, it is not possible to use a large steady dc signal across an illuminated $LiNbO_3$ device; however, the data may be impressed using an ac voltage.

Plans for the next quarter include the completion of the construction and testing of the initial 3- and 4-fold collimation devices. From the results of these tests, further adjustments in length and collimation will be made to maximize the performance in relation to a typical daisy chain system. In addition, new experiments may be carried out on diffused

guides in an attempt to create large index change, low loss guides. Alternatively, if very low loss guides can be created with a small index change, the lens structure will be explored further.

**APPENDIX B**

**INVESTIGATION INTO THE FEASIBILITY
OF DESIGNING A FAIL SAFE
OPTICAL DATA LINK**

Quarterly Status Report No. 2
Contract No. F19628-77-C-0055

Sperry Research Center
100 North Road
Sudbury, Massachusetts 01776

SCRC-CR-77-37
15 July 1977

Prepared for
ROME AIR DEVELOPMENT CENTER
DEPUTY FOR ELECTRONIC TECHNOLOGY
HANSCOM AIR FORCE BASE
BEDFORD, MASSACHUSETTS 01731

-77-

TABLE OF CONTENTS

## LIST OF ILLUSTRATIONS

Investigation into the Feasibility of Designing a Fail Safe Optical Data Link

## I.  INTRODUCTION

The objective of this program is to investigate and develop a data terminal suitable for use in constructing a highly reliable multi-terminal optical data link system.  This reliability is achieved through the development of a terminal structure that allows the link to continue in operation if the power fails at an individual terminal.  The specific data bus system is a daisy chain which uses single multimode fibers for the terminal interconnects as shown in the first Quarterly Status Report. Each individual terminal includes an electro-optic device that can impress information onto the data stream or monitor the data already on the channel and, if power failure does occur, allows adequate optical power to pass through the terminal with zero applied voltage.

This report covers the second three months of effort on this contract: April 1 through July 1, 1977.  This report presents experimental results on angle-collimation terminals.  A novel, improved fail-safe terminal that couples to fibers at normal incidence is also described.  Preliminary results on the improved terminal are given.

## II.  ANGLE COLLIMATION TERMINAL

The previous Status Report, QSR-1, presented the theory and design of electro-optical data terminals that use angle-butt-coupling at their input and output surfaces.  Multimode fibers are angle-coupled to the terminal ends to collimate fiber light entering the terminal and to re-inject all of the mainstream light into the output fiber.  Devices with 3:1 and 4:1 collimation have been built and tested as discussed below.

Specifications of the electro-optic terminals are given in Table 1. An attempt was made to minimize the device length, and a length of 0.5" was the smallest that could be attained. As Table 1 indicates, a pair of fibers cut at the proper angles was prepared for each device.

Table 1. Geometry and construction of angle terminals and fibers.

### 3:1 Terminal

Material = Z-cut, single crystal $LiTaO_3$

Optical collimation factor = 3

Terminal shape = parallelogram

Terminal length = 0.53 inches

Thickness of crystal = 61 $\mu$m

Angle at which terminal ends are cut = 40.1 degrees

Theoretical angle of terminal end = 40.3 degrees

Width of main channel electrodes = 10.2 mils

Width of side wall electrodes = 2.2 mils

Separation of main and side electrodes = 2.7 mils

Electrode metalization = 70Å Cr and 500Å Au

Fiber type = Corning low loss, step index

Fiber numerical aperture = 0.14

Fiber core diameter = 85 um

First end of fiber cut at zero degrees

Second end of fiber cut at 75.3 degrees

### 4:1 Terminal

Material = Z-cut, single crystal $LiTaO_3$

Optical collimation factor = 4

Terminal shape = parallelogram

Terminal length = 0.57 inches

Thickness of crystal = 78 um

Angle at which terminal ends are cut = 41.2 degrees

Theoretical angle of terminal end = 41.0 degrees

Width of main channel electrodes = 13.0 mils

Width of side wall electrodes = 2.5 mils

Separation of main and side electrodes = 3.0 mils

Electrode metalization = 70Å Cr and 500Å Au

Fibers same as 3:1 except second ends are terminated at 79.2 degrees

## A. RESULTS

Figure 1 shows the experimental set-up used for measuring the terminal's insertion loss and modulation depth. The full 0.14 NA of the fibers was excited by a laser beam ($\lambda$ = 0.63 μm) focussed onto fiber's flat end with a 20x objective. The angle-polished fiber end was butt-coupled to the terminal. There was a very small gap (less than 1 mil) between the fiber and crystal and this was filled with an n = 1.63 fluid. The high-index fluid was also inserted into the butt-coupling gap between the terminal output and second fiber as illustrated in Fig. 2. There were no anti-reflection coatings placed on the crystal ends, but the index-transition fluid does a good job of minimizing interface reflection losses. There are no polarizers in the system, and both TE and TM modes are launched in the electrooptic terminal.

At the output of the second fiber (Fig. 1) the light is gathered with an EMI 9558A photomultiplier tube whose output is fed to a logarthmic amplifier. The log-amp level is monitored with a digital milliameter that displays the optical level directly in dB. The channel waveguide in the terminal is actuated with a dc supply. As Fig. 3 shows, the central electrodes (high index region) and the side wall electrodes (low index region) are wired together in parallel with reversed polarities so that only one control voltage is needed.

The optical input level to the terminal must be recorded in order to determine the terminal's throughput loss. To do this, we contacted a $LiTaO_3$ prism to the angle-end of the input fiber as shown in
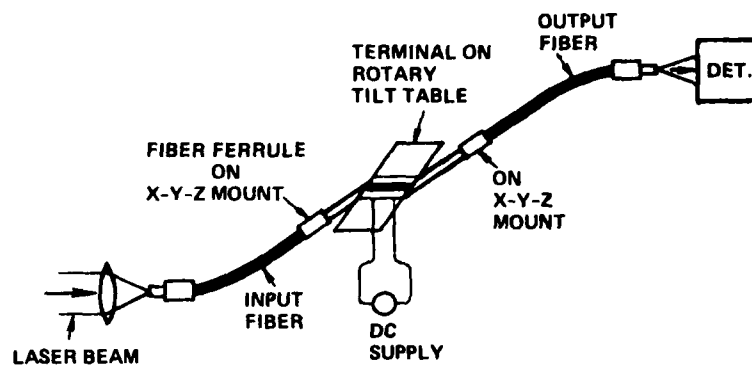
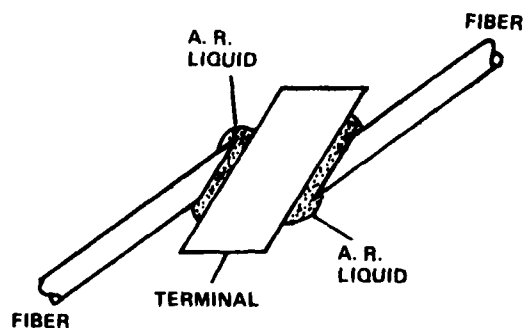FIG. 1     Arrangement for testing angle collimation terminal.



FIG. 2     Use of anti-reflecting liquid in angle butt coupling.

-83-

Fig. 4. Then the total emission from the fiber (the reference level) was measured. (If the prism were not used, most of the light would be internally reflected in the fiber).

Optical transmission through the Fig. 1 system was measured as a function of modulation voltage and the output was normalized with respect to the first fiber's output. Results for the two terminals are given in Figs. 5 and 6, respectively. The experimental uncertainty is shown by the shaded band in the Figure. The uncertainty is associated with the mechanical alignment between the fiber and the crystal channel. It is difficult to reproduce the optimum alignment from run to run.

The first Quarterly Report described the theoretical minimum loss of the terminal. The unavoidable sources of loss include optical beam spreading, an asymmetric beam profile, and a mismatch between the fiber cross-section and the fringing-field channel cross-section (a shape mismatch and a height mismatch). The ordinate in Figs. 5 and 6 is the total optical throughput loss from all sources. The observed fail-safe throughput loss is compared with its theoretical value in Table 2, which also lists modulation results.

## Table 2. Angle Terminal Results

### 3:1 device

Observed loss at V=0 is 10.6 dB total
Theoretical loss at V=0 is 6.6 dB avg. TE + TM
Optical transmission at +50V = 10.6%
Optical transmission at -50V = 8.1%
Depth of modulation, 50V to -50V = 24%

### 4:1 device

Observed loss at V=0 is 9.2 dB total
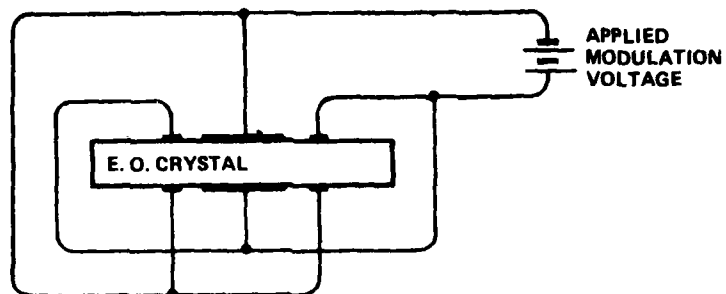Theoretical loss at V=0 is 4.5 dB avg. TE + TM

FIG. 3    Wiring diagram for stripe electrodes on crystal.
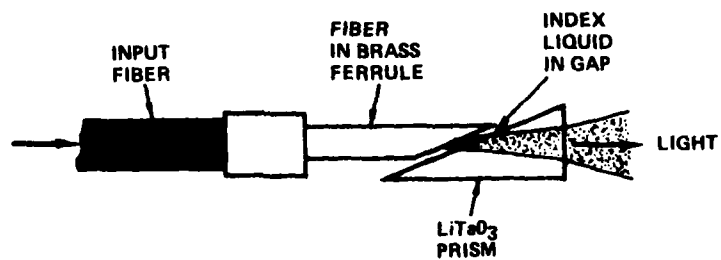


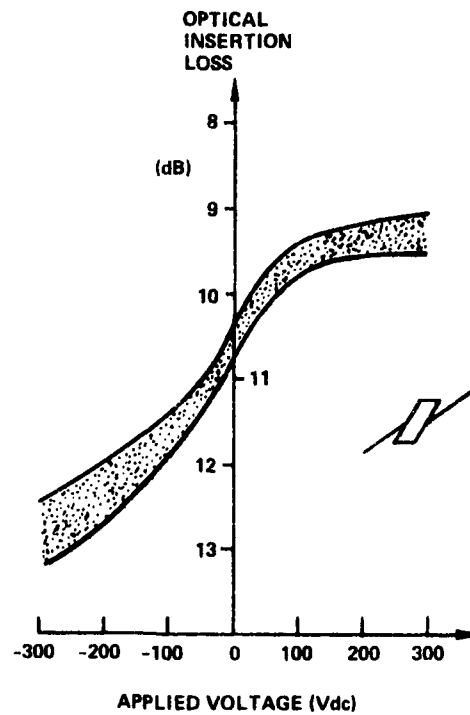FIG. 4    Means for measuring optical power from angle-terminated fiber.

FIG. 5    Total optical throughput loss of three-fold collimated
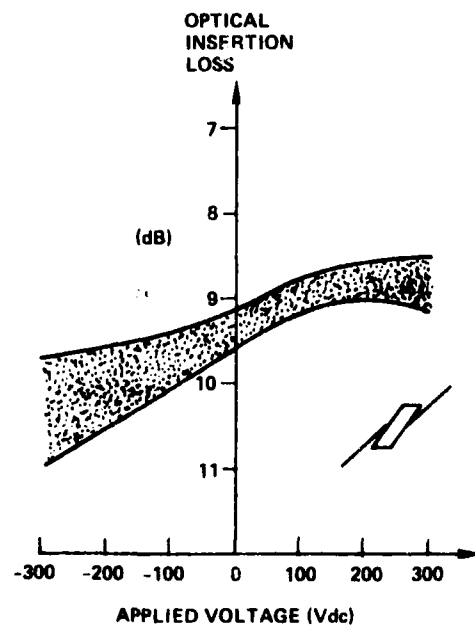terminal coupled to 0.14 NA fibers.



FIG. 6    Total optical throughput loss of four-fold collimated
terminal to 0.14 NA fibers.

-86-
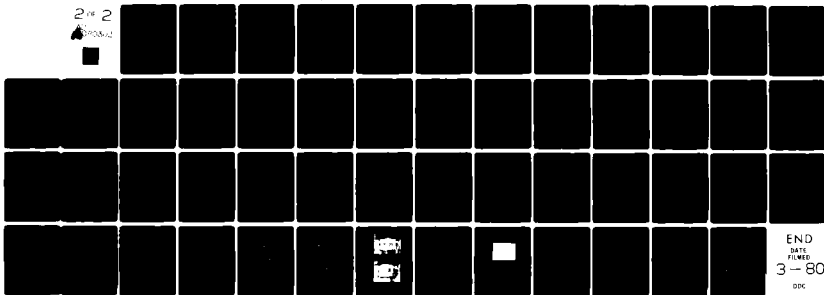
Optical transmission at +50V = 12.9%

Optical transmission at -50V = 11.7%

Depth of modulation, 50 to -50V = 9.3%

The measured loss is 4.7 to 5.0 dB larger than predicted. This excess loss comes from the following sources: flaws in the in/out surfaces of the LiTaO$_3$ crystal, imperfections in the input surface of the second fiber, multiple imperfect reflections off the metal electrode interfaces, and striae and imperfections within the crystal. With further development, it may be possible to reduce the excess loss to 1-2 dB and the fail-safe loss of the 4:1 device to 5-6 dB.

Starting at V=0 and going to V = 300 volts, the optical transmission goes up about 1.4 dB in the 3:1 case and about 0.6 dB in the 4:1 case. In principle, the increase should be greater than this as light becomes confined in the channel. At present, it is not well understood why the light-trapping is incomplete at high voltage.

As Figs. 5 and 6 show, reversing the voltage into the "anti-guiding" regime is effective for modulation. In this way, a large decrease in light transmission is obtained. The greatest change in optical throughput comes with the first 50 volts (approximately) applied in either the forward or reverse voltage regimes. Thus, a useful way to operate the terminal is to bias it at +50V and to apply 100V modulation in the reverse direction. Results for this modulation mode are given in Table 2, where the modulation depths are 24% and 9.3%, respectively.

It was mentioned in QSR-1 that one or two additional fibers would tap data off the optical mainstream. For the angle terminals, we estimate that the optical tap into two fibers would be 3.5 dB below the V=0 throughput in the 3:1 terminal, and 5.0 dB below the V=0 level in the 4:1 case. These tap ratios are -13.8 dB and -14.2 dB referred to the optical input level. The tap ratio is voltage dependent, decreasing in inverse proportion to the modulation.

-87-

## B. PROBLEM AREAS

The angle terminal presents fabrication and alignment pro-
blems: the fiber and crystal ends must be cut at the correct angles, and
the axis of the fiber emission cone must be in the plane of the crystal,
collinear with the electrooptic channel. These fabrication and alignment
operations must be accurate to within a fraction of a degree. From the
loss standpoint (Table 2), the 4-fold collimation is preferred to the
3-fold. Unfortunately, the above alignment problems increase as the
degree of collimation is raised. To summarize, we find that the 4:1 angle-
coupling terminal has the following disadvantages:

- the fail-safe loss is greater than 4.5 dB in theory
  and probably 6 dB in practice
- due to non-normal-incidence fiber coupling, the
  terminal is very sensitive to misalignments and to
  fabrication errors
- the modulation per volt is relatively low
- the fail-safe loss is inversely related to modu-
  lation sensitivity

These problem areas, particularly the insertion loss, led us
to seek a device structure offering improved performance characteristics.

### III. THE MIRROR TERMINAL--A NEW CONCEPT

If the fail-safe loss can be held to 2 dB, then the number
of data-bus terminals can be doubled or tripled relative to the 5-6 dB four-
fold terminals discussed above, so there is motivation for exploring
alternate approaches. Several means for eliminating oblique fiber in-
cedence were suggested in part III of QSR-1, but those means sacrificed
the fail-safe feature or were generally lossy, so they were not pursued
during the second quarter. After considering the problem further, we
conceived of a normal-incidence terminal that has very low loss when the
power is removed. We call this the "mirror terminal".

The idea of the mirror terminal is to focus divergent fiber

-88-

light (the input light) onto an output fiber using a curved reflecting surface on the crystal. In principle, very little light is lost in the process. The focussing is one-dimensional. In the other dimension, light is strongly trapped in a "thin" plate to keep control voltages low.

A. STRUCTURE

The structure is shown in the perspective drawing of Fig. 7 and in the top and side views of Fig. 8. As in earlier devices, the electro-optic material is a Z-cut plate of single-crystal $LiTaO_3$ sandwiched between protective glass plates using an insulating cement. The thickness of the crystal plate (for example, 75 $\mu$m) is chosen to match approximately the core diameter of the multimode fibers in the data bus system.

The input end of the terminal is ground and polished flat. With special grinding equipment, the other end is polished into the shape of a cylinder mirror. A metal coating is evaporated onto this curved surface to make it totally reflecting. Single strands of multimode fiber are butt coupled to the flat end at normal incidence as shown. The fibers include a bus input, bus output, and a local tapoff. To modulate the light passing through the terminal, metal electrodes of the appropriate shape are fabricated on both large surfaces of the crystal plate.

The operation of the terminal is shown in the optical ray diagram of Fig. 9. This is a top view of the terminal (X-Y plane) showing an input fiber and output fiber. Light emerging from the first fiber has a Z-component and makes multiple bounces in a vertical plane (not shown in the Figure). The mirror affects the propagation direction only in the X-Y plane as shown.

The simplest way to operate the device is to combine the input and output surfaces by locating them at the focal plane for 1-to-1 imaging. Mirror theory states that the 1-to-1 plane is located at a distance R from the mirror vertex V, perpendicular to the optic axis O.A.
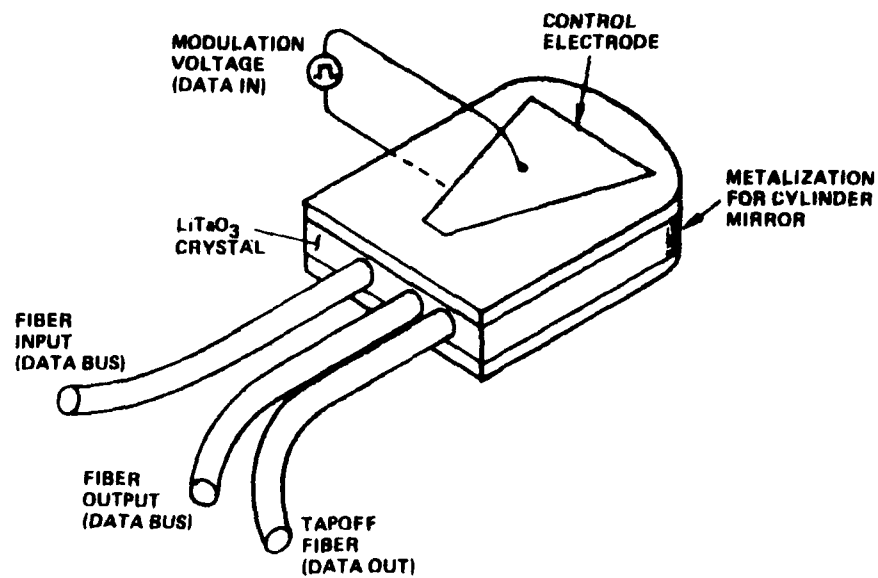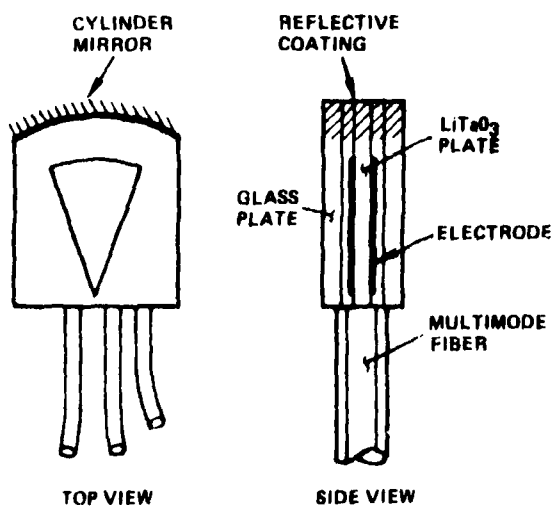
FIG. 7    Perspective view of fail-safe mirror terminal.



FIG. 8    Top and side views of mirror terminal.

-90-

as shown, where R is the mirror's radius of curvature, and R=2F, in which F is the focal distance. Hence, the flat in/out surface passes through the mirror's center of curvature C as indicated in the figure. The mirror has the useful property that an extended object (the fiber face) positioned a transverse distance d from C will be imaged to an extended object of the same size at an equal distance from C on the other side of the optic axis. Thus, the bus fibers are positioned symmetrically about C as shown.

Nearly all the divergent light from one fiber is re-gathered into the other. The focussing works equally well for TE and TM modes, and the desired focussing occurs regardless of how large the NA of the fiber is. Even if the crystal material is anisotropic (birefringent), the perturbation of the focal spot will be relatively small.

There can be several pairs of fibers that transmit at the same time without influencing each other. For example, there could be fibers A,B,C to the left of center and fiber D,E,F on the right with independent transmission paths A-F, B-E, and C-D. The example of simultaneous bidirectional transmission is shown in Fig. 10A.

The terminal is a tapoff device, that is, an active multi-mode directional coupler. The tapoff fiber can be located at one of three places: (1) adjacent to the output fiber, off-axis as in Fig. 7, (2) between the fibers, on the optic axis, and (3) on the optic axis at a small opening in the mirror film. In the third case, a 3-mil-diameter region of metal is removed from the mirror vertex and the tapoff fiber is butt coupled to the cylinder at that point. There the amount of light tapped off will not be changed greatly by the modulation voltage, so the tap is voltage independent.

It is also possible to have a voltage-dependent tap as shown in Fig. 7. There, the optical intensity in the tap fiber will swing from a small value at zero voltage to a much larger value at the designated modulation voltage. The terminal is "not listening" when the
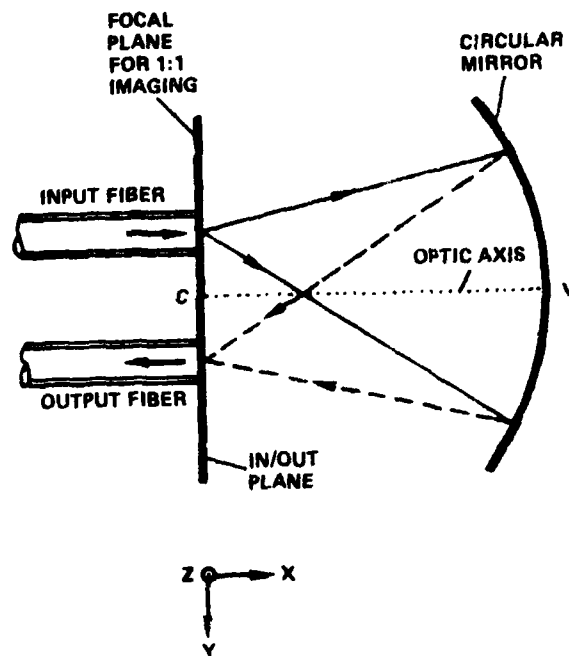
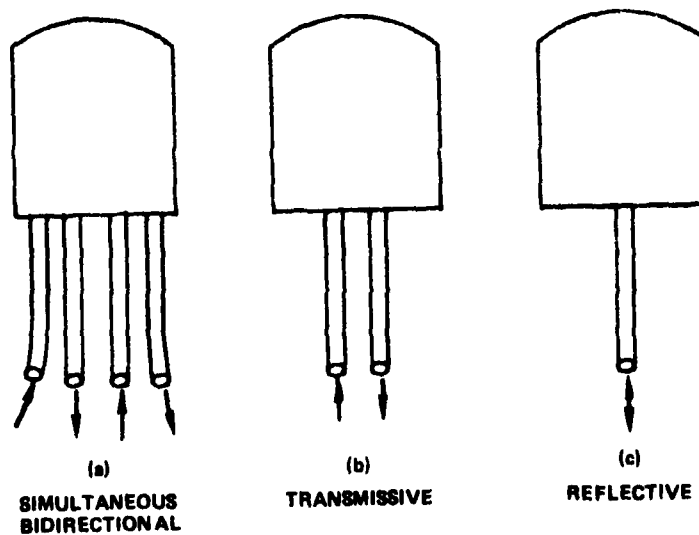FIG. 9    Optical ray paths within terminal.



FIG. 10    Three available operating modes for mirror terminal.

voltage is off, and this means the bus will not be loaded optically in that mode. The terminal will receive data when a dc potential is applied to the control electrodes. It is interesting to note that the voltage-dependent tap is a multimode optical switch, and that electrodes can be designed to make the mirror terminal perform multi-pole optical switching or multiplexing, if desired.

The modulation electrodes function by diverting or deflecting light rays from their paths in Fig. 9. This diminishes the amount of light that reaches the output fiber, thereby modulating the throughput. Voltage applied to the electrodes perturbs the TM modes through the $r_{33}$ electrooptic coefficient. The perturbation of TE modes is about 25% as strong through the $r_{13}$ coefficient. The estimated response of the mirror terminal to voltage is shown in the schematic graph of Fig. 11 for bus and tap fibers. Note that the terminal is definitely fail safe, with the optical transmission reaching its highest value at zero voltage.

A serial data bus is readily constructed using mirror terminals in the manner shown in Fig. 12, which illustrates two Tee-coupler terminals in the series array. As discussed in QSR-1, the overall link structure is an optical loop driven by one LED or laser source. An important feature of the system is that optical sources are not needed at the individual terminals. Electrical impulses on the terminal electrodes put optical data onto the bus. Data on the bus is sampled locally by the tap fiber at each terminal that feeds a photodetector. Note that the detector (a small, solid-state diode) could be directly butt coupled to the terminal, omitting the tap fiber.

The mirror terminals are optically symmetric and bidirectional. The terminal can function in a transmissive mode (Fig. 10B) or in a reflective mode (Fig. 10C) in which one fiber located on the optic axis serves as the transmission line for both directions. All three devices in Fig. 10 are modulatable and tapable. In addition, a branching-type mirror terminal can be built with one input and two
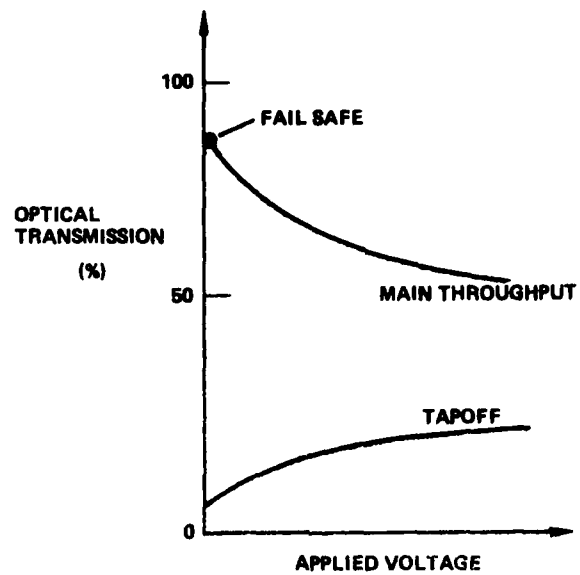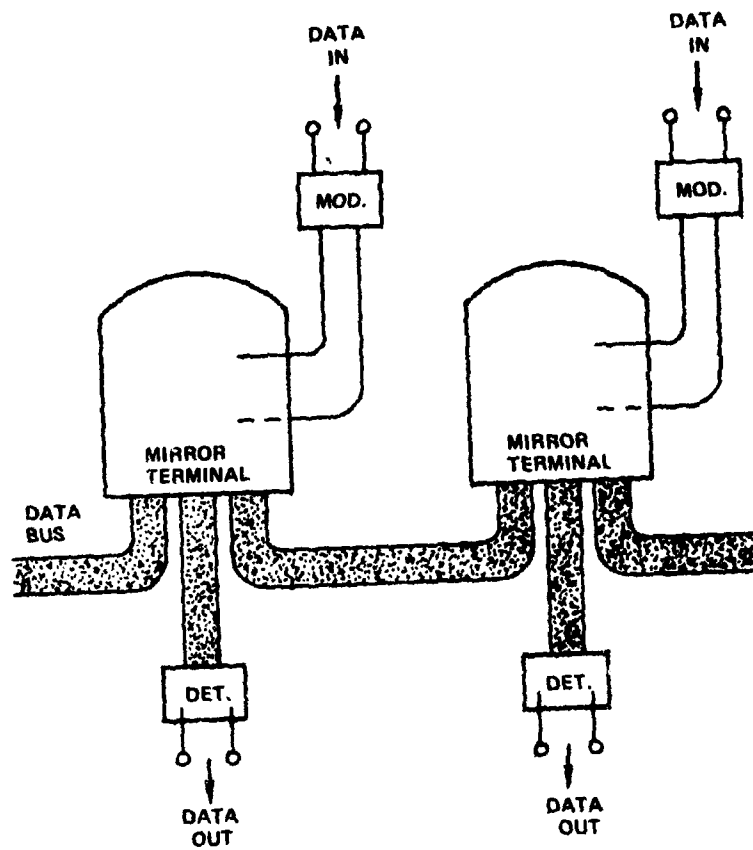
FIG. 11  Anticipated effect of modulation voltage.

FIG. 12   Portion of fail–safe data link.

equal-power outputs modulated in unison, which is like a modulated star coupler.

## B. INSERTION LOSS CALCULATION

Theoretically, the optical losses are quite low. One un-avoidable loss is mirror loss. For red light ($\lambda$ = 0.63 $\mu$m), the follow-ing reflection losses exist for the popular mirror coatings: chromium, 17.8% reflectance, 7.50 dB loss; aluminum, 80.0% reflectance, 0.97 dB loss; copper, 92.6% reflectance, 0.34 dB loss; gold, 92.0% reflectance, 0.36 dB loss. Thus, copper and gold are preferred. Irreducible loss also comes from distortion in the focal spot shape. To illustrate this, consider what happens when a laser beam is focussed to a tiny spot at the terminal input (Fig. 13A). Because the mirror focusses light in only one dimension, the "point" input is transformed into a line focus. Similarly, as in Fig. 13B, a circular fiber input turns into a rectan-gular output. This means some of the exit light will not be captured, assuming the output fiber has the same circular cross-section as the input. A similar coupling loss occurs if the input fiber has a greater core diameter than the plate height. The height-mismatch and shape mismatch loss is about 1 dB for a fairly wide range of crystal thick-ness (65 to 85 $\mu$m) as spelled out in Table 1 of QSR-1. A third but smaller loss is in/out relection loss at the fiber/crystal interface which can be kept below 0.3 dB by injecting an anti-reflection liquid (intermediate index) in the small fiber/crystal gap. Theoretical loss from the above three sources is about 1.6 dB.

We believe that the optical scattering losses that arise in a real terminal (excess loss) can be held to about 1 dB by careful construction. Putting this scattering loss together with the above theoretical loss, we expect it will ultimately be possible to have a total optical insertion loss of about 2 dB for these terminals.
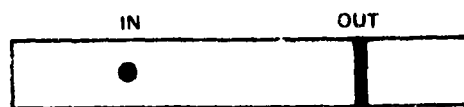
FIG. 13    End-view of mirror terminal showing incident and
emergent optical beam shapes.

## C. ADVANTAGES

The advantages of the mirror terminal  discussed above can be summarized as follows:

- fail-safe operation;
  highest throughput at V=0

- very low insertion loss,
  1-2 dB in principle

- normal-incidence butt-coupling
  of fibers

- easy to align terminal

- works for any fiber NA

- tapoff can be voltage dependent
  or constant if desired

- modulation sensitivity should be
  relatively high

- simple, compact,
  rugged construction

- device is bidirectional

- works reflectively with one
  in/out fiber if desired

## D. PRELIMINARY EXPERIMENTS

A motor-driven polishing apparatus is being constructed presently for grinding high-quality cylinder mirror surfaces as an integral part of the crystal sandwich.  While awaiting this equipment, we tried to see what could be done with an external mirror and a rudimentary polish on the curved crystal end.

We have demonstrated and tested the mirror-terminal concept with the set-up shown in Fig. 14.  The device was a 2.8 mil Z-cut plate of LiTaO$_3$ laminated between two glass microscope slides with 1-mil-layers of glycolpthalate.  One end was polished flat and the other end polished by hand into a cylinder shape with a 2.5 cm radius of curvature.  The sample was cemented to a 5 cm diam brass cylinder and polished with five
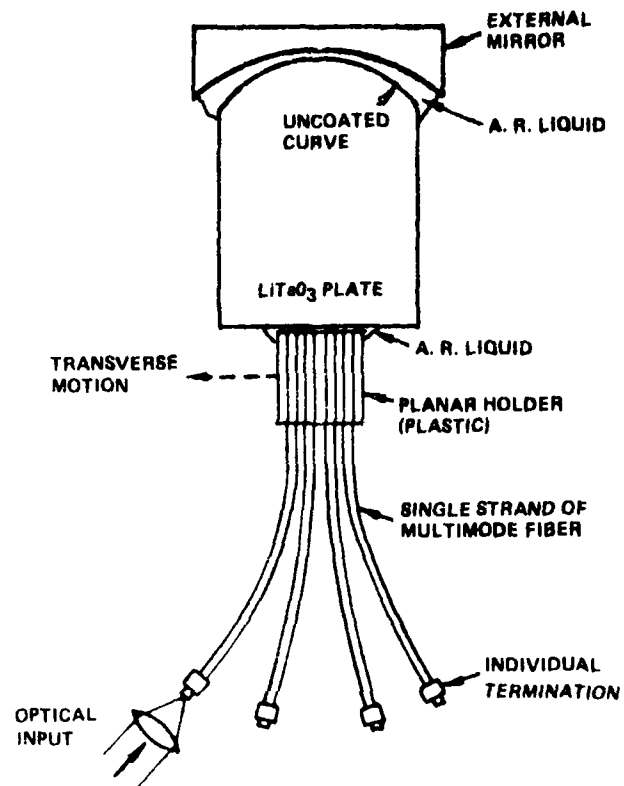
-98-

FIG. 14  Layout of external mirror terminal and multiple fiber coupling.

descending grit-sizes.  A concave aluminum-coated mirror from Edmund's Scientific was snugged against the crystal's curved end.  The mirror was spherical and it was self-centering when pressed against the smaller-radius crystal.  The mirror had a 3.2 cm radius of curvature, and the length of the crystal from vertex to flat was also 3.2 cm.  There was a 1-mil gap between mirror and crystal that was filled with an $n=1.63$ fluid to reduce reflections.

The fibers were 0.14 NA Corning step index with an 85 $\mu$m core. A linear (planar) array of four parallel fibers was prepared as shown in the figure.  The fibers were spaced 6 mils on centers on one end of the array and individually terminated at the other.  The array termination was attached to an x-y-z micromanipulator and the mirror device placed on a rotary tilt-table.  With an A.R. liquid intervening, the fibers were contacted to the terminal as shown.  Using a 40x objective, red laser light was focussed into fiber #1 and the outputs of fibers #2,3,4 examined.

E.  RESULTS

By positioning the fiber array at various transverse loca-tions, the optical output could be peaked up on either fiber #2, #3 or #4.  Moving the array to get maximum output on fiber #2, we found that the overall insertion loss was 6.7 dB, which is the optical throughput loss from all contributions.  The optical output from fiber #3 was 19 dB below #2, and #4 was 24 dB below #2.  The 6.7 dB loss is expressed rela-tive to the total light output from fiber #1 which was determined in a separate measurement with the terminal removed.  In this external mirror device, where the mirror surface is aluminum and the mismatch between fiber and crystal is 85 $\mu$m: 65 $\mu$m, the predicted $V=0$ loss is 2.0 dB.

We observed stray light coming from the crystal-to-mirror interface, and in a laser reflection experiment, we found that the

terminal's line focus was not completely sharp. Therefore, we feel that the 4.7 dB excess loss here comes from interface scattering and an imperfect focus in the in/out plane. Both of these difficulties can be remedied.

The observed 6.7 dB fail-safe loss is an encouraging result for two reasons: it is already 3 dB lower than the best result for the angle terminal, and it is amenable to significant reduction, hopefully with an internal mirror.

## IV.  PLANS FOR THE NEXT QUARTER

The general plan is to proceed with the development of the mirror terminal. The agenda for the next quarter consists of the following specific tasks: completion of the mirror grinding machine, debugging of the machine, construction of terminals with internal mirrors, design of photoresist masks for modulation electrodes, construction of a modulated terminal, and evaluation of these electro-optic mirror devices.

APPENDIX C

INVESTIGATION INTO THE FEASIBILITY

OF DESIGNING A FAIL SAFE OPTICAL DATA LINK

Quarterly Status Report No. 3
CONTRACT NO. F19628-77-C-0055

Sperry Research Center
100 North Road
Sudbury, Massachusetts 01776

SCRC-CR-77-73
1977 October 15

Prepared for
ROME AIR DEVELOPMENT CENTER
DEPUTY FOR ELECTRONIC TECHNOLOGY
HANSCOM AIR FORCE BASE
BEDFORD, MASSACHUSETTS 01731

# TABLE OF CONTENTS

## LIST OF ILLUSTRATIONS

Investigation into the Feasibility of Designing a Fail Safe Optical Data Link

## I.  INTRODUCTION

The objective of this program is to investigate and develop a
data terminal suitable for use in constructing a highly reliable multi-
terminal optical data link system.  This reliability is achieved through the
development of a terminal structure that allows the link to continue in
operation if the power fails at an individual terminal.  The specicic data
bus system is a daisy chain which uses single multimode fibers for the
terminal interconnects as shown in the first Quarterly Status Report.  Each
individual terminal includes an electro-optic device that can impress
information onto the data stream or monitor the data already on the channel
and, if power failure does occur, allows adequate optical power to pass
through the terminal with zero applied voltage.

This report covers the third three months of effort on this
contract:  July 1 through October 1, 1977.  During this period we have pro-
ceeded with device construction and testing on both the angle collimation
terminals and the newer mirror terminal structure.  The results on the angle
collimation terminal have been improved to the point that one device comes
close to meeting all contract goals, and requires an anti-reflection coating
to meet the goals.  The results on the mirror terminals are more preliminary,
but the main device concepts have been verified.  Modulation measurements
have been made, and 32% modulation depth was obtained for 50 V.

## II.  ANGLE COLLIMATION TERMINALS

In the second Quarterly Status Report (QSR-2),[1] we reported on the
performance of two fail safe terminals using 3:1 and 4:1 angle collimation.
At that time there was a fairly significant gap between theoretical and
experimental throughput loss (approximately 3 dB) with V=0.  In addition the
light gathering ability with an applied voltage was significantly lower than
predicted, in that the amount of light captured in the induced electro-optic

guide did not increase once the applied voltage exceeded approximately 100 volts. Since this collimation design should theoretically have characteristics that are quite favorable for the contract requirements and since the previous devices had unexplainably poor performance, some additional effort was applied in this area in order to resolve the previous discrepancies. To summarize the results obtained and reported on in this section, we have not found the precise explanation for the relatively high throughput losses measured with some angle collimation devices, although one possible cause is suggested. However, one additional device was constructed and tested this past quarter that did perform in agreement with theoretical predictions, and thus it is possible to use this design for the fail safe terminal.

## A. THEORETICAL LOSSES WITH V=0

The major contributions to the throughput loss of the collimation fail safe terminal have been explained in QSR-1 and QSR-2, and we review these results in this section. The most important loss component is due to the light emitted at a large angle from the fiber direction so that the rays miss the output fiber and are therefore uncollected (see Fig. 1). This loss obviously depends on the fiber NA, collimation factor, fiber core diameter, and the length of the crystal. A simple geometric diagram such as Fig. 1 can be used to estimate this loss. However, such an analysis is somewhat too simplified in that the variation of reflection loss with angle, the variation of the collimation effect with angle, and the circular nature of the emitting fiber are not taken into account. A computer program using ray tracing and taking into account the above effects has been developed,[1] and results obtained for a variety of device and fiber parameters. The most recent collimation device tested (LT-10) was 2.8 cm long, used three-fold collimation and was designed for a .15 NA. The computer results for this situation are shown in Fig. 2, which gives the output light intensity distribution at the end face of the crystal for both TE and TM polarizations. By measuring the area under the curves intercepted by the output fiber (core diam = 85 μm) and dividing by the total area under the curves, a relatively accurate estimate can be made of the throughput loss due to
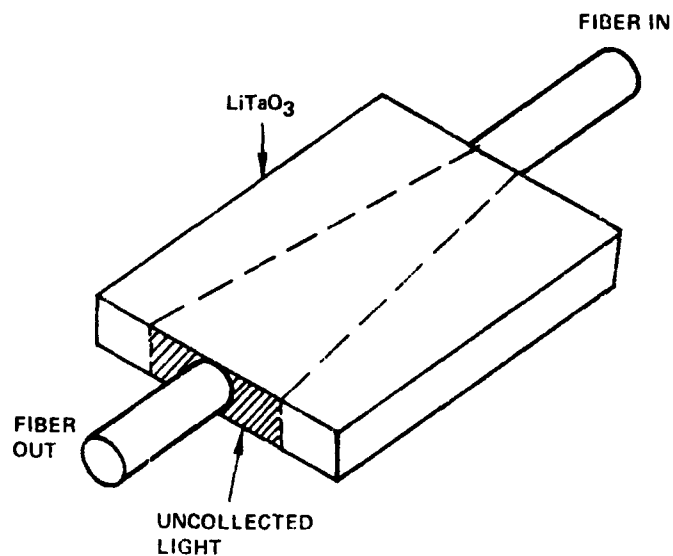
FIG. 1    Simplified diagram of device showing uncollected light.
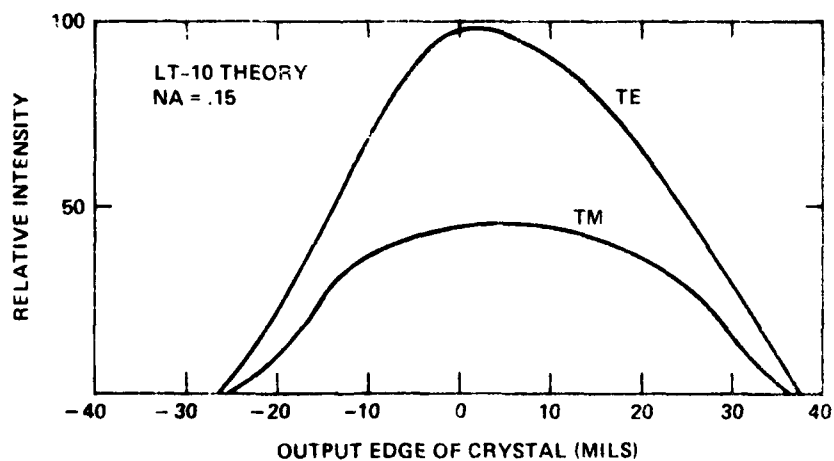Electrode pattern and non-normal incidence butt coupling
are not shown.



FIG. 2    Computer results for LT-10 output.

the spreading of the light emitted from the input fiber. For the case of LT-10 shown in Fig. 2, this loss is about 5 dB for TE light and 5.4 dB for TM light.

If there is not an anti-reflection coating on the ends of the crystal, the next largest loss component is due to reflections at the two crystal interfaces. The total (two interfaces) reflection loss for TE and TM modes and three- and four-fold collimation is tabulated in Table 1. The results are given in dB and assume that the index transition is from 1.47 (glass) to 2.18 ($LiTaO_3$). However, by inserting a higher index fluid between the fiber and crystal, it is possible to greatly reduce these reflection losses. For normal incidence the appropriate "anti-reflection index" is the mean of the two extreme indices, i.e., $n = \sqrt{n_1 n_2} = \sqrt{(1.47)(2.18)} = 1.79$. However, at non-normal incidence, the angle of incidence upon the fluid from the glass is much greater than the angle of incidence upon the crystal from the fluid. Therefore, the optimum index for the fluid is weighted more heavily toward the glass index. Calculations show that n 1.62 yields the lowest total reflection loss, and this loss is shown in Table 1 in parentheses. LT-10 used three-fold collimation, so that the total reflection loss with the fluid in place is .64 dB for TE modes and 2.4 dB for TM modes.

The third largest loss component is the size mismatch between the crystal and fiber, and the related shape mismatch between the rectangular crystal and the circular fiber (see QSR-1, Table 1). The actual thickness of LT-10 is 90 $\mu$m which is a fairly good match for the 85 $\mu$m diameter fiber. From Table 1 of QSR-1 the loss is estimated to be 24% or 1.2 dB.

Adding the effects of the three main loss components as shown in Table 2 yields 9 dB for TM and 6.8 dB for TE polarization, or approximately 7.8 dB average. In addition to these unavoidable loss components described above, there may also be some losses due to imperfections in the device construction, such as a slight rounding of the crystal edges, small scratches or chips in the crystal, and defects in the fiber end finish. For a well constructed device these effects should be small ($<$ .5 dB).

-109-

|      | 3-Fold | 4-Fold |
|------|--------|--------|
| TE   | 1.0 (.64) | 2.1 (1.6) |
| TM   | 4.4 (2.4) | 6.2 (3.6) |

Table 1. Reflection loss in dB after two glass/crystal
interfaces. Numbers in parentheses assume
$n = 1.62$ anti-reflection fluid.

|                      | TE  | TM  |
|----------------------|-----|-----|
| Spread Loss          | 5.0 | 5.4 |
| Reflection Loss      | .6  | 2.4 |
| Size & Shape Mismatch | 1.2 | 1.2 |
|                      | —   | —   |
| TOTAL                | 6.8 | 9.0 |

Average = 7.8 dB

Table 2. Summary of loss components (in dB) for $V = 0$.

## B. THEORETICAL LOSS WITH APPLIED VOLTAGE

A precise calculation of the throughput loss with an applied voltage requires much more effort than for the V=0 case. In particular, it is necessary to know the shape and strength of the fringing electric field precisely and then perform a complicated ray tracing for a two-dimensional system without circular symmetry. Exact solutions for the electric field in the dielectric are not possible to obtain, and the ray tracing in the two-dimensional graded index system is very complicated due to the asymmetry and requires extensive numerical calculations. A simplified calculation consideringonly ray motion in the plane of the crystal has been used for devices with normal incidence butt coupling. These calculations seem to indicate that the distribution shown in Fig. 3 will yield a good approximation to the real case. The device structure assumed is the "triple-stripe" geometry[1] as was used for LT-10 and shown in Fig. 4. The width W of the central stripe is the fiber core dimater times the collimation factor, or $3 \times 85 \ \mu m = 225 \ \mu m$ for LT-10. The guard channel electrodes are separated by an additional crystal thickness t from the central electrode to prevent electrical breakdown. Using a voltage sufficient to "capture" all of the TM light (approximately 100 V for LT-10), then results in the approximate light distribution shown in Fig. 3, with the light intensity falling from a maximum to zero in the "fringing field" region, whose width is approximately equal to the thickness of the crystal. The same approximate light distribution can be used for one-half of the TE light, since it is understood that the other one-half of this polarization is not captured by the electric field and is lost from the system.

The purpose of the above discussion is to obtain an expression for the throughput loss due to the light "captured" in the fringing field but lost to the output fiber. Using Fig. 3, we can estimate that this loss is $W/(W+t)$ or, for LT-10, 1.3 dB for TM and 1.3+3 dB = 4.3 dB for the TE polarization. In addition, there are the same reflection and size mismatch losses as before with V=0, so that the total losses (Table 3) are 5.5 dB. The actual voltage required to achieve this loss may be somewhat more than
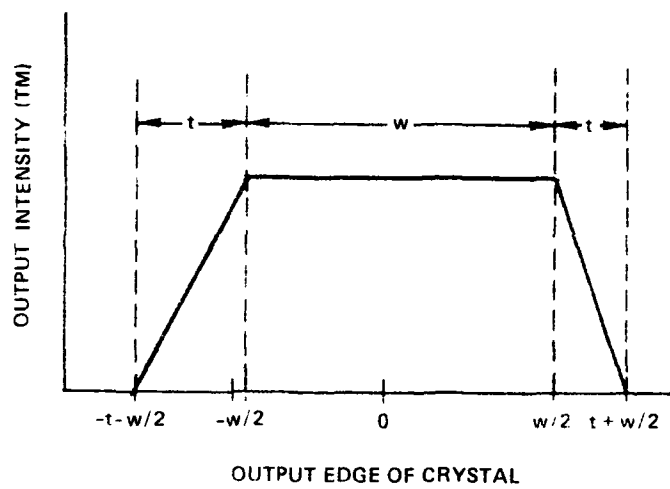
FIG. 3    Approximate output intensity distribution with applied voltage.
w = width of center electrode and
t  = thickness of crystal.



TOP VIEW

EDGE VIEW
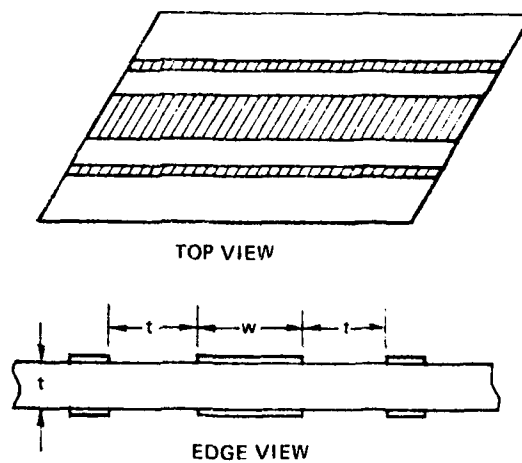
FIG. 4    Triple stripe electrode geometry used for LT-10.

|                        | TE   | TM   |
|------------------------|------|------|
| Fringing Field         | 1.3  | 1.3  |
| Not Captured           | 3.0  | 0    |
| Reflection Loss        | .6   | 2.4  |
| Size & Shape Mismatch  | 1.2  | 1.2  |
| TOTAL                  | 6.1  | 4.9  |

AVERAGE = 5.5 dB

Table 3. Summary of loss components (in dB) for
         $V \approx 120$ volts (LT-10).

100 V (for LT-10) since the actual fringing field distribution, and hence the light distribution, does not drop to zero after a distance of one crystal thickness, but rather falls to about 20% of the peak value. Thus, approximately 120 V is required for LT-10 for complete capture of the TM light, and further increases in voltage will continue to capture more of the TE light.

## C. EXPERIMENTAL RESULTS FROM LT-10

The preceding two sections have outlined the theoretical throughput losses expected for a collimation fail safe terminal with specific results calculated for a particular device LT-10. In Fig. 5 the throughput is given as a function of applied voltage for LT-10. In addition, we also present the theoretical throughput calculated for V=0 and estimated as a function of applied voltage in the manner outlined in the preceding section. For this device we have obtained very reasonable agreement between theory and experiment.

In Table 4, we summarize the results obtained with LT-10 and compare with some of the goals set for this contract. As can be seen from the table, the present results are close to the desired goals. However, since the performance of LT-10 is at its theoretical maximum, there is no possible further improvement in performance by improved construction techniques alone. Losses can be reduced further only by addressing the three major components responsible for the observed loss: loss due to the natural spreading of the light (V=0) or the fringing field (V≠0), size and shape mismatch loss, and reflection loss.

The spreading loss (V=0) is a function of a number of parameters such as fiber NA and device length as explained in Sec. 2.A. This contribution to the total throughput loss can be lowered arbitrarily by shortening the crystal or increasing the collimation factor. However, these procedures do not improve the performance of the device with the guiding voltage applied, since the main loss component when $V = 100$ V is due to the fringing electric field. Therefore, reducing the free spreading loss for V=0 merely
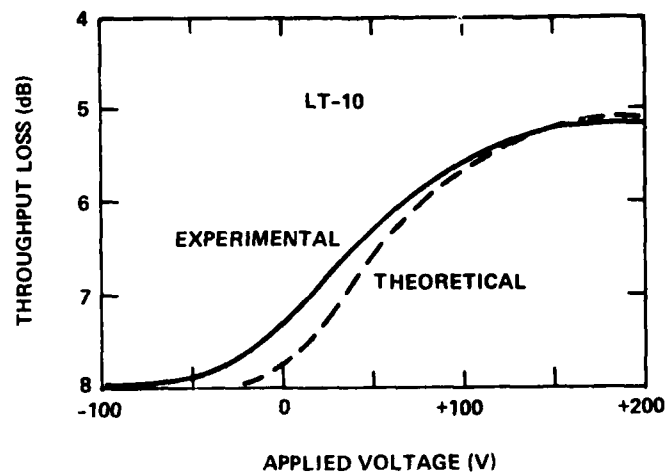
FIG. 5    Theoretical and experimental throughput loss vs. voltage for LT-10.

|                        | Goals | Collimation Terminal (LT-10) |
|------------------------|-------|------------------------------|
| Loss (V=0)             | 6 dB  | 6.3 dB                       |
| Loss (V on)            | 4 dB  | 5.6 dB                       |
| Modulation Depth       | 38%   | 32%                          |
| Voltage                | 40 V  | 100 V                        |

Table 4.   Comparison of contract goals with performance
of LT-10.

-115-

lowers the device modulation depth and does not improve the performance of the terminal in the normal state of operation with V on.

The second factor, size and shape mismatch loss, can be improved slightly by matching the crystal thickness and fiber diameter more perfectly. As shown in QSR-1, the optimum thickness for an 85 $\mu$m core diameter fiber is about 75 $\mu$m. However, this results in a loss of 1.0 dB as opposed to 1.2 dB for LT-10, so that the improvement is small.

The third factor cited above, reflection loss, affects both the V off and V on states of the device identically and therefore is capable of reducing the throughput loss in a useful manner, i.e., without affecting the modulation depth. At present, an anti-reflection fluid layer (n=1.62) of arbitrary thickness is used to reduce losses. However, a 1.62 index layer with an optimum thickness of 3000 Å can be used to obtain cancellation of the reflected wave still further. Figure 6 shows the calculated percent reflection as a function of input angle for an anti-reflection coated crystal with four-fold collimation and a fiber incident angle of 79$^{\circ}$. The half angle in glass for a .15 NA fiber is 5.8$^{\circ}$, and thus the light cone range is from 73 to 85$^{\circ}$. For this range of angles we can calculate that the total reflection loss is well under .5 dB. Figure 7 gives the reflection coefficient as a function of the refractive index of the anti-reflection layer. There is a wide range of indices (1.55 to 1.70) that will still yield a low reflection coefficient. Thus, with this anti-reflection coating, the performance characteristics shown in Table 4 would be improved sufficiently to meet the goals set for throughput loss both with V on and V off.

The possibility of anti-reflection coatings is being investigated at this time. It appears that SiO is a good candidate for an evaporated coating of the proper index on the edge of the crystal. There may be some problem in cleaning the crystal edges properly before evaporating the SiO, and this construction problem is being addressed.
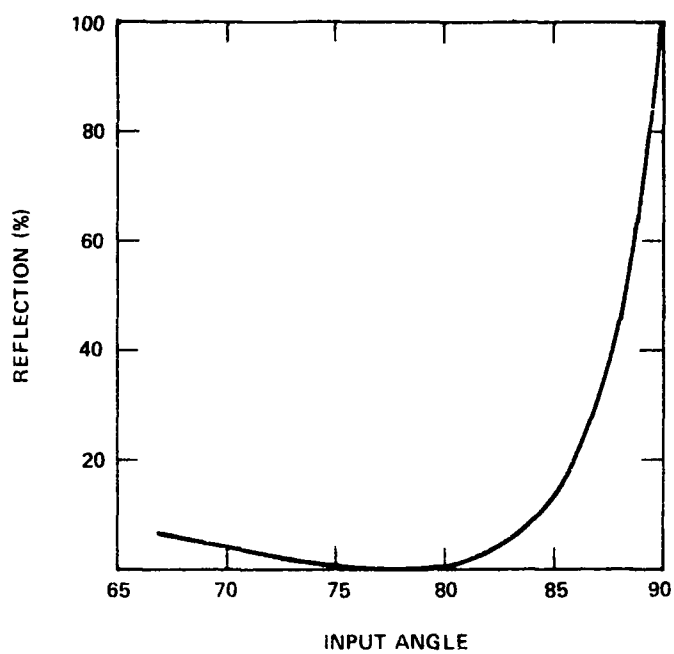
-116-

FIG. 6    Reflection vs. fiber input angle for LiNbO₃ with AR coating.
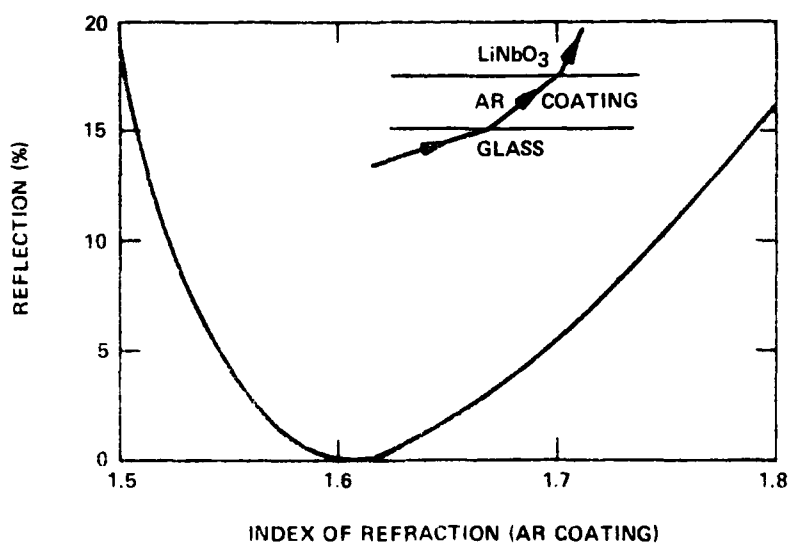


FIG. 7    Reflection vs. index of refraction of AR coating.

-117-

D. STATUS OF ANGLE COLLIMATION TERMINALS

One uncertainty that must be resolved before proceeding with the angle collimation terminals is the possible lack of reproducibility in constructing or testing these devices. Several of the terminals have been made thus far: one with two-fold collimation, two with three-fold collimation, and one with four-fold collimation. Only one device, LT-10, has been measured to have performance in agreement with theory while, as described in QSR-2, the performance of two earlier devices had throughput losses approximately 3 dB higher than theory. One possible explanation is the alignment difficulty encountered in using the angle collimation devices. The proper positioning of each fiber relative to the device requires the correct simultaneous alignment relative to three coordinate positions and three angular degrees of freedom. In particular, for large incident angles, the precision required to properly align the input and output fibers is increased greatly over the case of normal incidence. Thus, it is possible that the devices made previously are functioning properly but that the correct alignment was not obtained during testing.

The second area for further work is the use of anti-reflection coatings. Such coatings seem feasible if the edges of the crystal can be cleaned properly after most of the other device fabrication steps have been completed. As explained before, with these coatings the device performance will equal the contract goals with total throughput losses of only 4 dB. However, to some extent the amount of effort expended on the anti-reflection coatings and the angle collimation devices, in general, will depend on the success obtained with the mirror terminal structure, as discussed in the next section.

# III. MIRROR TERMINALS

The mirror terminal concept was introduced in QSR-2 and a theoretical description was given of the device operation including throughput losses. For completeness, we reproduce here two figures from QSR-2, Figs. 8 and 9, showing the design of the mirror terminal. The operation is straightforward: the light from an input fiber freely spreads in the plane of the crystal, strikes the circular mirror at the far end of the crystal, and is reflected and focused back into the output fiber. An appropriate electrode pattern is used to spoil the focus and hence produce modulation in response to an applied voltage.

During the past quarter, an electrode pattern has been designed and additional terminals have been constructed and tested. Before describing those results, we discuss in more depth the theoretical losses typically encountered using the mirror terminal concept.

## A. THEORETICAL THROUGHPUT LOSSES

As described in QSR-2, there are several mechanisms responsible for an inherent throughput loss using the mirror terminal. A gold coating for the mirror yields approximately .4 dB loss upon reflection. Again there will be a height and shape mismatch loss of approximately 1 dB as described in detail in QSR-1. Also, there is a reflection loss taken twice at the input and output fiber interface with the crystal. In addition, if an external mirror is used, there are two more reflections for a total loss of about .6 dB.

The fourth loss component is illustrated in Fig. 10 and is due to the finite numerical aperture of the fibers used. As shown in the drawing, the reflected light cone from the mirror strikes the output fiber at an angle relative to the normal entrance light cone of the fiber, so that some of the light will enter at too large an angle for capture by the fiber and will be lost. This loss has been estimated using simple formulas derived from Fig. 10, and the results are shown in Table 5 for a fiber NA of .15 and device radius R=1". For small separations of less than 15 mils, the loss
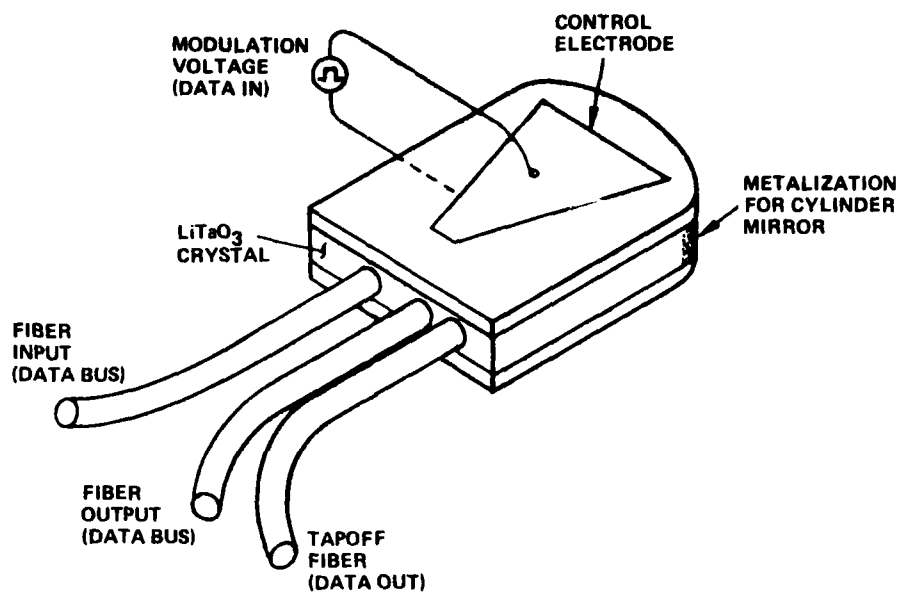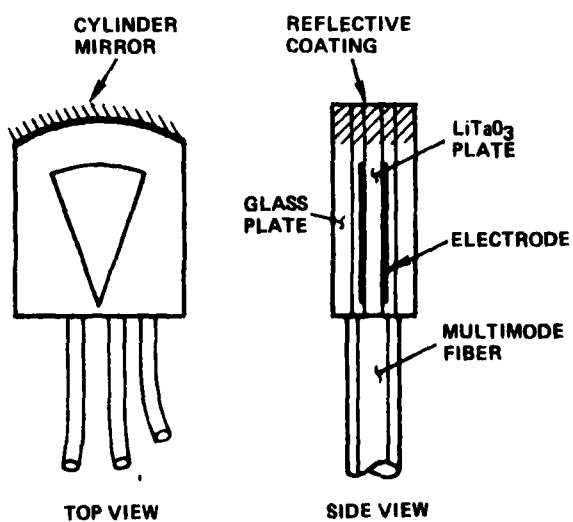
FIG. 8    Perspective view of fail-safe mirror terminal.



TOP VIEW                    SIDE VIEW

FIG. 9    Top and side views of mirror terminal.
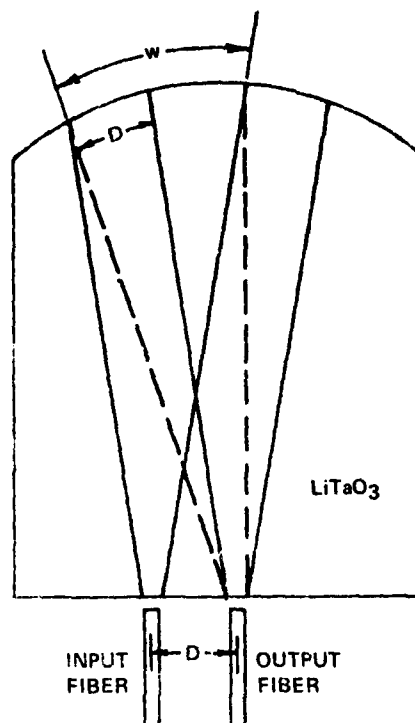
FIG. 10    Throughput loss due to finite numerical aperture of output
fiber.

| D(mils) | Loss(%) |
|---------|---------|
| 5       | 3.3     |
| 10      | 6.7     |
| 15      | 10.0    |
| 20      | 13.0    |
| 30      | 20.0    |

$$Loss = D/W$$

$$W = \left(\frac{2 \times N.A.}{n_{LT}}\right) \times R \approx N.A. \times R$$

$$N.A. = .15 \qquad R = 1"$$

Table 5.    Throughput loss due to center-to-center separation D
between input and output fibers.

is less than .5 dB. This loss can actually be avoided entirely if the fibers are appropriately tilted but, for the present, the fiber terminations are made with all fibers parallel.

The above losses are summarized in Table 6, 2.2 dB total for a mirror evaporated on the crystal face and 2.5 dB for an external mirror. These losses are felt to be "inherent" losses in that they are unavoidable using the mirror terminal structure, as opposed to losses that are due to imperfections in construction.

There will be other losses present that can be minimized as the construction techniques are perfected. Figure 11 illustrates the loss due to missed focus of the light cone on the output fiber. In this case it arises from the fact that the length of the crystal exceeds the radius of curvature of the mirror by a distance d. This situation may also arise with an external mirror if the radius of the external mirror is shorter than the crystal length. Table 7 gives the losses as a function of the error d for two different fiber core diameters, fd = 3.3 mils and 10 mils. As can be seen from the table, the losses are quite serious for the small core 3.3 mil fiber, with losses greater than 1 dB for only a 4 mil error in focus. The 10 mil fiber yields losses less than one-half the smaller fiber.

A similar situation arises if the crystal length is shorter by a distance d from the mirror radius of curvature. In this case the fibers can be adjusted correctly for focusing, but the focal plane position is a distance d away from the edge of the crystal. This leads to a relatively severe loss due to the spreading of the light perpendicular to the plane of the crystal. Again, the percentage loss is much lower for the larger fiber diameter.

Previously in our program, we had considered only the small core, 2 to 4 mil diameter, all-glass fibers for use with crystals of comparable thickness. However, as shown by the previous calculations, the misalignment losses are considerably lower when using a large core diameter fiber, as might be expected. The main drawback to this approach, however, is that the voltage required for modulation should be directly proportional to the
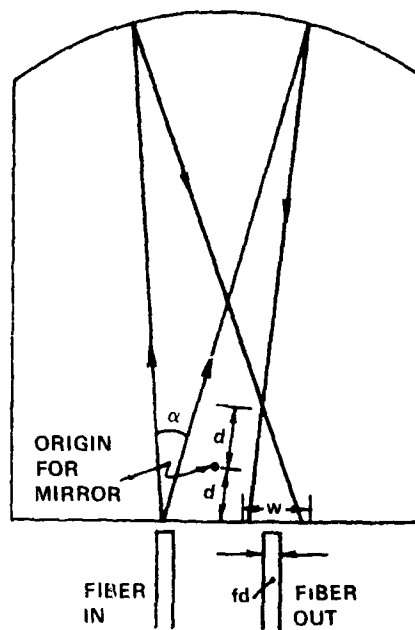
$$w = 4d \tan\alpha + fd$$
$$LOSS = fd/w$$

FIG. 11   Error caused by crystal length exceeding mirror radius of curvature.

| MINIMUM MIRROR TERMINAL LOSSES | |
|---|---|
| Reflection (gold mirror) | .4 dB |
| Size & Shape Mismatch | 1.0 dB |
| Crystal Interface Reflections | .3 dB |
| (with external mirror) | .6 dB |
| Numerical Aperture Loss (typical) | .5 dB |
| TOTAL | 2.2 dB |
| (2.5 dB with external mirror) | |

Table 6.   Unavoidable losses associated with mirror terminal design.

| Deviation, d(mils) | Loss (%) | |
|---|---|---|
| | fd = 3.3 mil | fd = 10 mils |
| 1 | 7 | 3 |
| 2 | 13 | 5 |
| 4 | 23 | 10 |
| 6 | 31 | 15 |
| 10 | 43 | 20 |

$$\alpha = 3.6^{0}$$

$$W = 4d \tan\alpha + fd$$

$$Loss (\%) = fd/W$$

Table 7. Loss due to missed focus. See Fig. 11.
fd = fiber core diameter.

-124-

thickness. Therefore, if 50 V is required to obtain adequate modulation depth with a 3 mil crystal, 150 V will be needed for a 9 mil crystal. There are three possible remedies for this situation: (1) the actual voltage required may be lower than cited above, (2) the criterion for "adequate" modulation depth may be lowered and (3) new driving techniques may be used which effectively lower the required voltage. At this point we feel that the 10 mil crystal represents a possible means for obtaining low throughput losses, and such devices have been built as will be described later. It is not definite that means will be found to alleviate the high voltage require- ments, but the approach has enough promise to be pursued further.

## B. EXTERNAL VS INTERNAL MIRROR

Thus far in the program, several devices have been made with external and internal mirrors. In most cases, it appears that the devices using an external mirror operate with lower throughput loss. A model of the reflection process will be presented here that attempts tr explain the throughput loss related to reflection as due to imperfections in the crystal end face.

Imagine a small portion of the mirror end of the crystal that is mis-oriented at a small angle $\theta$ relative to its correct orientation for proper reflection. If an internal mirror is used, that is, if the end face itself is to be used as the mirror, then the directional misalignment from this small section will yield an error in the light ray direction of $2\theta$.

This error of $2\theta$ must be compared with the external mirror case diagrammed in Fig. 12. The surface misalignment by the small angle $\theta$ will now cause the incident ray at $\theta_1 = 0^0$ to be refracted to a new direction $\theta_2 = (n_1/n_2-1)\theta$. The ray now reflects from the mirror in a direction $\theta_3 = -\theta_2$, and then is refracted a second time into the direction $\theta_4 = 2(1-n_2/n_1)\theta$. Using $n_1 = 2.2$ for LiTaO$_3$ and $n_2 = 1.5$ for the index fluid used between the crystal and the mirror, we obtain $\theta_4 \approx \frac{2}{3}\theta$. Thus, the final deviation of the light ray due to the error $\theta$ is $\frac{2}{3}\theta$ for the external mirror case and $2\theta$ for the internal mirror. This assumes that the perfection of the external mirror is much greater than that of the crystal,
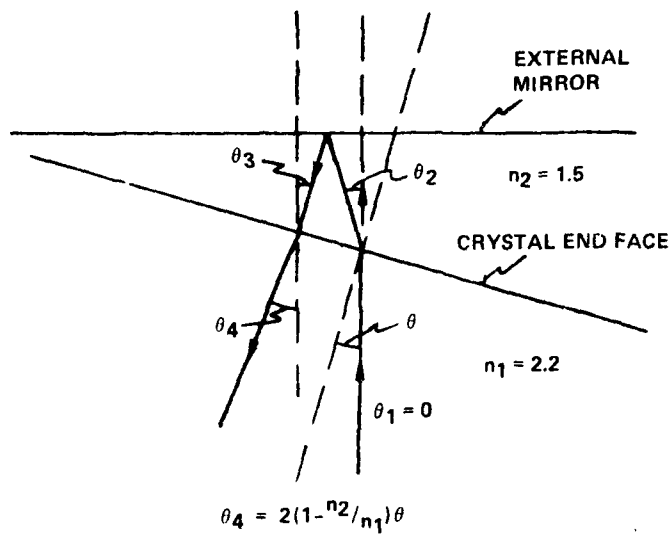
EXTERNAL
MIRROR

$\theta_3$

$\theta_2$

$n_2 = 1.5$

CRYSTAL END FACE

$\theta_4$

$\theta$

$n_1 = 2.2$

$\theta_1 = 0$

$$\theta_4 = 2(1 - \tfrac{n_2}{n_1})\theta$$

FIG. 12    Deviation of incident ray due to misalignment of crystal end face by angle $\theta$.

which is likely to be true due to the difficulties inherent in polishing the thin, fragile crystal.

While the external mirror is much more tolerant of imperfections in the crystal end face, there are other loss mechanisms associated with its use. Clearly, any physical separation between the end of the crystal and the mirror itself will lead to loss due to the spreading of light from the crystal that is not reflected back into the crystal, as shown in Fig. 13. These losses might be due to a variety of causes such as the mismatch between a spherical mirror (Fig. 14a) and the circular crystal end face, a mismatch between radii of curvature of the mirror and the crystal (Fig. 14b), or simple experimental error. A computer program was used to calculate the exact results for this loss for two different crystal thicknesses, 3 mils and 9 mils, and the results are presented in Table 8. As would be expected, the thicker crystal has much lower losses, especially for small separations.

The actual distance separations for the two cases shown in Fig. 14a and b can easily be estimated for our present devices. For the spherical mirror misalignment (case a), assuming 50 mil thick glass slides and a 1" long crystal (radius of curvature = 1"), it is easily calculated that $D = 1.25$ mils. According to Table 8, this is a loss of about 7% for a 3 mil crystal and only 2.5% for a 9 mil crystal. Obviously, this loss could be eliminated by using cylindrical lenses. For case b, two different radii of curvature, we can assume that the radii certainly will differ by less than 100 mils. Using a 1" long crystal, the separation D is then only .2 mil at an angle of $3.6^o$ from the center direction. (A numerical aperture of .14 implies $\pm 3.6^o$ light cone in $LiTaO_3$.) Thus, the loss from this situation should be negligible.

Finally, in discussing the use of an external mirror relative to an internal one, it should be mentioned that the external mirror approach is implemented more easily when an electrode structure is used for modulation. The electrode pattern is evaporated on the crystal in an approximately centered position and the fibers are adjusted relative to the electrode. Then the external mirror can be positioned exactly for reflection from the
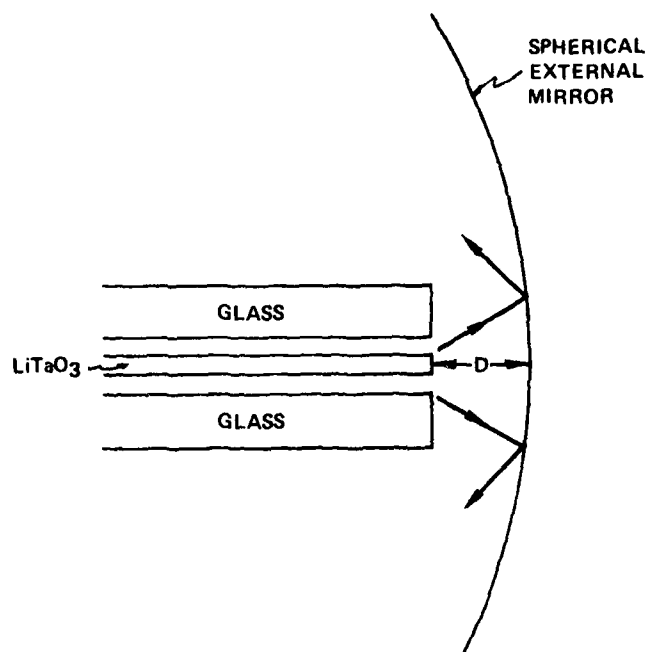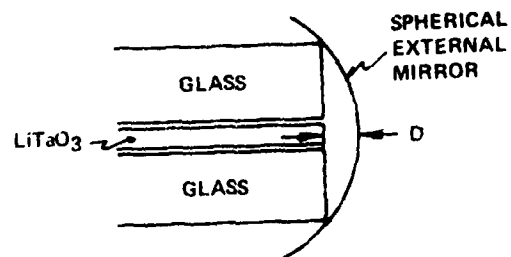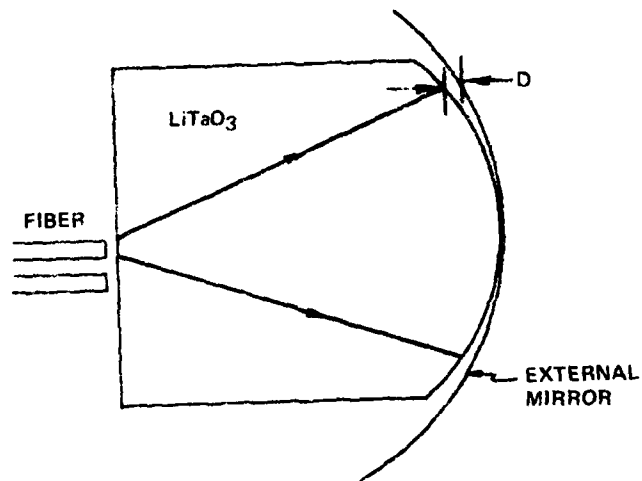
-127-

FIG. 13   Loss due to physical separation of an external mirror and
the crystal end face.

(a)



(b)

FIG. 14    Mirror/crystal separation due to (a)  spherical mirror or
(b)  different radius of curvature.

input fiber to the output fiber. When using an internal mirror, the location of the internal mirror is fixed, and thus the simultaneous alignment of electrode pattern, fibers, and mirror is much more difficult.

## C. EXPERIMENTAL RESULTS

An electrode pattern was designed using a series of electrodes to "spoil" the focus of the light when a voltage is applied. The pattern was created with the aid of a computer and is shown in Fig. 15 for a 3.5 mil crystal and in Fig. 16 for a 9 mil crystal. The only difference in the two patterns is that the thicker crystal allows a wider lateral fringing field between electrodes, and therefore a larger separation is needed between adjacent electrodes with the larger crystal. The same pattern is used on top and bottom of the crystal. All dimensions given in Figs. 15 and 16 are in mm.

Two devices were constructed, one using 3.5 mil $LiTaO_3$ (Fig. 17) and the other using a 9 mil crystal (Fig. 18). Also, two multifiber terminations were fabricated for the device with 3.3 mil core Corning fiber and 10 mil core Valtec fiber. The devices were tested using the experimental arrangement of Fig. 19, except that for the 3 mil devices an internal mirror was also tested. In all cases a He-Ne laser was used with focusing optics to yield an excitation cone of .15 NA.

Figure 20 shows a portion of the near field pattern at the cylindrical surface for the 3.5 mil crystal with 300 V applied across the crystal. The alternate bright and dark areas are evidence of the action of the electrodes in disturbing the uniform input beam and thereby causing modulation.

The light throughput as a function of voltage is shown in Fig. 21 for both the main bus fiber and a local tapoff fiber. The pattern is nearly symmetrical about -25 V. Normally, it would be expected that maximum throughput should occur at V=0, but all of the devices when initially constructed exhibit a built in "bias voltage" that yields an index change underneath electrodes with zero applied voltage. This bias fades to zero with time, but at the time of the measurements of Fig. 21 there was still a

| Separation | Loss (%) | |
|---|---|---|
| D (mils) | 3 mil Crystal | 9 mil Crystal |
| 2 | 14 | 5 |
| 4 | 27 | 9 |
| 6 | 40 | 14 |
| 8 | 54 | 18 |
| 10 | 63 | 23 |
| 12 | 69 | 27 |
| 14 | 74 | 32 |
| 16 | 77 | 36 |
| 18 | 80 | 41 |
| 20 | 82 | 45 |
| 30 | 88 | 63 |
| 40 | 91 | 72 |

Table 8.  Loss due to physical separation D between crystal end
face and external mirror.
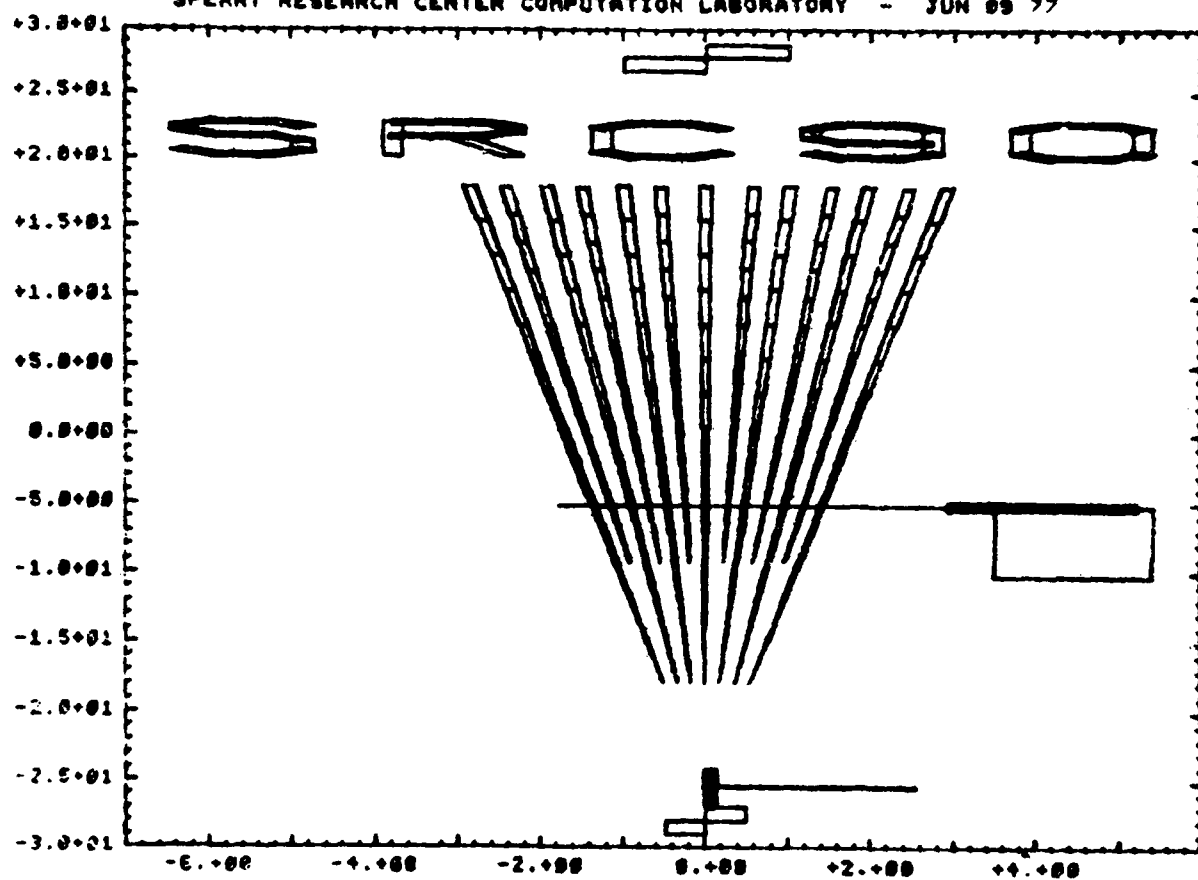
FIG. 15 Electrode pattern for 3.5 mil crystal.
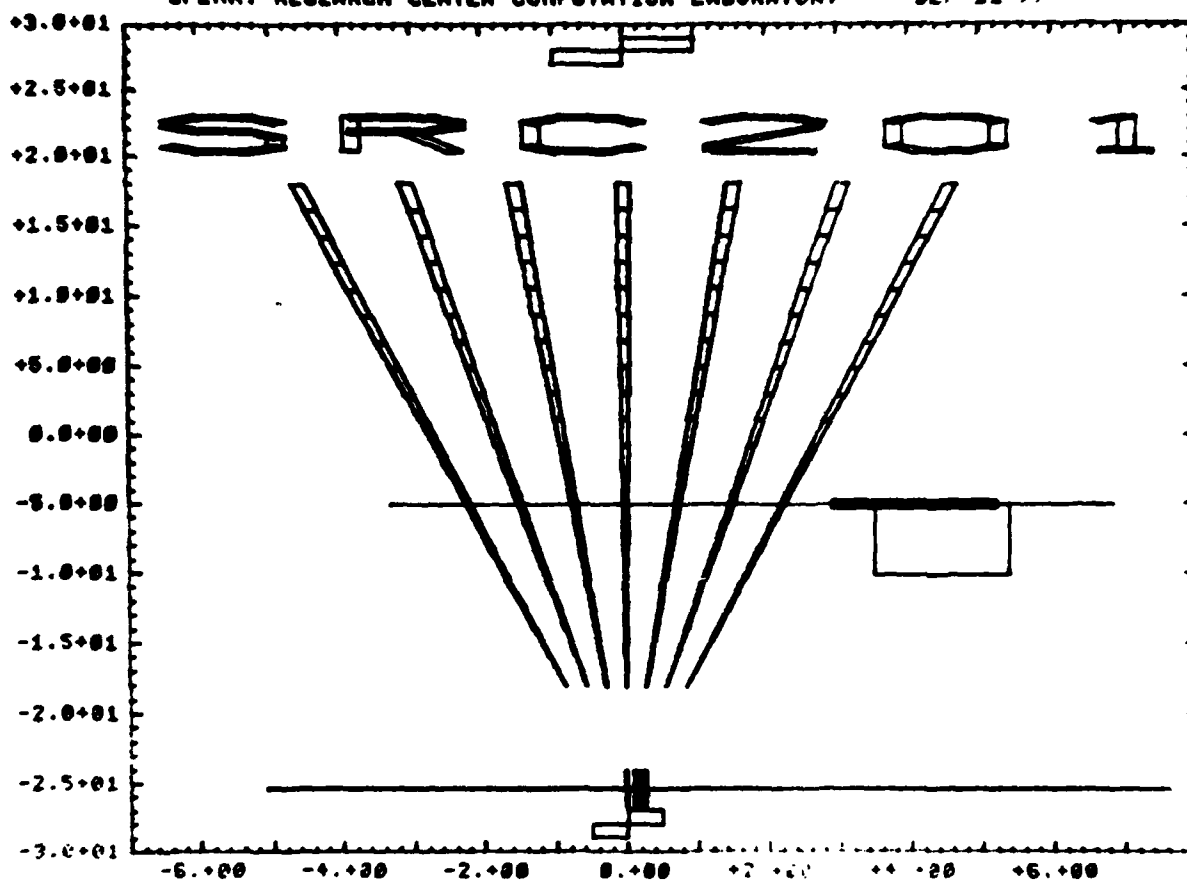
-132-

FIG. 16    Electrode pattern for 9 mil crystal.

FIG. 17   Mirror terminal using 3.5 mil crystal.


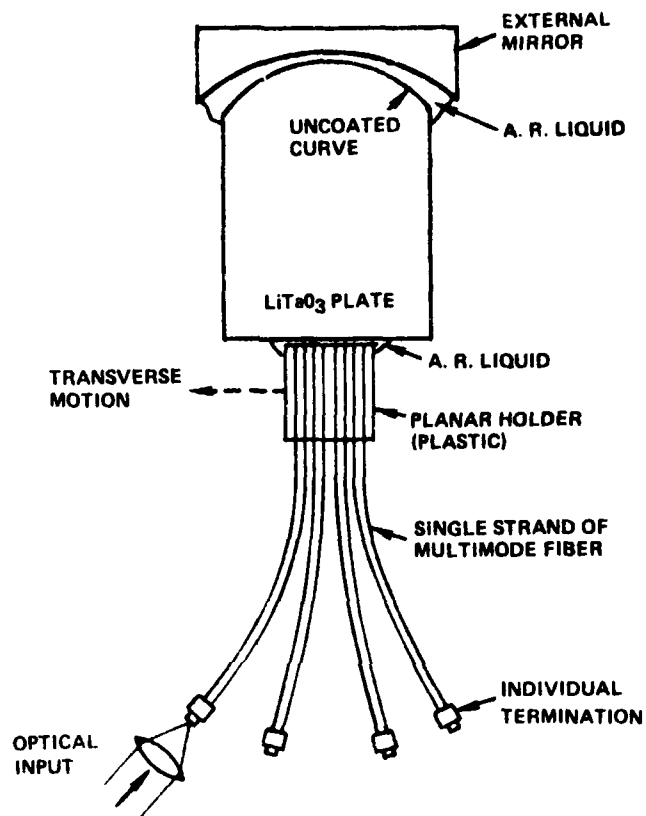
FIG. 18   Mirror terminal using 9 mil crystal.

FIG. 19   Layout of external mirror terminal and multiple fiber coupling.
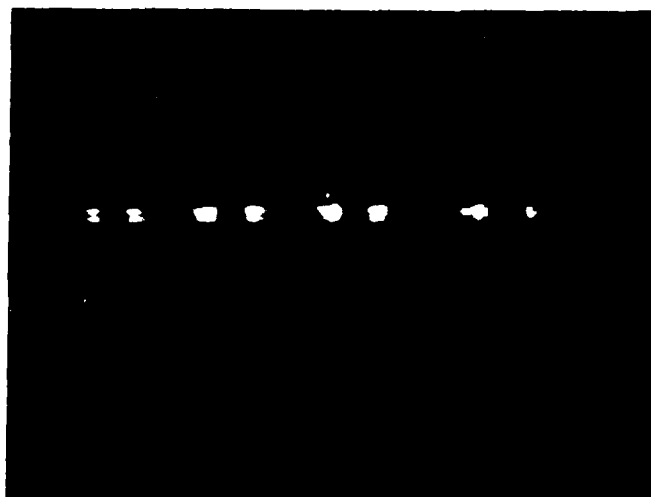
FIG. 20    Near field pattern of 3.5 mil crystal with 300 V applied.

residual effect equivalent to about 25 V of applied voltage. The exact cause of the effect$^2$ is not known at this time, except that it can be created by heating the crystal at about $100^\circ C$, that the initial strength seems to vary from crystal to crystal, and that the index change fades in approximately one week's time without any apparent detrimental effect.

As shown in Fig. 21, the output from the tapoff fiber is relatively constant with this electrode structure. Figure 22 is a plot, made from the data of Fig. 21, of the modulation depth vs voltage. A depth of 32% may be obtained with 50 V as opposed to 100 V for the collimation terminal. The modulation depth increases at a slower rate with higher voltages, giving an approximate square root dependence. However, very low voltages do give a significant modulation depth, e.g., 10% for only 10 V.

Soon after beginning measurements on the 3.5 mil device, it was discovered that the crystal was cracked. Most of the electrode pattern remained intact so that the modulation measurements could be taken, although a new crystal may yield better results than those shown in Fig. 22. However, throughput loss measurements are not accurate due to the scattering and reflection losses at the crack. A new, identical 3.5 mil device has been constructed and will be tested but not soon enough to be reported on for this quarter.

The thicker 9 mil crystal has also not been fully tested at the time of this report. The effect of the initial passive bias had not faded sufficiently to take modulation measurements, although this will be possible in the near future. Another problem area with the thicker crystal was the Valtec fiber termination. The large core fiber is plastic coated, and a better polish can usually be obtained without the plastic. In our first try with this fiber, the plastic cladding was removed for the length of the termination, and this made the fibers quite lossy. Some information on the throughput loss of the 9 mil device, however, was obtained by allowing for the extra fiber loss. Using a spherical mirror and no device, the loss for the Valtec termination was measured to be 8.2 dB (ratio of output of input fiber to output of output fiber). Normally, this loss is about 2 dB, so
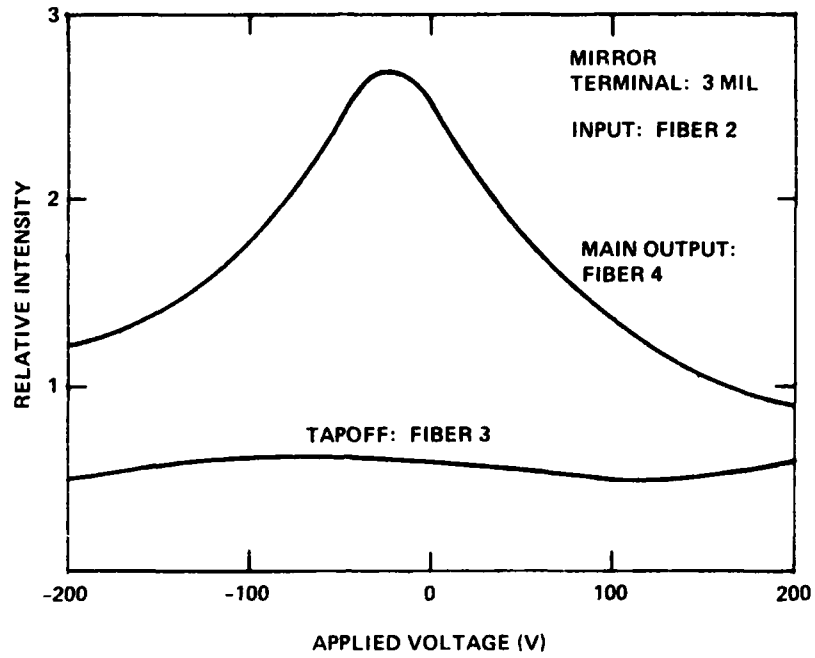
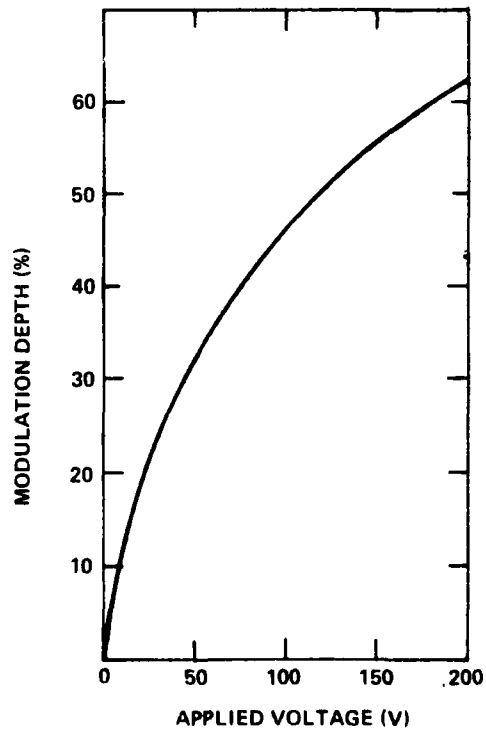FIG. 21 Throughput vs. voltage for the main bus and local tapoff fiber.



FIG. 22 Modulation depth vs. applied voltage for 3 mil mirror terminal.

-138-

that the excess loss of this termination is more than 6 dB. With the device inserted, the total loss rose to 11.8 dB, but allowing for the excess fiber loss this translates to a device loss of less than 6 dB. In addition, with the built-in bias in effect, this loss corresponds to a nearly maximum modulation depth, so that the loss with $V=0$ should be a few dB lower. During the next quarter, a new Valtec fiber termination will be constructed and, after the built-in bias has faded, the 9 mil mirror terminal will be remeasured to confirm the results on throughput loss.

References

1. Quarterly Status Reports Nos. 1 and 2 of this same contract.

2. The cause of this phenomenon is apparently derived from ionic motion in the crystal and is related to the results found by others (e.g., J. J. Amodei and D. C. Staebler, Appl. Phys. Letters 18, 540 (1971)) to fix holograms in $LiNbO_3$.

# MISSION
## of
## Rome Air Development Center

*RADC plans and executes research, development, test and selected acquisition programs in support of Command, Control Communications and Intelligence ($C^3I$) activities. Technical and engineering support within areas of technical competence is provided to ESD Program Offices (POs) and other ESD elements. The principal technical mission areas are communications, electromagnetic guidance and control, surveillance of ground and aerospace objects, intelligence data collection and handling, information system technology, ionospheric propagation, solid state sciences, microwave physics and electronic reliability, maintainability and compatibility.*